Understanding the Role of MLCL AT-1 and Tafazzin in Mitochondrial Function

by

Edgard Marcello Mejia

A Thesis submitted to the Faculty of Graduate Studies of the University of Manitoba

in partial fulfillment of the requirements of the degree of

Doctor of Philosophy

Department of Pharmacology and Therapeutics

University of Manitoba

Abstract

Cardiolipin (CL) is a phospholipid found exclusively in mitochondria and is required for normal mitochondrial function. CL biosynthesis requires a crucial remodelling step that incorporates specific acyl chains onto its molecular structure. The enzyme primarily responsible for CL remodelling is Tafazzin (TAZ), a mitochondrial protein encoded by the *TAZ* gene localized to chromosome Xq28.12. Mutations on the *TAZ* gene result in a rare yet severe disease known as Barth Syndrome (BTHS). BTHS is characterized by symptoms that include cardiomyopathies, neutropenia and skeletal myopathies. The mitochondrial enzyme Monolysocardiolipin Acyltransferase -1 (MLCL AT-1) also exhibits the ability to remodel CL with specific acyl chains. The aims of our study were to 1) determine if a relationship exists between TAZ and MLCL AT-1 , 2) determine if MLCL AT-1 expression in BTHS lymphoblasts leads to improvements in mitochondrial function, and 3) to use the Taz knockdown (KD) mouse model to get a better understanding of the phenotypes displayed by BTHS patients. Our results showed that in normal healthy lymphoblasts, expression of MLCL AT-1 was inversely dependent on TAZ expression. However, in BTHS lymphoblasts, expression of MLCL AT-1 was significantly lower compared to healthy controls. With the use of a MLCL AT-1-carrying plasmid, we expressed MLCL AT-1 in BTHS cells. This resulted in increased MLCL AT-1 gene, protein and enzyme activity. In addition, expression of MLCL AT-1 in BTHS cells resulted in increases in CL mass, improved mitochondrial function and a reduction in reactive oxygen species (ROS) production. However, no changes were detected in mitochondrial respiratory chain supercomplex (SC) assembly in BTHS cells expressing MLCL AT-1 compared to healthy controls. SC formation was disrupted in

the hearts and skeletal muscle, but not the liver, of the *Taz* KD mice compared to wild-type (WT) animals. These results correlated with an elevated generation of hydrogen peroxide (H_2O_2) in the heart and skeletal muscle mitochondria of *Taz* KD mice compared to WT. Liver mitochondria from *Taz* KD mice, on the other hand, generated significantly less H_2O_2 compared to WT mice. The results from this study and our other published work demonstrate that MLCL AT-1 expression varies depending on the health of mitochondria and is tissue specific. In addition, our results reveal that TAZ expression is essential for various aspects of mitochondrial function including SC formation and ROS production.

Acknowledgements

This thesis was made possible by the financial support provided by the Barth Syndrome Foundation of Canada/USA and the Canadian Institutes for Health Research. Edgard M. Mejia received financial assistance from the Research Manitoba in conjunction with the Children's Hospital Research Institute of Manitoba.

I would like to thank my supervisor, Dr. Grant Hatch, for giving me the opportunity to pursue my PhD under his guidance. Working in his laboratory has been a privilege and an experience I will never forget. I would also like to thank all of my lab members, both past and present. Their kindness, help and support made my time here both productive and enjoyable. I would also like to thank all the members of the department of Pharmacology and Therapeutics. It takes an entire department to ensure a student successfully completes their training, and I appreciate what each and every one of you have done for me. For her contribution to my lipid mass spectrometry data, I would like to thank Dr. Genevieve Sparagna. I would also like to acknowledge my committee members which include Dr. Donald Miller, Dr. Donald Smyth and Dr. Barbara Triggs-Raine. They have provided me with invaluable guidance throughout my training and helped ensure my thesis was properly evaluated.

I would like to extend a special thanks to the late William Taylor. He was a constant source of advice and helped me develop my skills in the laboratory. Bill was always patient and always willing to help. I would not have made it this far without his guidance.

Last but not least, I would like to thank my friends and family. I dedicate this work to them and thank them for their unshakeable support throughout these past

years. To my girlfriend Ngoc, thank you for your encouragement and for always giving me great advice. You know better than anyone what I have gone through to get this far. Thank you for always being there. To my mother and father, thank you for always believing I could do this and for teaching me to never give up. I will never forget the sacrifices you have made for me. Without you, none of this would be possible.

Table of Contents

List of Tables

List of Figures

List of Copyrighted Material

Abbreviations

2D	2 Dimensional
3-MGA	3-Methylglutaconic Acid
AA	Antimycin A
A/A	Antibiotic/Antimycotic Solution
ADP	Adenosine Diphosphate
ALCAT1	Acyl-CoA:Lysocardiolipin Acyltransferase 1
αTFP	Alpha Trifunctional Protein
ATP	Adenosine 5'-Triphosphate
βTFP	Beta Trifunctional Protein
BN-PAGE	Blue Native Polyacrylamide Gel Electrophoresis
BSA	Bovine Serum Albumin
BTHS	Barth Syndrome
cat.#	Catalogue Number
cDNA	Complementary Deoxyribonucleic Acid
CDP-DAG	Cytidine Diphosphate Diacylglycerol
C. elegans	*Caenorhabditis elegans*
Ci	Curie
CI	Complex 1
CII	Complex 2
CIII	Complex 3
CIV	Complex 4
CL	Cardiolipin

CLS	Cardiolipin Synthase
CO_2	Carbon Dioxide
Ct	Cycle Threshold
CTP	Cytidine Triphosphate
CV	Complex 5
DDM	n-dodecyl β-D-maltoside
DLDH	Dihydrolipoamide Dehydrogenase
DMEM	Dulbecco's Modified Eagle Medium
DNA	Deoxyribonucleic Acid
dox	Doxycycline
DTNB	5, 5'-Dithiobis-(2-Nitrobenzoic Acid)
ECAR	Extracellular Acidification Rate
ECL	Enhanced Chemiluminescence
EDTA	Ethylenediaminetetraacetic Acid
EGTA	Ethylene Glycol Tetraacetic Acid
ER	Endoplasmic Reticulum
ESI-MS	Electrospray Ionization - Mass Spectrometry
ETC	Electron Transport Chain
FBS	Fetal Bovine Serum
FCCP	Carbonyl Cyanide 4-(Trifluoromethoxy) Phenylhydrazone
GPAT	Glycerol-3-Phosphate Acyltransferase
H_2O_2	Hydrogen Peroxide
HPLC	High Performance Liquid Chromatography

h	Hours
HRP	Horseradish Peroxidase
IGAA	In-gel Activity Assay
IgG	Immunoglobulin G
iPSC-CM	Induced-Pluripotent Stem-Cell Derived Cardiomyocytes
kDa	Kilo Dalton
kg	Kilogram
IMM	Inner Mitochondrial Membrane
KD	Knockdown
kg	Kilogram
L_4-CL	Tetralinoleoyl Cardiolipin
LPA	Lysophosphatidic Acid
M	Molar
MAP1LC3	Microtubule-Associated Protein 1Light-Chain 3
MAPK	Mitogen-Activated Protein Kinase
µg	Microgram
µL	Microlitre
mg	Milligram
mins.	Minutes
mL	Millilitre
MLCL AT-1	Monolysocardiolipin Acyltranferase-1
MLCL	Monolysocardiolipin
mm	Millimeter

MMP	Mitochondrial Membrane Protein
mtDNA	Mitochondrial Deoxyribonucleic Acid
Mtpa	Mitochondrial Trifunctional Protein Alpha
ng	Nano Gram
nmol	Nano Mole
ns	Not significant
OCR	Oxygen Consumption Rate
Oligo.	Oligomycin
OMM	Outer Mitochondrial Membrane
PA	Phosphatidic Acid
PBS	Phosphate Buffered Saline
PC	Phosphatidylcholine
PCR	Polymerase Chain Reaction
PE	Phosphatidylethanolamine
PG	Phosphatidylglycerol
PGP	Phosphatidylglycerol Phosphate
PHB	Prohibitin
PI3K	Phosphoinositide 3 Kinase
pmol	Pico Mole
PTFE	Polytetrafluoroethylene
PTPMT1	Protein Tyrosine Phosphatase Mitochondrion 1
PVDF	Polyvinylidene Difluoride
RISP	Rieske Iron-Sulfur Protein

RNA	Ribonucleic Acid
RNAi	Interference Ribonucleic Acid
ROS	Reactive Oxygen Species
RPM	Rotations Per Minute
RPMI	Roswell Park Memorial Institute
RT	Room Temperature
RT-PCR	Reverse Transcriptase Polymerase Chain Reaction
SDS-PAGE	Sodium Dodecyl Sulfate Polyacrylamide Gel Electrophoresis
SC	Supercomplex
SHR	Spontaneously Hypertensive Rats
shRNA	Short Hairpin Ribonucleic Acid
SLP-2	Stomatin-Like Protein 2
Tam41	Mitochondrial Translocator Assembly and Maintenance Protein Homolog
TAZ	Tafazzin
tBid	Truncated BH3 Interacting Domain Death Agonist
TBS	Tris-Buffered Saline
TBS-T	Tris-Buffered Saline - Tween
TLC	Thin-Layer Chromatography
TMRM	Tetramethylrhodamin-methylester
Tris	Trizma Buffer
TUP	Theoretical Upper Phase
VDAC	Voltage-Dependent Anion Channel
WT	Wild-Type

Introduction

1) Barth Syndrome

Barth Syndrome (BTHS) is a rare X-linked recessive disease that manifests itself as various cardiomyopathies, neutropenia (cyclic, chronic or intermittent), skeletal myopathies, 3-methylglutaconic aciduria and cognitive difficulties [1-3]. It was first described in 1983 by Dr. Peter Barth in a family of Dutch pedigree [1]. Upon closer analysis, it was revealed that substantial mitochondrial ultrastructural damage was present in the cardiac and skeletal tissue of these patients [1]. It was later determined that the disease was caused by mutations in the tafazzin (*TAZ*) gene (previously known as gene G4.5) located on the distal portion of Xq28 and responsible for producing the enzyme known as tafazzin [4-6]. Tafazzin (TAZ) is a transacylase that preferentially transfers linoleoyl groups from phosphatidylcholine (PC) and/or phosphatidylethanolamine (PE) to monolysocardiolipin (MLCL) to produce CL [7]. Thus, TAZ is crucial for CL biosynthesis and function.

2) Cardiolipin

CL is a polyglycerphospholipid that is unique to mitochondrial membranes [8-10]. It was first isolated by Dr. Mary Pangborn in 1942 and was named cardiolipin due to the fact that it was isolated from cow hearts [11]. CL is synthesized and localized in the inner mitochondrial membrane (IMM) with trace amounts found in the outer mitochondrial membrane (OMM) [12, 13]. In the IMM, CL makes up about 15-20% of all lipids in yeast and mammals [14]. The molecular structure of CL (a polar head group,

glycerol backbone with four acyl chains) is thought to be one of the characteristic elements behind its role in mitochondrial membranes (reviewed in[15]). Due to its small polar head group and large hydrophobic tail, CL has a conical structure which introduces tension into mitochondrial membranes. This allows proteins to be properly accommodated in the inner membrane and also induces negative curvature on membranes [15, 16]. CL has two negative charges, allowing it to easily interact with proteins in the OMM and IMM. These traits are believed to be the reason why CL is present in such large quantities in mitochondria, particularly in the IMM where there are not only a large amount of proteins, but also extensive curvature (cristae) compared to the OMM (Fig.1). However, the mere presence of CL in mitochondrial membranes is not enough to ensure proper mitochondrial function. Specific molecular species of CL make up the bulk of all CL found in tissues such as the heart and liver, predominantly species containing unsaturated fatty acids [10, 17]. For example, the major CL molecular species found in rat liver (comprising of ~57% of total CL), bovine heart (~48% of total) and human heart (~80% of total) is referred to as tetralinoleoyl-CL (L_4-CL) [18]. Thanks to the extensive work of several laboratories, many of the roles that CL plays have been described. CL has been shown to be directly or indirectly involved in mitochondrial protein transport [19], cross-talk between mitochondria and vacuoles [20] and mitochondrial-mediated apoptosis [21-24]. CL is also reported to play a major role in mitochondrial bioenergetics by acting as the 'glue' that holds complexes from the electron transport chain together, forming higher order structures known as supercomplexes (SCs) [25-28]. CL's promiscuous ability to interact with

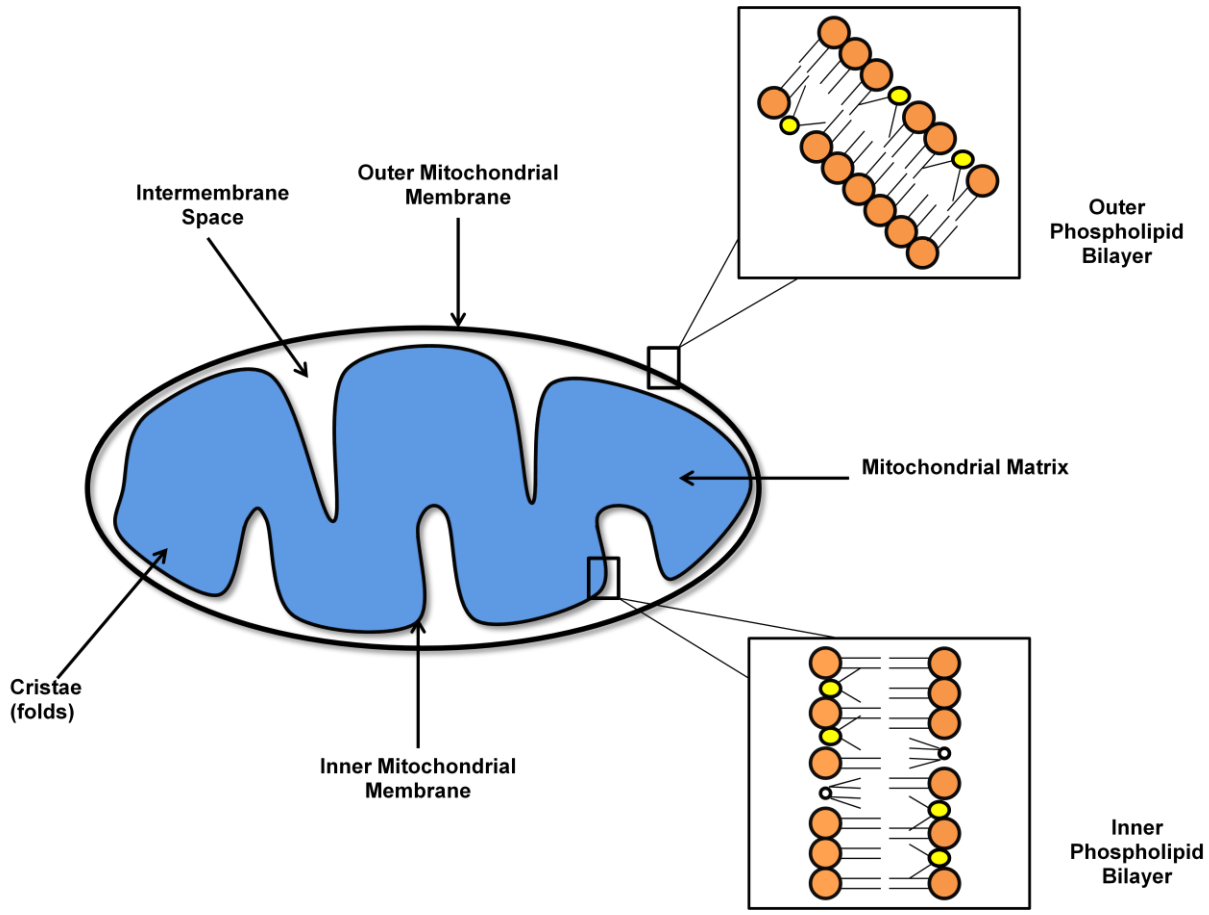

Figure 1: Distribution of the major phospholipids in mitochondrial membranes.

The outer mitochondrial membrane (OMM) and inner mitochondrial membrane (IMM) contain structural phospholipids such as phosphatidylcholine (PC), phosphatidylethanolamine (PE) and cardiolipin (CL). Phospholipid abundance varies between the OMM and IMM. PC and PE make up the majority of phospholipids, and PE and CL are more abundant in the IMM compared to the OMM. The tubular formation of PC allows for the formation of planar bilayers in both the OMM and IMM. Non-bilayer forming phospholipids such as PE and CL have a smaller hydrophilic head group compared to their hydrophobic acyl groups, thus favouring hexagonal phase formations. This introduces tension into mitochondrial membranes which allows the incorporation of proteins and can also contribute to the negative curvature of the membrane thereby facilitating specific mitochondrial functions such as fusion and/or fission. [15]

various proteins is the main reason why it is involved in many mitochondrial and sometimes cellular mechanisms.

3) CL-Protein Interactions

As mentioned above, CL has been reported to play an important role in mitochondrial-mediated apoptosis [21-24]. As the name implies, mitochondrial-mediated apoptosis (also known as the intrinsic apoptotic pathway) is mediated by a number of mitochondrial factors (reviewed in [29]). The extrinsic apoptotic pathway on the other hand, is mediated by receptors on the plasma membrane and their corresponding ligands, although reports indicate that both the intrinsic and extrinsic pathways may not be independent of each other (reviewed in [29]). In the intrinsic pathway, CL has been shown to interact with caspase-8, acting as a platform that recruits caspase-8 to the OMM where it undergoes oligomerization [21]. Using BTHS lymphoblasts, Gonzalvez *et al* demonstrated that mitochondria were unable to bind caspase-8, thus blocking the signal transduction [22]. The direct interaction of CL with apoptotic factors is not always necessary however. Studies have shown that even though CL is required for the recruitment of intrinsic apoptotic factors such as tBid to mitochondria, CL does not bind directly to tBid *in vitro*, but is instead believed to be necessary for the recruitment of tBid from the cytosol to the IMM [23].

An important cellular process known as mitophagy, involves the selective removal of mitochondria via autophagy (reviewed in [30]). It is a necessary process required to ensure that damaged mitochondria are promptly removed and may also be required to regulate mitochondrial numbers to match metabolic demands [30]. Various

studies have shown that CL also plays a role in mitophagy. Much like apoptosis, CL has been shown to be involved in mitophagy via lipid-to-protein interactions. For example, Chu *et al* demonstrated that microtubule-associated protein 1 light-chain 3 (MAP1LC3), a protein that interacts with cellular and sub-cellular membranes to act as a marker for autophagosome recruitment, interacts with CL [31]. Chu *et al* also showed that the inhibition of this CL-MAP1LC3 interaction prevented the recruitment of autophagosomes and lysosomes to mitochondria and thus prevented mitochondrial loss [31]. Thus, it is evident that CL plays an important role not only in apoptosis but also in mitophagy, which helps eliminate aberrant mitochondria and may prevent cells from eventually undergoing apoptosis or even necrosis. However, some of CL's most crucial roles involve its function in the assembly rather than the breakdown of membranes, as will be discussed later on.

Another example of CL-protein interactions involves a mitochondrial protein known as stomatin-like protein 2 (SLP-2). SLP-2 is a protein that belongs to the stomatin family [32, 33] and has been reported to be up-regulated when T lymphocytes are activated *in vitro* and *in vivo* [34]. However, despite the wide expression of this protein in mitochondria, the actual function of SLP-2 is currently unknown [35]. What we do know about SLP-2 is that it not only interacts with prohibitins-1 and 2 (PHB-1 and PHB-2) [36], but it also interacts with CL [35]. Prohibitins are proteins found in eukaryotic cells that are involved in cellular functions such as cellular signalling and transcriptional control as well as mitochondrial biogenesis (reviewed in [37]). Prohibitins form a ring-like structure that is composed of alternating subunits of PHB-1 and PHB-2 in the IMM of yeast, mammals and *C. elegans* [38-40]. Christie *et al* reported that

elevating the expression of SLP-2 in T lymphocytes led to significantly higher levels of CL which correlated with increased complex I (CI) and complex II (CII) activities [35]. Increasing SLP-2 expression also resulted in increased resistance to apoptosis (intrinsic pathway) as well as elevated ATP levels [35]. The authors of this study proposed that SLP-2 functions by recruiting prohibitins to CL where they can then perform their biological functions [35]. Thus, SLP-2 interacts with CL allowing prohibitins to be targeted to mitochondria.

One of the earliest and most widely documented CL-protein interactions reported is the interaction between CL and the ADP/ATP carrier found on the IMM. Studies conducted by Beyer and Klingenberg in 1985 using beef heart mitochondria demonstrated that the ADP/ATP carrier is tightly bound to 6 molecules of CL [41]. Later studies showed that, surprisingly, CL did not need to have a specific acyl composition in order to bind to the ADP/ATP carrier [42]. This finding could be due to experimental conditions as later studies have shown that specific species of CL, such as L_4-CL, are the most abundant forms of CL found in mitochondrial membranes [18]. Subsequent studies showed that not only are 6 CL molecules tightly bound to the ADP/ATP carrier, but CL was also required for ADP/ATP carrier activity [43]. A study conducted by Jiang *et al* further demonstrated how important the presence of CL is for the proper function of the ADP/ATP carrier [44]. Using *S. cerevisiae* cells deficient for CL synthase (CLS), an enzyme required for CL biosynthesis [45], Jiang *et al* showed that even though ADP/ATP content was not affected, the significant reduction in CL led to the inactivation of the carrier [44]. Therefore, these studies have shown that CL in the IMM interacts with the ADP/ATP carrier and that this interaction is necessary for the carrier's function.

CL-protein interactions have been studied extensively in eukaryotic cells, but important findings have also been made in other organisms. Work conducted in photosynthetic bacteria has shown that CL is essential for the proper function of the photoreaction centre, a protein complex found on bacterial membranes required for light-driven electron transfer for the production of ATP [46]. X-ray crystallography results revealed that both the head group and tail region of CL were bound to various amino acid residues of the photoreaction center [46]. This interaction between CL and the photoreaction centre has been reported in a number of photosynthetic species of bacteria, but the actual function of this interaction has not been fully elucidated [47]. It is believed that CL may be necessary for the potential dimerization of the photoreaction centre in photosynthetic bacteria, however, further work is still required to better understand this mechanism [47].

4) Mitochondrial Supercomplexes

The role that CL plays in the formation and maintenance of SCs has been heavily investigated by many laboratories in recent years. Not only is the specific role CL plays in SC formation unknown, but the role that SCs themselves play in different tissues is still not fully resolved. Research into CL's role in SC formation is fairly recent, but knowledge of the interaction that exists between complexes of the electron transport chain (ETC) dates back to work conducted by Chance and Williams in 1955 [48]. Since this time there has been extensive debate over which model better describes the true nature of the ETC complexes. The 'solid state' model hypothesizes that complexes of the ETC interact with one another and form what are known as SCs, while the 'fluid

state' model predicts that complexes from the ETC do not interact with each other and function in an independent manner (reviewed in [49]). Even though evidence has emerged that shows individual respiratory complexes do indeed have biochemical activity [50], the fluid state model cannot explain the isolation of various SCs as demonstrated by Blue Native Polyacrylamide Gel Electrophoresis (BN-PAGE) [51] and single-particle electron microscopy [52]. Not only can these SCs be visualised and resolved via techniques such as BN-PAGE, but they are also biochemically active as shown by in-gel activity assays [51, 53]. Studies have also shown that optimal enzymatic function can be achieved when complexes interact with each other, and point mutations that affect one complex can result in the impaired function of others [49, 52]. However, the fluid state model argues that if indeed SCs exist in a supramolecular assembly, then they should not be individually active (reviewed in [49]). A number of studies that used fluorescence recovery after photobleaching and flux control analysis showed that the electron transfer between different complexes mediated by ubiquinone and cytochrome c occurred over a long range distance of 36 nm [54-56]. This observation is a direct argument against the solid state model that predicts close contact between ETC complexes. Another study questioning the relevance of SCs provides evidence that shows that cytochrome c is not trapped within SCs and is easily able to diffuse within the ETC without restrictions [57]. This study acknowledges that interactions between complex IV (CIV) and cytochrome c may exist, but these interactions are very short lived and do not appear to serve a specific physiological purpose. Despite these type of reports, evidence continues to build that supports the solid state model, especially when the role that CL plays in SC formation is considered

(discussed in a later section). The continuing research on this topic has lead to the emergence of a new model that accommodates findings from both pro-solid state and pro-fluid state models. In a recent review by Acin-Perez *et al*, the authors expertly describe how recent studies have lead to the hypothesis that optimal mitochondrial function is achieved when you have a balance between free respiratory complexes and SCs [58]. This new model is referred to as the 'plasticity' model and it hypothesizes that the organization of SCs can be adjusted depending on the cell type and also on the different metabolic demands of different tissues. Various studies conducted on yeast, plant and mammalian cell lines have reported that changing the growth and physiological conditions of these cells (i.e. replacing glucose with lactose or galactose as carbon sources or hypoxic conditions) results in a change in the dynamics of SC formation [58, 59]. These studies show that by forcing the mitochondria to work at maximum capacity, SC expression can be increased. This predicted dynamic nature that SCs possess would prove to be invaluable information when considering the various diseases that arise as a result of mitochondrial dysfunction. This topic will be discussed in a later section.

The specific interactions that occur between all five complexes of the ETC (complexes I-V) have been described. It has been demonstrated that in various organisms, complexes I, III and IV associate with each other to form SCs [51]. Most studies report that complex II (CII) does not associate with other complexes in both plant and mammalian mitochondria [51, 60, 61]. Complex V (CV) on the other hand appears to co-migrate with other complexes on BN-PAGEs, but only interacts with itself to form a dimer [51, 62]. Our *in vitro* work primarily focused on studying CI SC

formation because research has shown that unlike the other complexes of the ETC, CI predominantly exists in SCs rather than as an individual unit [51]. It has been hypothesized that CI function depends on its interactions with CIII and CIV. Li *et al* demonstrated that in the absence of CIII, CI function was significantly unstable in mammalian mitochondria [63]. The absence of CIV was even more detrimental, resulting in complete loss of function in CI [63]. However, CIII and CIV function is not significantly affected in the absence of CI [63, 64]. Not only is the function of CI dependent on SC formation, but potentially, so is its assembly. A comprehensive study conducted by Marques *et al* demonstrated that CI/III SC formation occurs before individual CI formation [65]. Another study showed that the association of CIV and CIII (in that order) to a partially assembled CI acting as a scaffold, was necessary before additional subunits (NDUFS4 and NDUFV1) could be incorporated into complex I [66]. Thus, it can be seen that interactions between complexes I, III and IV are not only present in mitochondrial membranes, but these interactions are necessary for their function and overall assembly (particularly for CI).

5) Mitochondrial supercomplexes and reactive oxygen species production

The complexes of the ETC mediate the transport of electrons via redox reactions in an oxygen-dependent manner that ultimately results in CIV reducing O_2 to H_2O. In addition, complexes I, III and IV pump protons into the mitochondrial intermembrane space which generates the proton motive force that drives CV (F_1F_o ATP synthase) to produce ATP. These biochemical reactions are collectively referred to as oxidative phosphorylation, and they are also responsible for mitochondria being a large

contributor to the production of reactive oxygen species (ROS) in cells. Despite the fact that electron transport along the ETC is a tightly coupled process, about 1-3% of the O_2 is incompletely reduced leading to the formation of superoxide and ultimately hydrogen peroxide (H_2O_2) [67]. ROS production is often seen as a negative side-effect of oxidative phosphorylation, but previous and ongoing studies have shown that it is an essential biochemical process. ROS has been shown to play a major role in the regulation of mitogen-activated protein kinase (MAPK) and phosphoinositide 3-kinase (PI3K) signalling pathways (reviewed in [68]). ROS also play an important role in the signalling pathways of the innate and adaptive immune responses as well as acting as an antimicrobial agent produced by phagocytes (reviewed in [69]). The problem lies in the potential imbalance that may occur between excess ROS production and the antioxidant responses typically employed by cells such as the production of superoxide dismutase (SOD), which converts the significantly more harmful superoxide to H_2O_2 [68]. A number of diseases are associated with elevated levels of ROS, including cardiovascular diseases [70], diabetes [71], and neurodegenerative diseases [72]. Elevated ROS levels can cause mtDNA mutations [73], can oxidize the complexes of the ETC [74] and also cause phospholipid peroxidation [75]. In addition, ROS has been shown to increase with age [76]. Thus, it is not surprising that imbalanced ROS levels are associated with a number of diseases and cellular dysfunction. And so it is evident that mitochondria are a major source of ROS, but if we take a closer look at the mitochondrial sites responsible for ROS production we can begin to appreciate the importance SC formation has on disease progression.

The major sites of ROS production in mitochondria are CI and CIII [77, 78]. Aside from the fact that SCs aid in improving the efficiency of electron transport and also improve the kinetics of substrate channeling, their formation is also predicted to minimize ROS production by CI and CIII. A direct correlation between SC formation and ROS production was shown by Maranzana *et al* who observed that ROS production was significantly raised when SC assembly was impaired in bovine heart mitochondria [79]. Another study looking at mouse lung fibroblasts lacking the Rieske iron-sulfur protein (RISP, a catalytic subunit of CIII), found that not only was SC formation decreased, but it was accompanied by increases in ROS [80]. Therefore, we can infer from these studies that SC formation may be an essential factor for mitochondrial health by minimizing excessive ROS production. Excessive ROS production due to decreases in SC formation would be detrimental for mitochondria but would also lead to cellular damage. When we now consider the fact that CL is reported to be essential for SC formation, we may begin to understand the role that SCs play in BTHS.

6) Cardiolipin interacts with mitochondrial supercomplexes

Work by Zhang and Pfeiffer has shown that CL acts as the glue that stabilizes SCs [25, 26]. Further advances have been made in understanding the role that CL plays in SC formation thanks to the research being conducted on BTHS. A number of studies using yeast, BTHS animal models or cells from BTHS patients have demonstrated that SC formation is disturbed in BTHS. Brandner *et al* reported that TAZ1 (orthologue of human TAZ) deletion leads to the release of CIV from the III_2/IV_2 SC [81]. Other studies using a *Taz* KD mouse model observed that SC formation as

well as CI SC activity was significantly reduced in *Taz* KD mice compared to WT [28, 82]. Studies were conducted by Mckenzie *et al* that showed levels of the SC containing CI, $CIII_2$ and CIV were significantly reduced in BTHS lymphoblasts compared to age-matched controls [83]. As mentioned previously, a lack or decrease in SC formation may lead to increases in ROS production. One of the consequences of excessive ROS production is the susceptibility of phospholipids to undergo peroxidation. Due to its molecular structure (including four unsaturated fatty acid chains), CL is highly susceptible to lipid peroxidation. Reports have shown that CL peroxidation leads to a loss of its molecular interaction with cytochrome c [84]. The release of cytochrome c is a signal for the initiation of apoptosis and leads to programmed cell death [85-87]. These processes where by decreased CL leads to decreased SC formation resulting in increased ROS production which in turn peroxidizes CL that leads to apoptosis, generates a vicious cycle that may explain the pathology behind BTHS. In fact, various studies focussing on understanding the pathophysiology behind BTHS have reported a potential correlation between BTHS and increased ROS production. One example is a study conducted by Wang *et al* that used BTHS induced-pluripotent stem-cell derived cardiomyocytes (iPSC-CMs) and observed an elevation in mitochondrial membrane potential which led to increases in ROS production [88]. Thus, dysfunctional ROS production may be playing a key role in the development of BTHS.

7) Cardiolipin Biosynthesis

CL biosynthesis is redundant in yeast, mammals and plants, and takes place in the inner mitochondrial membrane via the cytidine-5'-diphosphate-1,2-diacyl-*sn*-glycerol

phosphate pathway [9, 89]. However, this biosynthetic pathway begins in the endoplasmic reticulum (ER) and includes a number of precursors and enzymes that ultimately result in the formation of bis-(1,2-diacyl-sn-glycero-3-phospho)-1'-3'-sn-glycerol, or CL (Fig.2). The *de novo* biosynthesis of CL begins with the transfer of a fatty acid from acyl coenzyme A to the *sn-1* position of glycerol-3-phosphate by glycerol-3-phosphate acyltransferase (GPAT) to form lysophosphatidic acid (LPA) [90]. GPAT enzymes have a microsomal localization, found in both perinuclear and cortical endoplasmic reticula in cells that are actively proliferating [91]. LPA is then acylated at the *sn-2* position by 1-acyl-*sn*-glycerol-3-phosphate acyltransferase to form phosphatidic acid (PA). This is followed by a condensation reaction between PA and cytidine triphosphate (CTP) which is catalyzed by an enzyme called mitochondrial translocator assembly and maintenance protein homolog, or Tam41, to form the high energy intermediate CDP-DAG [92]. It is only until recently that this enzyme's role in CL biosynthesis was elucidated by Tamura *et al* [92]. It is important to note that both LPA and PA are synthesized on the outer surface of the mitochondrial outer membranes, and PA has to be transported into the IMM for CL synthesis [93]. Importing CDP-DAG into the IMM has been shown to be significantly less efficient than importing PA for CL biosynthesis [92]. Next, an activated phosphatidyl group from CDP-DAG is transferred to the *sn-1* position of *sn*-glycerol-3-phosphate by phosphatidyl glycerol phosphate (PGP) synthase to yield PGP [10]. The following step in this pathway was described by Zhang *et al* (2011), who showed that an enzyme called protein tyrosine phosphatase mitochondrion 1(PTPMT1) is responsible for the hydrolysis of PGP to yield phosphatidyl glycerol [94]. PTPMT1 is localized exclusively in the IMM with its expression reported in

bacteria, plants and animals [94]. The final step in this pathway is catalyzed by an IMM enzyme called CL synthase (CLS) and it involves the transfer of an activated phosphatidyl group from another CDP-DAG to PG to form nascent CL [45].

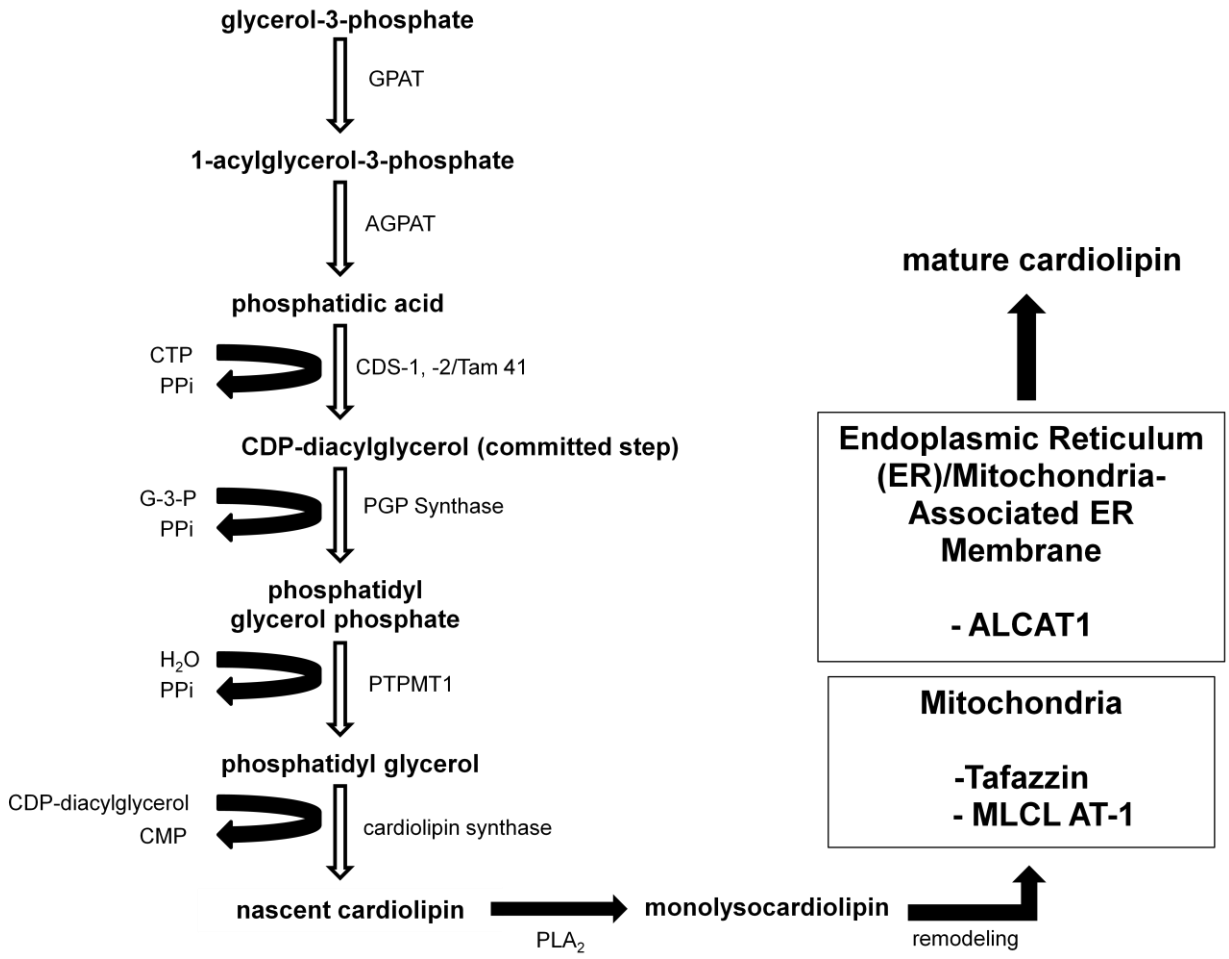

Figure 2: CL *de novo* biosynthesis pathway and remodelling enzymes.

CL must be remodelled with specific fatty acid chains prior to its incorporation into mitochondrial membranes. CLS does not have acyl chain specificity, while TAZ on the other hand, remodels CL by transferring specific acyl chains from phospholipids such as PC and PE to a MLCL molecule to produce mature CL. [95]

8) Tafazzin

CL found in mitochondria of various organisms and tissues contains specific acyl chains. As mentioned previously, the most abundant CL species found in heart and liver is rich in linoleic acid [18]. However, CLS has limited acyl specificity for its substrates for the production of consistent CL [96-98], which is indicative of additional steps required for CL biosynthesis. A crucial step required for proper CL function and homeostasis following *de novo* CL biosynthesis is known as CL remodelling. The primary enzyme required for this process is known as tafazzin (TAZ). TAZ is a transacylase found in the intermembrane space of mitochondria [99] that has been shown to transfer specific acyl chains (such as linoleic acid) from various phospholipids such as phosphatidylcholine (PC) and phosphatidylethanolamine (PE) to monolysocardiolipin (MLCL) (reviewed in [100]). The fatty acyl configuration of CL is tissue specific, such that highly oxidative tissues like the heart and skeletal muscle are rich in CL with four linoleic acid moieties. This type of CL is known as tetralinoleoyl-CL (L_4-CL) and research has shown it is the most affected CL species in BTHS [101]. The locus of the gene responsible for the production of TAZ is Xq28, also known as the *TAZ* gene [6]. This gene, composed of 11 exons, can undergo alternative splicing to produce a full length isoform or species that are missing exon 5, exon 6, exon 7 or all three exons [6]. The TAZ proteins produced can range from 129 to 292 amino acids and usually have a molecular weight of approximately 33.5kDa [6]. Despite the existence of a number of TAZ isoforms, only the isoform missing exon 5 has been reported to produce the functional protein responsible for CL remodelling [102]. However, both the isoform missing exon 5 and the full-length isoform are the most

abundant in mammalian heart, skeletal muscle and leukocytes [6]. Similar results have been reported in yeast [102]. An interesting observation made in this mammalian study was the presence of a TAZ isoform that was only present in heart and skeletal muscle [6]. This isoform was the smallest out of all the others and it helps raise the question: why do other TAZ isoforms exist in the first place? This topic will be discussed in a later section. Even though the previously discussed mammalian study made monumental strides towards the understanding of TAZ, they were limited by their use of regular reverse transcriptase PCR analysis on total RNA isolated from different tissues to quantify differences in splice variants. A later study conducted by Houtkooper *et al* [103] that used quantitative real-time PCR to compare the different isoforms using human cDNA provided a more effective approach. Houtkooper *et al* analysed six different splice variants in 16 different tissues and, surprisingly, found that the different isoforms were (for the most part) equally expressed in all tissues analyzed [103]. In addition, the tissues with the highest TAZ expression were the pancreas and the spleen [103]. Considering the fact that CL in tissues such as the heart and skeletal muscle are enriched with specific unsaturated fatty acids (linoleic and oleic acid) while tissues such as the pancreas and spleen have CL with more acyl variability, these observations raise many questions. The authors themselves acknowledge the limitations of their study by indicating that mRNA levels do not necessarily correlate with protein expression. However, Houtkooper *et al* hypothesize that aside from TAZ protein expression, other factors such as cellular microenvironment and substrate availability, may contribute to TAZ-mediated CL remodelling [103]. In brain tissue, TAZ mRNA expression is among the lowest compared to all tissues [103]. This could explain why brain CL has the most

diverse acyl species compared to other tissues. However, the microenvironment of the brain is also unique in that it is rich in fatty acids such as arachidonic acid and docosahexaenoic acid. The diverse acyl species of CL in the brain could also be the result of the different acyl substrates available compared to other tissues like the heart and skeletal muscle.

As mentioned previously, TAZ is a transacylase that transfers acyl chains from a phospholipid to MLCL to produce CL. However, recent experiments conducted with the purified recombinant enzyme showed that TAZ reacts with a wide variety of phospholipids as well as their lysophospholipid analogs [104, 105]. The same studies found that TAZ does not distinguish between acyl groups in the *sn*-1 and *sn*-2 positions. These data indicate that TAZ does not have the acyl specificity necessary to remodel CL with specific acyl chains. Thus, how is it possible that CL incorporated in mitochondrial membranes is enriched in specific unsaturated fatty acids? It is important to keep in mind that even though *in vitro* work is able to demonstrate the functions of TAZ, it may not necessarily predict how this enzyme works *in vivo*. This is illustrated by an important characteristic of TAZ that may explain the documented acyl specificity of CL. Schlame *et al* observed that TAZ does not react with lipids in a bilayer formation [105]. Instead, TAZ appears to require significant positive or negative curvature of the lipid-water interface in order to perform its enzymatic function. This is a puzzling observation considering phospholipids of both the inner and outer mitochondrial membranes are predominantly found in bilayer formations with PC and PE making up the large majority (~75%) of lipids found in these membranes (reviewed in [15]). However, when you consider the lipid composition of the IMM as well as the molecular

characteristics of the lipids within it, TAZ's function begins to make a little more sense. As mentioned previously, CL is found in higher concentrations in the IMM making up about 15-20% of all lipids [14]. CL is described as a non-bilayer forming lipid favouring hexagonal formations due to its small polar head group and large hydrophobic tail giving it a conical shape (reviewed in [15]). This conical shape is one that is difficult to pack into an otherwise compact lipid bilayer composed primarily of PC (~40-50% of all mitochondrial lipids) which, thanks to its tubular/cylindrical shape, organizes itself into planar bilayers in an aqueous environment (reviewed in [15]). PE on the other hand, also makes up a large portion of all mitochondrial phospholipids (~30%) and is found in slightly higher amounts in the IMM [14], but due to its molecular structure (small ethanolamine head group relative to its hydrophobic tail), is a non-bilayer lipid. Like CL, PE has a conical shape that favours hexagonal formations and can exert negative curvature on lipid membranes. Due to the presence of extensive curvature on the cristae of the IMM, it is not surprising that both PE and CL are found in such great quantities at this location. The findings by Schlame *et al* [106] indicating that TAZ does not interact with lipid bilayers can potentially explain the relative specificity of TAZ for CL. Since CL is a non-bilayer lipid, this may facilitate its interactions with TAZ while simultaneously minimizing other TAZ-lipid interactions [106].

9) Barth Syndrome - Current Knowledge

Studies have confirmed that TAZ is involved in the metabolism of CL by remodelling its acyl chains to contain specific fatty acids [107, 108]. TAZ gene mutations result in dysfunctional CL remodelling and ultimately the development of

BTHS (OMIM 302060). The only known disease that is exclusively associated with dysfunctional CL remodelling is BTHS [108]. Despite the fact that over 100 TAZ gene mutations have been identified [109], there is no correlation between the genotype and phenotype of this disease [110]. The prevalence of BTHS is reported to be 1 in every 300,000 - 400,000 births in the United States (reviewed in [111]). However, the world wide prevalence of BTHS is unknown. This is due, in part, to the unpredictable display of symptoms by patients. BTHS patients may experience sudden cardiac deterioration followed by unexplained remission [112]. Not only does this make it difficult to report the disease incidence, but also makes diagnosis and treatment challenging. Current methods used to diagnose BTHS include: quantification of 3-methylglutaconic acid (3-MGA), cardiolipin analysis (e.g. in platelets, muscle), *TAZ* gene sequencing and echocardiograms [113]. One of the most effective and least intrusive methods to diagnose BTHS is the bloodspot assay. This assay can determine the MLCL:CL ratio in bloodspots [114]. Patients with BTHS are unable to acylate MLCL to form CL, leading to elevated levels of MLCL which can be detected by the bloodspot assay. The most common symptoms of BTHS include various cardiomyopathies, neutropenia, skeletal myopathy, growth retardation and organic aciduria [1, 2]. The cardiomyopathies can include: isolated left ventricular non-compaction, ventricular arrhythmia and hypertrophic cardiomyopathy (reviewed in [115]). These symptoms can begin very early and can cause fetal cardiomyopathy, male fetal loss and stillbirth [115]. Neutropenia in BTHS patients is not only life threatening (due to the recurring bacterial infections), but is difficult to diagnose [116]. This due to the fact that some BTHS patients can experience chronic, cyclic and intermittent neutropenia, while others

experience no neutropenia at all [2]. Some advances have been made in our understanding of the mechanism of neutropenia in BTHS patients, but more work is still required to find new therapeutic strategies. Various studies have examined the bone marrow characteristics in neutropenia-associated disorders and all have shown that myeloid differentiation is blocked in these cells [117-120]. This could explain the significantly low levels of neutrophils observed in some BTHS patients. Another potential explanation for the observed neutropenia exhibited by BTHS patients could be an early clearance of neutrophils by macrophages. However, Kuijpers *et al* have demonstrated that BTHS neutrophils are not recognized by circulating macrophages, and thus, the neutropenia is not caused by early clearance [121]. Another possible explanation is that the neutropenia in BTHS patients may be due to increased mitochondrial-directed apoptosis in neutrophils. However, mitochondrial levels in neutrophils are actually quite low [116]. Myeloid progenitor cells, on the other hand, have significantly higher levels of mitochondria and studies focussed on neutropenia-associated disorders show that certain apoptotic markers are significantly elevated in these cells and ultimately lead to a reduction in circulating neutrophils [117, 122]. This could also be a potential mechanism taking place in BTHS patients causing neutropenia.

Many studies have been conducted in an attempt to better understand the sub-cellular and molecular mechanisms of BTHS and have lead to a better understanding of the disease. Xu *et al* used lymphoblasts from a number of BTHS patients to study the fatty acid composition of the major mitochondrial lipids including: PC, PE and CL [123]. The authors found that all three phospholipids were affected in BTHS patients, and as

expected, CL experienced the greatest changes. Stearic (18:0) and palmitic acid (16:0) were the most abundant acyl chains in CL from BTHS patients compared to controls which were rich in linoleic (18:2) and palmitoleic acid (16:1) [123]. In this study, the PE composition from BTHS patients was more or less normal. PC on the other hand, did experience some acyl changes leading the authors to conclude that fatty acid transfer between PC and CL was significantly affected in BTHS patients [123]. In addition, an examination of the mitochondria from BTHS patients using transmission electron microscopy revealed an increase in mitochondrial mass in these patients [123]. This could be an indication of a compensatory mechanism employed by BTHS cells to compensate for decreased CL levels and therefore decreased mitochondrial function. In a different study conducted by Acehan *et al,* electron microscopic tomography was used to study the internal three-dimensional organization of mitochondrial membranes in BTHS lymphoblasts and controls [124]. The images obtained revealed that BTHS lymphoblasts contained a greater mitochondrial volume compared to controls, however, individual mitochondrial size was more variable in BTHS cells. The mitochondria in these BTHS cells were also more fragmented with poorly formed cristae [124].

Currently, there is no cure for BTHS. Treatment options for BTHS patients may involve a combination of surgical procedures and pharmacological interventions. These can include heart transplants, granulocyte colony stimulating factor (G-CSF) administration, and treatment with drugs such as ACE inhibitors. However, there is currently no one treatment available that can treat this disease at a systemic level. A potential agent that may be used to treat BHTS is known as monolysocardiolipin

acyltransferase-1 (MLCL AT-1), an enzyme that has been shown to also be able to remodel CL with specific acyl species [18, 125].

10) Monolysocardiolipin Acyltransferase-1

MLCL AT-1 is a splice variant of the α-subunit of the mitochondrial Trifunctional Protein (αTFP) [126] and its gene is located on chromosome 2p23 [127]. MLCL AT-1 is a 59kDa protein that is identical to the 74kDa αTFP minus the first 227 amino acids (Fig.3) [18]. The MLCL AT-1 enzyme is located on the inner leaflet of the inner mitochondrial membrane where it is reported to remodel CL with specific acyl chains [18]. The mitochondrial Trifunctional Protein (TFP) is an enzyme complex localized in the IMM and functions by catalyzing three out of the four steps in the β-oxidation cycle [128]. This enzyme is a hetero-octamer composed of four α (αTFP) and four β-subunits (βTFP) [129, 130]. Previous studies conducted in rat heart and pig liver have shown that the CL in these tissues was rich in linoleic and oleic acid and that MLCL was rapidly reacylated to CL in an acyl-coenzyme A dependent manner [125, 131]. Using rat heart and radiolabelled fatty acids, Ma *et al* showed that unsaturated fatty acids were incorporated into CL via deacylation followed by reacylation [131]. This study also showed that *in vitro* mitochondrial acylation of MLCL to CL did not occur in the absence of coenzyme-A. In another study using pig liver, Taylor *et al* isolated a 74kDa protein that was able to catalyse the acylation of MLCL to CL using ^{14}C linoleoyl coenzyme A [125]. The isolated enzyme did not utilize other lysophospholipids (except for MLCL) as substrates for the formation of CL. This same study also used liver from thyroxine treated rats, and using a polyclonal antibody raised in rabbits to probe for the isolated

Figure 3: Alignment of αTFP and MLCL AT-1 peptide sequences.

Peptide sequence alignment of NP_000173 (human α trifunctional protein) and AAX93141 (unknown human protein - MLCL AT-1) using Constraint-based Multiple Alignment Tool (COBALT). MLCL AT-1 is a splice variant of NP_000173, missing the first 227 amino acids.

74kDa protein, it was found that the expression of the 74kDa protein was significantly higher compared to euthyroid controls. The authors concluded that the expression of monolysocardiolipin acyltransferase may be regulated by thyroid hormone. These studies have further demonstrated that CL remodelling is a necessary step following *de novo* CL biosynthesis and that other enzymes besides TAZ have the capability to perform this function. Why multiple enzymes exist to perform the same function is still unknown, but another study conducted by Danos *et al* began to shed some light on this question. With the use of H9c2 cardiac myoblast cells, Danos *et al* showed that incubating these cells with 2-deoxyglucose (2-DG) lead to increases in cleaved caspase-3 and poly(ADP-ribose) polymerase compared to untreated controls [132]. This was an indication that apoptosis was being induced in these cells. However, CL pool sizes and fatty acid compositions did not differ between 2-DG treated cells and controls. Expression of the remodelling enzyme TAZ also remained unaltered between controls and 2-DG treated cells. In addition, mitochondrial phospholipase A2 and monolysocardiolipin acyltransferase activity was significantly elevated in 2-DG treated cells compared to controls. The authors hypothesized that the monolysocardiolipin acyltransferase enzyme may play a compensatory role that allows cells to maintain their CL pool size under situations of cellular duress [132]. In 2009, Taylor *et al* were able to identify a previously uncharacterized protein that utilized unsaturated fatty acids for the acylation of MLCL to CL and named it MLCL AT-1 [18]. Using pig liver mitochondria and matrix-assisted laser desorption ionization time-of-flight mass spectrometry analysis followed by searches on the Mascot protein database, a peptide match consistent with a 59kDa protein was found. This previously unknown protein (with a GenBank™ protein

accession number of AAX93141) was purified as mentioned in [18], and showed that it could acylate MLCL to produce CL using linoleoyl coenzyme A > oleoyl coenzyme A > and palmitoyl coenzyme A [18]. By transfecting HeLa cells with an *MLCL AT-1* plasmid, Taylor *et al* showed that they could increase MLCL AT-1 enzyme activity and incorporation of ^{14}C linoleic acid into CL. This study also demonstrated that MLCL AT-1 could be used to elevate MLCL AT-1 enzyme activity, remodelling of CL with linoleic acid and CL mass in BTHS lymphoblasts [18]. However, the specific role that MLCL AT-1 plays in organisms is currently unknown. Our current studies demonstrate that MLCL AT-1 expression may be dependent on TAZ expression. In addition, MLCL AT-1 can be manipulated in BTHS cells to improve various aspects of the disease.

Objectives

For this project our objectives were as follows: 1) to determine if a relationship exists between TAZ and MLCL AT-1, 2) to determine if MLCL AT-1 expression in BTHS lymphoblasts leads to improvements in mitochondrial function, and 3) to use the *Taz* KD mouse model to get a better understanding of the phenotypes displayed by BTHS patients.

Materials and Experimental Methods

1) Materials

Epstein-Barr virus transformed lymphoblasts (identifier 3798) were obtained from the Coriell Institute for Medical Research (Camden, NJ, USA). BTHS lymphoblasts

(patient 618) were generously donated by Dr. Richard Kelly (John Hopkins University). Transgenic mice were obtained from the Jackson Laboratory (Bar Harbour, ME, USA). Rodent chow was obtained from Harlan Laboratories (Mississauga, ON, Canada). RPMI 1640 media, OptiMEM, stealth RNAi and other cell culture components and supplements were ordered from Life Technologies Inc. (Burlington, ON, Canada). RNAprotect® Reagent, RNeasy® Plus Mini Kit and Qiashredder homogenizer columns, QuantiTect® Probe RT PCR Kit and other RT-PCR components were obtained from Qiagen® (Cambridge, MA, USA). Primers used for RT PCR detection were ordered from Invitrogen (Burlington, ON, USA). Antibodies used for western blot analysis were obtained from Abcam (Cambridge, MA, USA) and Santa Cruz Biotechnology Inc. (Dallas, TX, USA). Other western blot components were obtained from Bio Rad (Mississauga, ON, Canada) and GE Healthcare Life Sciences (Mississauga, ON, Canada). Radiolabels were obtained from Perkin Elmer (Boston, MA, USA). Ecolite scintillant was obtained from ICN Biochemicals (Montreal, QC, Canada). Lipid standards were obtained from Serdary Research Laboratories (Englewoods Cliff, NJ, USA). Thin-layer chromatographic plates (silica gel G, 0.25mm thickness) were obtained from Merk (Darmstadt, Germany). BN-PAGE components and reagents were obtained from Invitrogen (Burlington, ON, Canada) and Sigma-Aldrich (St. Louis, MO, USA). Mitochondrial stress test and glycolytic analysis components were obtained from Seahorse Bioscience (North Billerica, MA, USA). MitoSOX and Amplex UltraRed Molecular Probes were obtained from Invitrogen (Burlington, ON, USA). All other biochemical agents, components and drugs were ASC grade and were obtained from either Sigma-Aldrich (St. Louis, MO) or Thermo Fisher Scientific (Carlsbad, CA).

2) Cell Culture

Experiments were conducted using Epstein-Barr virus transformed lymphoblasts that were obtained from the Coriell Institute for Medical Research (Camden, NJ, USA). These control cells were age-matched to Epstein-Barr virus transformed BTHS lymphoblasts (patient 618) that were generously donated by Dr. Richard Kelly (John Hopkins University). Please refer to Table 1 for cell line details. These lymphoblasts were grown in RPMI—1640 medium containing 10% FBS and 1% A/A (GIBCO) at 37 ^{o}C and 5% CO_2 in a Thermoscientific Steri-cycle CO_2 incubator HEPA Class 200. Cell media was changed every 48 h and the cells were passaged every five days.

Table 1

Healthy and BTHS lymphoblast information.

Cell Line (Identifier)	Phenotype	Age of Diagnosis	Age at Cell Harvest (years)	Tafazzin Mutation
3798	Healthy Control	-	10	none
618	BTHS	5 months	9	Exon 2, c. 171 del. A (frameshift)

3) Doxycycline-inducible *Taz* knockdown mouse model

Taz knockdown (KD) mice were generated by mating transgenic mice (B6.Cg-Gt(ROSA)26Sortm1(H1/tetO-RNAi:Taz,CAG-tetR)Bsf/ZkhuJ, Jackson Laboratory, Bar Harbour, ME, USA) containing doxycycline (dox) inducible tafazzin specific short-hair-pin RNA (shRNA) with female C57BL/6J mice (Jackson Laboratory, Bar Harbour, ME, USA). *Taz* KD was induced *in utero* and was maintained postnatally by administering dox (625 mg of dox/kg of chow) as part of the standard low-fat 6% (w/w) fat rodent chow (Harlan, Rodent diet cat.#: TD.01306) as previously described [133]. Female C57BL/6J mice consumed the dox diet (TD.01306) for at least 4 days prior to breeding. A low-fat diet lacking dox was used during the 4 day mating period to prevent knock-down of tafazzin in the transgenic males. The dams were then returned to the dox diet (TD.01306) for their entire pregnancy, birth and suckling period. Only male offspring were used experimentally and were weaned at 3 weeks of age onto the low-fat (6%, w/w) (Harlan, Rodent diet cat# TD.01306) dox-containing diet (625 mg/kg). Male mice positive for the tafazzin shRNA transgene were identified by PCR as described previously [133]. Male transgenic mice not treated with dox served as controls. (Cole L.K., unpublished data)

4) Cell Transfection

Lymphoblasts were transfected via electroporation with a BTX Electroporation System Manipulator 600 at 250V for 15-20 milli seconds. To 5 X 10^6 cells, 2nmol of Stealth RNAi (Invitrogen) were added. To knock down *TAZ*, cells were transfected with

a *TAZ* RNAi sequence (scrambled sequence used as a negative control, Table 2). BTHS cells were transfected with either 20 µg of a MLCL AT-1-containing plasmid or with 20 µg of an empty vector (Fig.4). After transfection, cells were incubated in 5mL RPMI-1640 medium without the addition of FBS or A/A solution for 6 h at 37^{o}C and 5% CO_2. After 6 h, 15 mL of RPMI media with 10% FBS and 1% A/A solution were added to each sample and incubated at 37ºC and 5% CO_2 for an additional 42 h.

Table 2

RNAi sequences used.

Name	RNA Sequence
TAZ RNAi Control (sense)	CCUGAUCCGUUUCGGCAACACAGUA
TAZ RNAi Control (anti-sense)	UACUGUGUUGCCGAAACGGAUCAGG
TAZ RNAi (sense)	CCUACAGCUGCUUCUGGACCAAGUA
TAZ RNAi (anti-sense)	UACUUGGUCCAGAAGCAGCUGUAGG

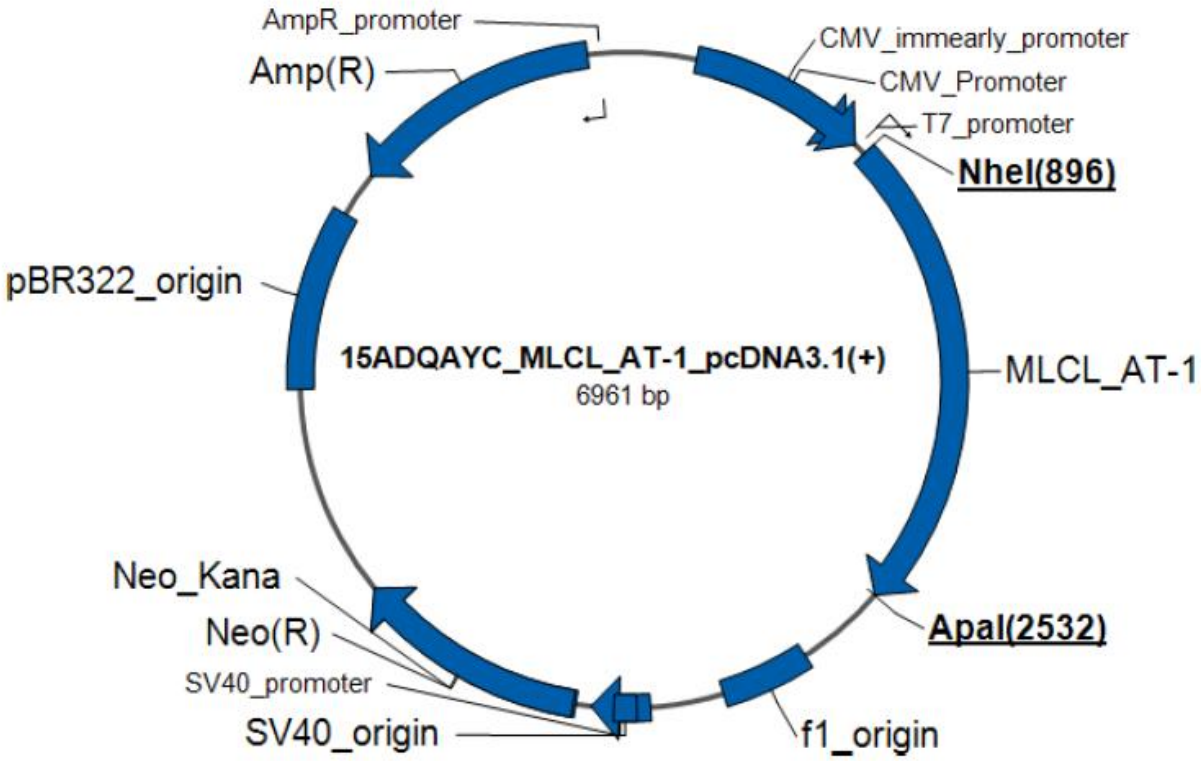

Figure 4: Synthetic MLCL AT-1 plasmid.

The MLCL AT-1 gene was incorporated into the vector backbone pcDNA3.1(+). The plasmid was transformed into and then purified from ampicillin-resistant *E. coli* bacteria. *Image obtained from Quality Assurance Documentation provided by Thermofisher Scientific.*

5) MLCL AT-1 Plasmid Preparation

The *MLCL AT-1* plasmid was prepared as described by Taylor *et al* [18]. Briefly, the primers for the MLCL AT-1 protein were amplified using 1 µg of HeLa cell RNA. The full-length cDNA sequences were incorporated into pcDNA 3.1(+) (Figure 4) using the TOPO cloning reaction (Invitrogen). Once the plasmid was constructed, it was transformed into E. coli One Shot® bacteria via a chemical reaction using S.O.C. media (Invitrogen) followed by inoculation into ampicillin-containing agar and allowed to grow over-night. The next day, colonies were isolated and inoculated into 5 mL of ampicillin-containing LB media and cultured at 37ºC in an orbital shaker set at 200 rpm over-night. Plasmid purification from E. coli was conducted using a Qiagen® Plasmid Midi Kit (cat.#: 12143) as described by the manufacturer's protocol. DNA sequencing (Manitoba Institute of Cell Biology) was used to verify the plasmid sequences.

6) Cell Harvesting

After the cells were transfected and grown at 37 ^{o}C and 5% CO_2 for 48 hours, they were pelleted (1400 rpm for 10 mins at room temperature) and washed twice with chilled phosphate buffered saline (PBS).

7) RNA Isolation & Relative Gene Expression

RNA was isolated from healthy and BTHS lymphoblasts using RNAprotect® Reagent, the RNeasy® Plus Mini Kit and Qiashredder homogenizer columns. To

stabilize the RNA, $1X10^7$ cultured cells (maximum amount used) were pelleted (as mentioned previously) and re-suspended in 1mL of RNAprotect® Reagent. This mixture was then vortexed for about 30 seconds to allow for cell re-suspension. The mixture was then stored at -80^oC until it was ready for use. To begin RNA isolation, the cells in RNAprotect® Reagent were thawed and then centrifuged at 9000 X g for 5 mins. The supernatant was then discarded and the cell pellet was re-suspended in 600 µL of buffer RLT Plus. This mixture was vortexed for at least 30 seconds to re-suspend the pellet (additional mixing by pipetting was sometimes necessary). The entire volume was then transferred to a QIAshredder placed in a 2 mL collection tube followed by centrifugation at 9000 X g for 2 mins. This step was performed in order to homogenize the cell lysate. The resulting volume was then transferred to a gDNA eliminator spin column placed in a 2 mL collection tube and centrifuged for 30 seconds at 9000 X g. To the solution/flow through in the 2 mL collection tube, 600 µL of 70% ethanol was added and mixed well by pipetting. A maximum of 700 µL was then transferred to an RNeasy spin column placed in a 2 mL collection tube and centrifuged for 30 seconds at 9000 X g. The flow-through was discarded and the spin column was re-used for successive aliquots of the corresponding samples (since each sample volume exceeded 700 µL). To the RNeasy spin column placed in a 2 mL collection tube, 700 µL of buffer RW1 was added and centrifuged for 30 seconds at 9000 X g. The flow-through was discarded and to the RNeasy spin column in a 2 mL collection tube, 500 µL of buffer RPE was added to wash the spin column membrane (please note that four volumes of 96-100% ethanol must be added to buffer RPE before use). This was followed by a 30 second centrifugation step at 9000 X g. The flow-through was again discarded and to the

RNeasy spin column in a 2 mL collection tube, 500 µL of buffer RPE was added and was centrifuged for 2 mins at 9000 X g for a final wash of the spin column membrane. The RNeasy spin column was then placed in a new 1.5 mL collection tube and 30-50 µL of RNase-free water was added to the spin column followed by centrifugation for 1 min at 9000 X g. The RNA in the collected eluate was then quantified (UV spectroscopy), aliquoted and stored at -80^{o}C for future use. The absorbance of the RNA sample was measured at 260 and 280 nm (an A260 reading = 1.0 is equivalent to 40 µg/mL was assumed). One-step PCR was performed using the QuantiTect® Probe RT PCR Kit (please see Table 3 for list of primers) and the double stranded DNA stain SYBR green as indicated by the manufacturer. Final primer concentration was 0.4 µM and final RNA template concentration was 8.0 ng/µL in a reaction mixture volume of 25 µL. Relative gene expression analysis was performed using a Master Cycler ep Realplex system. Relative gene expression was calculated using the $2^{-\Delta\Delta Ct}$ method as described in [134].

Table 3

Primers used for RT PCR (gene detection).

Primer Name	Primer Sequence
TAZ Forward (human)	GCAGACATCTGCTTCACCAA
TAZ Reverse (human)	TCTGGTAGACGCCATCTCCT
Taz Forward (mouse)	CCATGGAATTCGAACGCTGACGTC
Taz Reverse (mouse)	TATGGGCTATGAACTAATGACCC
MLCL AT-1 Forward	GAAGTCATCCGAATCCTCCA
MLCL AT-1 Reverse	TTTCGCTACATCCACACCAA
18S Forward	AAACGGCTACCACATCCAAG
18S Reverse	CCTCCAATGGATCCTCGTTA

8) Lipid Mass Spectrometry

CL mass and fatty acyl molecular species and tri-linoleoyl MLCL (L_3-MLCL) mass were quantified using electrospray ionization - mass spectrometry (ESI-MS) coupled to high performance liquid chromatography (HPLC) as previously described [135].

9) Lipid Isolation and Sensitive Lipid Phosphorous Assay

Transfected cells were harvested as described above and the cell pellet was re-suspended in 2mL of a 1:1 DDH_2O and methanol solution. The re-suspended samples were placed in dimethyldichlorosilane-coated test tubes. Next, 500 µL of 0.9% NaCl (saline solution) and 250 µL of butanol were added to each sample, followed by the addition of 2 mL of chloroform. The samples were then vortexed and allowed to sit at room temperature for 15-20 mins. Samples were then centrifuged at 2000 rpm for 10 mins. This resulted in the separation of the aqueous and organic layer, the latter (bottom layer) is carefully placed in a new dimethyldichlorosilane-coated test tube. To the organic layer, 3 mL of theoretic upper phase (TUP) solution is added (49% methanol, 48% saline solution and 3% chloroform) and vortexed. Samples were centrifuged at 2000 rpm for 10 mins at RT. Once separation was achieved, the top aqueous layer was aspirated and discarded, leaving behind the bottom organic layer. Samples were then dried down using N_2. Dried samples were re-suspended in ~25 µL of chloroform and spotted onto a 0.4M Borate-coated silica thin-layer chromatography (TLC) plate (uncoated plates obtained from Merk) using a 50 µL glass syringe. The first dimension of the Two-dimensional TLC involved placing the spotted plates in a chamber

containing the solvent system made up of 67% chloroform, 28.1% methanol, 2% ammonium hydroxide and 2.9% DDH_2O for 1.5 h. The plates were then taken out and allowed to dry in a fume hood for about 15 mins before being placed in an oven at 60ºC for 1hr. After this time, the plates were taken out and allowed to cool for 15mins before being placed in the second dimension for 20 mins (plates were turned 90º counter clockwise relative to original spotting corner). The second dimension solvent system consisted of 62% chloroform, 33.3% methanol and 4.7% DDH_2O. After the second dimension step, the plates were allowed to dry in a fume hood for about 15 mins. To visualize the separated lipids, the plates were inserted into an iodine chamber and exposed to the vapours for about 5 mins. The CL could now be visualized (light brown spot) and was isolated by carefully scraping the spot from the TLC plate and collecting the material. CL was quantified by performing a sensitive lipid phosphorous assay (described in [136]). Briefly, using sodium phosphate to make standards, a 1mM solution was made (in DDH_2O) and incremental volumes (0, 1, 2.5, 5, 10, 25, 50 µL) were placed in respective 13X100mm glass test tubes. The standards were placed in a heat block at 180ºC in a fume hood until they were dry. Next, 500 µL of 70% perchloric acid was added to all standards and collected samples and heated for 1.5 h in a fume hood. After this time, the standards and samples were allowed to cool for 10 mins before the addition of 2.5 mL of DDH_2O to each tube. To each tube, 500 µL of a 2.5% ammonium molybdate solution (in DDH_2O) was added and vortexed immediately. Then, 500 µL of a 10% ascorbic acid solution (in DDH_2O) was added to each tube and vortexed immediately. All tubes were then placed in 95ºC water for 15 mins. After a 10min cooling period, all tubes were centrifuged at 2000 rpm for 10 mins. The

absorbance of the resulting supernatant was then measured at 820nm using a Gen5 plate reader.

10) Radiolabelling Studies (using ^{14}C Linoleic Acid)

Healthy and BTHS lymphoblasts were transfected as described above with one alteration. The FBS typically used to supplement the RPMI media was replaced with delipidated FBS. The purpose of this alteration was to minimize the effects of other lipids present in FBS and study the use of linoleic acid by the lymphoblasts in this experiment. After 24 h, the cells were incubated with 1µCi of ^{14}C linoleic acid bound to bovine serum albumin in 1:1 molar ratio (to facilitate entry into cells) for an additional 24 h. After this time, the cells were harvested, the lipids were extracted and then separated via 2D TLC as described above. CL (along with other phospholipids such as PC, PE, phosphatidylinositol (PI), and phosphatidylserine (PS)) was isolated from TLC plates, placed in a scintillation vial containing 5 mL of Ecolite scintillant and the incorporation of ^{14}C linoleic acid into CL was measured using a Beckman LS 6500 liquid scintillation counter. Results were reported as a % of ^{14}C linoleic acid incorporated into CL.

11) Mitochondrial Isolation for BN-PAGE

Cellular mitochondrial fractions were isolated using commercial ABCAM Kit (cat.#: ab110170) as described in the kit's protocol with some minor alterations. This kit was chosen due to its ability to isolate intact mitochondria using reagents that are

compatible with BN-PAGE work. All isolations were performed at 4^{o}C. Cultured cells were initially harvested as mentioned previously. The washed and pelleted cells (10-15 mg) were frozen at -80^{o}C for 1.5 h to weaken their plasma membrane. The frozen cell pellets were then allowed to thaw and were then re-suspended in 1 mL of Reagent A. The re-suspended cells were incubated on ice for 10 mins. The cells were then transferred to a 2 mL borosilicate glass douncer (chilled on ice prior to use) and were homogenized using 30 strokes from a polytetrafluoroethylene (PTFE) pestle with a stainless steel rod. To ensure that at least 50% of the cells were ruptured, an aliquot of the homogenized cells was stained with trypan blue (0.4%) and then observed under a phase contrast microscope. The homogenate was then centrifuged at 1000 X g for 10 mins at 4^{o}C. The resulting supernatant (SN # 1) was transferred to a 2 mL eppendorf tube while the pellet was re-suspended in 1ml Reagent B. The homogenization and centrifugation steps were repeated with the re-suspended pellet, and the resulting supernatant (SN # 2) was mixed with SN # 1. The SN # 1 and SN # 2 mixture was centrifuged at 12000 X g for 15 mins at 4^{o}C. The supernatant was discarded while the mitochondrial pellet was re-suspended in 80-100 µL of Reagent C supplemented with protease inhibitors. The mitochondrial protein concentration was determined via the Bradford method [137].

Mitochondria were isolated from tissue using commercial Sigma kit (cat.#: MITOISO1) as described in the kit's protocol with some minor alterations. All mitochondrial isolations were conducted at 4^{o}C and only freshly harvested tissues were used. Mitochondria isolated from liver required the use of Extraction Buffer A, an isotonic solution that prevents mitochondrial swelling. Mitochondria isolated from heart

or skeletal muscle required the use of Extraction Buffer B, an ionic solution that prevents the homogenate from becoming gelatinous. Freshly harvested tissue was washed twice with 2 volumes of 1X Extraction Buffer (A for liver, B for heart or skeletal muscle) and was then cut into 50-100 mg pieces which were placed on a cooled glass or plastic surface where it was further cut into smaller portions. The tissue sample was transferred to an eppendorf tube and re-suspended in 10 volumes of 1X Extraction Buffer (A containing 2mg/mL albumin for liver, B containing 0.25 mg/mL trypsin). For heart and skeletal muscle tissue, a 3 min incubation on ice was required followed by centrifugation at 1000 X g for 15 seconds. The supernatant was discarded and the heart or skeletal muscle was re-suspended in 8 volumes of 1X Extraction Buffer B containing 0.25 mg/mL trypsin and incubated on ice for 20 mins. An albumin solution (Sigma cat.#: A0474) was added to the heart or skeletal muscle solution to a final concentration of 10 mg/mL to quench the proteolytic reaction and mixed well by vortexing. The heart or skeletal muscle sample was centrifuged at 1000 X g for 15 seconds and the supernatant was discarded. The pellet was washed by adding 8 volumes of 1 X Extraction Buffer B and centrifuging at 1000 X g for 15 seconds (this step was repeated twice). Liver, heart or skeletal muscle samples were then transferred to a 2 mL borosilicate glass douncer (chilled on ice prior to use) and were homogenized using a PTFE pestle with a stainless steel rod. For liver, 10-15 strokes were sufficient, while heart and skeletal muscle required 30 strokes. The homogenized samples were transferred to 2 mL eppendorf tubes and centrifuged at 600 X g for 10 mins. The supernatant was placed in a new 2 mL eppendorf tube and centrifuged at 11000 X g for 15 mins. The supernatant for liver samples had to undergo the low and high spin steps

a second time. Once the mitochondrial pellet was isolated, it was re-suspended in 40 µL of 1X storage buffer and was assayed for protein concentration using the Bradford assay.

12) BN-PAGE

Once cellular mitochondria were obtained, 100 µg were treated with 50 µL of sample buffer (Invitrogen, cat.#: BN2003) containing 0.2% n-dodecyl β-D-maltoside (DDM, Invitrogen cat.#: BN2005) and placed on ice for 15 minutes. For mitochondria isolated from tissue samples, 50 µg were treated with 50 µL of sample buffer containing 1% digitonin (Invitrogen cat.#: BN2006) and placed on ice for 15 mins. The samples were then centrifuged at 20,000 x g for 30 mins at 4^{o}C. The supernatant, or mitochondrial membrane fraction (MMF), was collected and stored at -80 ^{o}C. To perform the BN-PAGE, 1 µL of Coomassie® G-250 additive (charge shift molecule) was added to 20 µL of MMF and the mixture was then placed into each well of a 3-12% gradient acrylamide bisacrylamide gel (Invitrogen cat.#: BN2011BX10). To perform the electrophoresis, 1X running buffer (50 mM BisTris, 50 mM Tricine, pH = 6.8) was used for the outer chamber (600 mL) of the XCell™ Surelock™ Mini-Cell , and either the dark blue cathode buffer (1X running buffer with 0.02% Coomassie® G-250) or light cathode buffer (1X running buffer with 0.002% G-250) was added to the inner chamber (200 mL). The gel was run at 150 V for 1.5 hours, then at 250 V for the last 30 mins (electrophoresis performed at 4ºC). If performing western blots or in-gel activity assays, then the gel is run as previously described. However, after the dye front has migrated to 1/3 of the gel, the run is paused and the dark cathode buffer is replaced with 200 mL

of pre-chilled light cathode buffer and the run is then continued. Coomassie-stained gels (dark cathode buffer used throughout the entire run) had to undergo a fixing and destaining step to be able to visualize proteins. Immediately after the electrophoresis run, the gel was fixed by submerging it in a 40% methanol and 10% acetic acid solution (in a glass container with a lid) and heated using a microwave (medium heat) for 45 seconds. The gel was then placed in a rocker for 15 mins with the lid covering the container. After this time the fixing solution was replaced by a destaining solution (8% acetic acid) and the gel was placed on a rocker for at least 2 h (an overnight incubation was sometimes required to visualize the proteins on the gel). Images were captured using a ChemiDoc™ MP imaging system using a white light conversion screen.

13) In-gel activity assays (complexes I, II and IV)

To detect complex I activity, BN PAGE was performed as described previously. After electrophoresis, the gel was submerged in a solution containing 5 mM Tris (pH = 7.4), 0.3 mM β-Nicotinamide adenine dinucleotide and 0.1 mM nitrotetrazolium blue (NTB) and placed in a rocker at room temperature (RT) for 2 hours. To stop the reaction, the gel was washed twice with DDH_2O and was then placed in 60 mL of fixing solution (40% methanol, 10% acetic acid) for 15 mins. This process also helps remove some of the residual coomassie stain that remains after running the gel. After 15 mins, the gel is then placed in a de-stain solution (8% acetic acid) for about 1 hour. To detect complex II activity, following electrophoresis, the gel was submerged in a solution containing 2mM Tris (pH = 7.4), 20 mM sodium succinate, 0.2 mM phenazine methasulfate and 0.1 mM NTB. The gel was incubated for 1hr at RT and the reaction

was stopped as previously described. For complex IV detection, following electrophoresis, the gel was submerged in a solution containing 50mM sodium phosphate (pH = 7.2), 0.5mg/mL 3, 3' - diaminobenzidine tetrahydrochloride hydrate, and 0.12mg/mL cytochrome c for 1hr at RT protected from light. The reaction was stopped as previously described. Images were captured using digital photography.

14) ROS (H_2O_2) measurement

Mitochondria were isolated from freshly excised heart, skeletal muscle and liver tissue using a commercial kit (Sigma-Aldrich). Levels of mitochondrial H_2O_2 were measured using 15-20 µg of mitochondrial protein per well (96-well plate) and the Amplex® UltraRed reagent (50 µM, Invitrogen) in a reaction buffer containing: 125 mM KCl, 4 mM KH_2PO_4, 14 mM NaCl, 20 mM HEPES, 1 mM $MgCl_2$, 0.020 mM EGTA, 0.2 % BSA, 5 mM Sodium succinate, 0.5 µM Antimycin A, 0.1 U/mL Horse Radish Peroxidase, pH 7.4 with KOH. Prepared plate was incubated at 37^{o}C (protected from light) for 20 mins and fluorescence was measured using a Gen5 microplate reader (wavelength settings: 530/590nm).

15) Immunoblotting (SDS PAGE)

Mitochondrial protein was isolated according to the Abcam manufacturer's protocol (ab110170). For SDS PAGE, mitochondrial protein was prepared as described above. To 15 µg of mitochondrial protein, an equal volume of 2X Laemmli buffer (BioRad cat.#: 1610737) supplemented with 5% 2-mercaptoethanol was added and mixed by pipetting.

The samples were boiled at 95 °C for five mins and then allowed to cool before centrifugation at 2000 rpm for 1 min. The entire volume was then loaded onto individual wells of a 4-15% polyacrylamide pre-cast gel (BioRad cat.#: 4561086) and electrophoresis was performed at 100V for 1 hour. This was followed by a wet transfer of proteins onto a polyvinylidene difluoride (PVDF) membrane performed at 100V for 1 hour at 4°C. The membrane was then blocked for 1 hour at room temperature using 5% Amersham ECL Prime blocking reagent (GE Healthcare cat.#: RPN418) in 0.5% tween-20/Tris-buffered saline (TBS-T). The membrane was then washed 3 times at 5 min intervals with TBS-T before an overnight incubation (4ºC) with the respective primary antibody in a blocking buffer solution of 3% BSA/TBS-T (please refer to Table 4 for antibody information list). The next day, the primary antibody solution was removed and the membrane was washed 3 times at 5 min intervals with TBS-T (room temperature). The membrane was then incubated in a secondary antibody blocking solution of 3% BSA/TBS-T for 1hr at room temperature (please refer to Table 4 for secondary antibody information). The secondary antibody solution was then removed and the membrane was washed with TBS-T 3 times at 10 min intervals. To develop the membrane for protein band visualization, ECL blocking agent (GE Health Care cat.#: RPN2125) was used as specified by the manufacturer's protocol. A ChemiDoc™ MP imaging system was used to visualize protein bands and capture images and the relative band intensities were determined using ImageJ software.

Table 4

Antibodies used for western blot analysis.

Primary antibody	Secondary antibody
Anti-Tafazzin (cat.#: ab105104. Abcam)	Goat anti-rabbit IgG-HRP (cat.#: sc-2004. Santa Cruz Biotech.)
Anti-HADHA (cat.#: ab137663. Abcam)	Goat anti-rabbit IgG-HRP (cat.#: sc-2004. Santa Cruz Biotech.)
Anti-VDAC1 (cat.#: ab15895. Abcam)	Goat anti-rabbit IgG-HRP (cat.#: sc-2004. Santa Cruz Biotech.)

16) MLCL AT-1 Enzyme Activity Assay

Enzyme activity assay performed as described in [125, 131]. Briefly, mitochondria from transfected healthy and BTHS lymphoblasts were isolated by first re-suspending cell pellets (10-15 mg) in 600 µL of a 10 mM Tris, 2 mM EDTA and 0.25 M sucrose buffer solution. The cells were then transferred to a 2 mL borosilicate glass douncer (chilled on ice prior to use) and were homogenized using 30 strokes from a PTFE pestle with a stainless steel rod. The samples were then centrifuged at 1500 rpm for 10 mins at 4ºC. The supernatant was then collected and centrifuged at 13000 rpm for 20 mins at 4ºC. The supernatant was discarded and the isolated mitochondrial pellet was re-suspended in 30 µL of the 10 mM Tris, 2 mM EDTA and 0.25 M sucrose buffer. Mitochondrial protein concentration was determined using the Bradford assay [137]. To perform the MLCL AT-1 enzyme activity assay, 10 µg of mitochondrial protein was placed in a solution containing 50 mM Tris-HCl buffer (pH = 8.0), 0.3 mM MLCL, [1-^{14}C]linoleoyl coenzyme A (120,000 dpm/nmol), made up to a volume of ~120 µL using DDH_2O. These substrates were placed in dimethylchlorosialine-coated glass test tubes and were then incubated at 37ºC for 1 hour. After the incubation period, the reaction was stopped by adding 3 mL of a 2:1 chloroform-methanol solution plus 800 µL of 0.9% KCl. After vortexing briefly, the tubes were centrifuged for 10 mins at 2000 rpm. The top layer was discarded and to the bottom layer, 2 mL of theoretical upper phase (TUP) solution (50% methanol, 47% of 0.9% NaCl and 3% chloroform) was added and vortexed briefly. The samples were then centrifuged for 10 mins at 2000 rpm. The resultant upper layer was discarded while the bottom layer (organic fraction) was dried down using N_2. The dried down lipid fraction was re-suspended in 25 µL of chloroform

and then spotted on a 0.4 M borate-coated TLC plate (obtained from Merck, silica gel coated glass) and two-dimensional TLC was performed as described previously. CL was visualized using iodine vapours and then scraped from the plate and placed in a scintillation vial containing 5 mL of Ecolite scintillant. The sample radioactivity (disintegrations per minute, or dpm) was measured using a Beckman LS 6500 liquid scintillation counter.

17) Cell-Tak XF-24 Plate Coating for Mitochondrial Function and Glycolysis Assays

Lymphoblasts are non-adherent cells that must be immobilized in order to perform mitochondrial and glycolytic function experiments using the XF 24 analyzer. Cell-Tak (Corning cat. #: 354240) is used to prepare an adherent monolayer of cells in each well of an XF 24 microplate. Cell-Tak is a non-immunogenic extracellular matrix protein that is isolated and prepared from *Mytilus edulis* (marine mussel) [138]. To coat the XF 24 microplates, Cell-Tak was first diluted in a 0.1M solution of sodium bicarbonate to a concentration of 22.4 µg/mL. To each of the 24 wells, 50 µL of the diluted Cell-Tak was added (1.12 µg per well) followed by a 20 min incubation period at room temperature. After 20 mins, the Cell-Tak was aspirated and the wells were rinsed once with 200 µL of UltraPure DNase/RNase-free water (ThermoFisher Scientific cat. #: 10977-023). The wells were allowed to dry for at least 10 mins prior to seeding cells.

18) Mitochondrial Function (Seahorse XF 24 Flux Analyser)

Transfected lymphoblasts were re-suspended in 1 mL of XF assay media (modified DMEM) containing 1 mM sodium pyruvate and 11 mM D-Glucose (media was warmed to 37^{o}C, pH = 7.4 and filter sterilized using a 0.22 µm filter before use). Cells were counted using a haematocytometer and were then diluted to achieve a concentration of 3000 cells/µL for healthy lymphoblasts and 2000 cells/µL for BTHS lymphoblasts. This difference is due to the difference in cell size that exists between healthy and BHTS lymphoblasts (which are about 35%-40% larger). Cell number optimization experiments demonstrated that these respective concentrations are necessary to achieve a monolayer of cells in each well of the XF analyzer plate. A volume of 100 µL of the diluted samples was added to corresponding wells of a Cell-Tak-coated XF analyser 24-well plate (Cell-Tak was diluted in a 0.1M solution of sodium bicarbonate to a concentration of 22.4 µg/mL and 1.12 µg per well was added) . The plate was centrifuged at room temperature for 10 mins at 1200 rpm and was then placed at 37^{o}C in a CO_2-free incubator for a maximum of 20 mins. During this incubation period an XF sensor cartridge, calibrated overnight at 37^{o}C (in a CO_2-free incubator), is loaded with oligomycin (port A = 75 µL of a 10 µM solution), FCCP (port B = 83 µL of a 10 µM solution) and Rotenone/Antimycin A (port C = 93 µL of 10 µM solution). The goal is to achieve a concentration of 1µM for each of the drugs in each plate well. Once loaded, the sensor cartridge is placed in the XF analyser and calibrated. After the incubation period, the plate wells are topped-off with 575 µL of the supplemented XF assay media and the plate is then placed in the XF 24 analyser.

19) Glycolytic Function

Cultured lymphoblasts were centrifuged at 1400 rpm for 10 mins to pellet the cells. The growth media was discarded and the cells were re-suspended in 1mL of XF assay media (unbuffered DMEM, 0mM glucose, warmed to 37^{o}C, pH = 7.35, filter sterilized using 0.22 µm filter) supplemented with L-glutamine (final concentration = 2 mM). The cells were seeded onto the XF microplate as described above and incubated at 37^{o}C in CO_2-free incubator for 1 hour. During this time, an XF sensor cartridge, calibrated overnight at 37^{o}C, is prepared by adding 80 µL of an 83 mM D-glucose solution to port A (final concentration per well = 10 mM). After the sensor cartridge calibration, the XF microplate with the seeded cells is loaded into the XF Analyzer. The rate of glycolysis was measured by detecting the change in extracellular acidification rate (ECAR) after injecting glucose into each well (final concentration = 10 mM).

22) Citrate synthase assay

Mitochondria were isolated from 3798 healthy and 618 BTHS lymphoblasts as described above (section 11 - 'Mitochondrial isolation for BN-PAGE', of the Materials and Experimental Methods section). Citrate synthase activity was measured using the citrate synthase assay kit (Sigma cat.#: CS0720) as described by the manufacturer's protocol. Briefly, 25 µg of mitochondrial protein from each sample were re-suspended in 200 µL of CellLytic M reagent. From the re-suspended mitochondrial samples, 8 µL were added to each well of a 96-well plate followed by 200 µL of the reaction mixture that was composed of 1X assay buffer, 30 mM acetyl CoA, 10 mM DTNB and 10 mM

oxaloacetic acid. Using a plate reader, absorbance was measured at 412 nm on a kinetic program and enzyme activity was calculated.

21) MitoSOX staining and detection by Flow Cytometry

For the detection of ROS, cells were incubated with 5 µM of the mitochondrial-specific superoxide indicator MitoSOX (obtained from Molecular Probes-ThermoFisher) as described in [139]. After a 20 min. incubation at 37ºC (protected from light), cells were washed twice with Hank's balanced salt solution containing calcium and magnesium (HBSS, Gibco cat. #: 14025-092), re-suspended in HBSS and then fluorescence was detected using a BD LSRII flow cytometer and the FACSDiva software (488nm excitation in the FL2 and FL3 channels). As a positive control, additional samples were incubated with MitoSOX plus 10 µL antimycin A (AA). AA is a known inducer of superoxide production.

Results

1) Lipid Mass Spectrometry

The fatty acyl molecular species of CL and MLCL was quantified in healthy (3798) and BTHS (618) lymphoblasts using ESI-MS coupled to HPLC as described in the Experimental Methods section. This experiment was conducted to detect any differences in the amount and types of CL and MLCL in healthy and BTHS lymphoblasts. A number of different CL and MLCL species were detected in both cell lines (see Table 5 for CL and MLCL species identification). Our results showed that all major CL species are found in significantly higher concentrations in 3798 healthy lymphoblasts compared to 618 BTHS cells (Fig.5 and Fig.6A). In addition, the major CL species found in lymphoblasts are the 1426 (16:1-18:1-18:1-18:2) and 1428 (16:1-18:1-18:1-18:1) species (Fig.6A). As predicted, the total CL pool was significantly lower in BTHS cells compared to healthy controls (Fig.7A). The total pool of MLCL was significantly higher in BTHS cells compared to healthy controls (Fig.7B), with the 1192 (18:1-18:1-18:1) species being the most abundant (Fig.6B).

Table 5

Major CL and MLCL species found in 3798 and 618 lymphoblasts.

m/z	Number of each fatty acyl substituent on individual CL molecular species							
	16:0	**16:1**	**18:0**	**18:1**	**18:2**	**18:3**	**20:4**	**22:6**
1422		1			3			
1424		1		1	2			
1426		1		2	1			
1428		1		3				
1448					4			
1450				1	3			
1452				2	2			
1454				3	1			
1456				4				
1472					3		1	
1474				1	2		1	
1476				2	1		1	
1478				3			1	
1496					3			1
1498				1	2			1
1500				2	1			1
1502				3				1

Monolysocardiolilpins

1186					3			
1188				1	2			
1190				2	1			
1192				3				

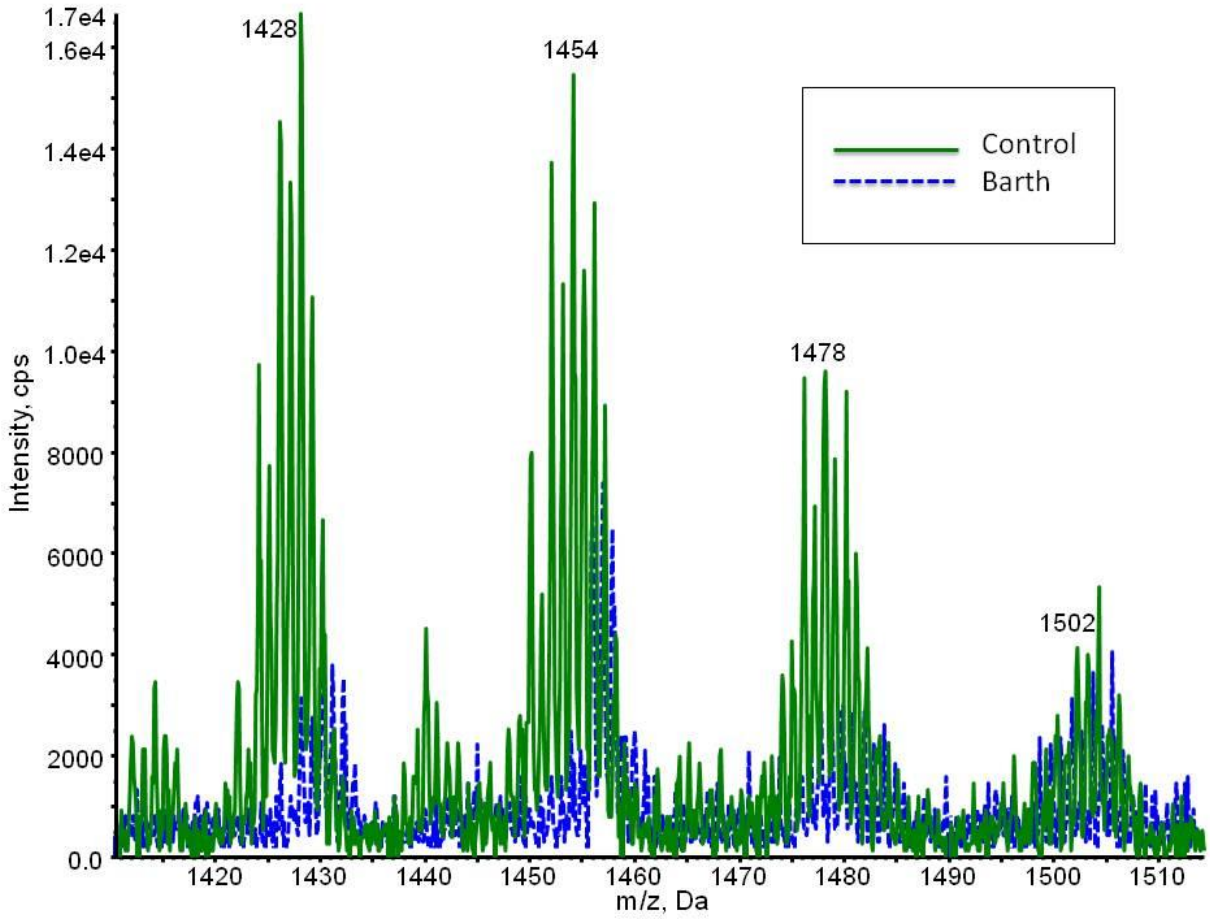

Figure 5: Comparison of the different CL fatty acyl molecular species between 3798 healthy and 618 BTHS lymphoblasts.

Representative chromatograph of the major CL species quantified using ESI-MS coupled with HPLC (as described in the Experimental Methods section) in 3798 healthy control and 618 BTHS lymphoblasts.

A.)

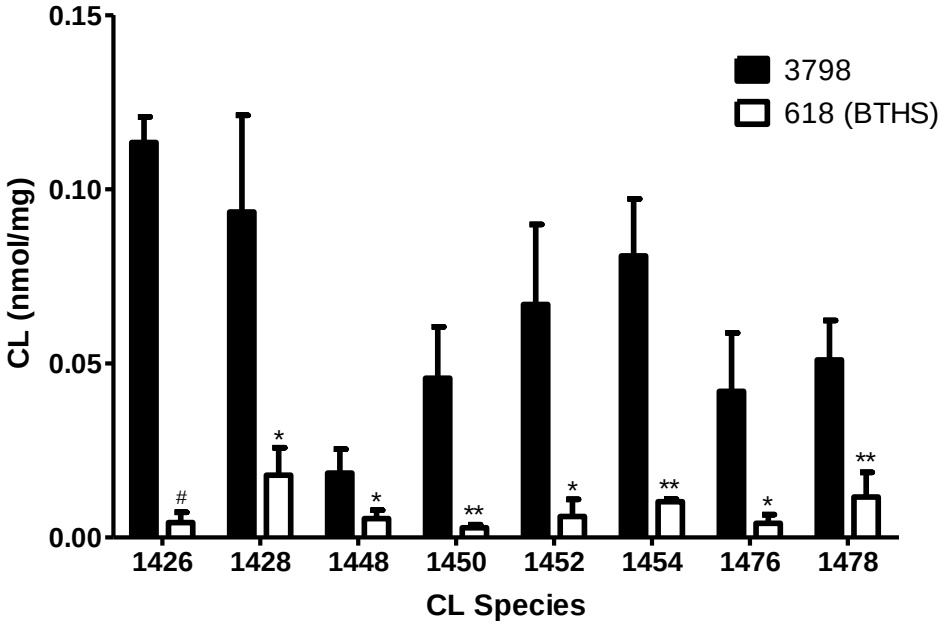

B.)

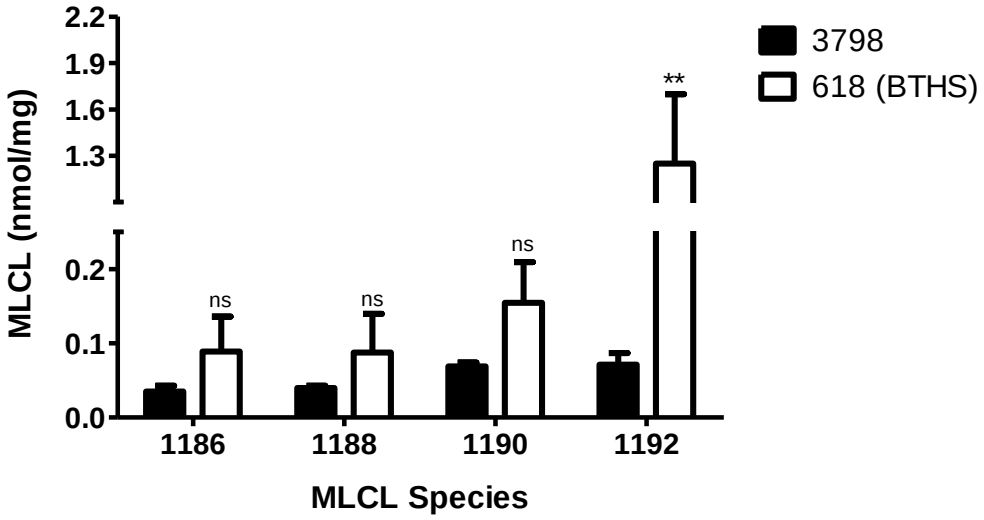

Figure 6: CL and MLCL fatty acyl molecular species found in 3798 healthy and 618 BTHS lymphoblasts.

Quantification of the major A.) CL and B.) MLCL fatty acyl molecular species in 3798 and 618 lymphoblasts (Data represent the mean ± SD, n = 3, #p<0.001, **p<0.01, *p<0.05, ns = not significant). Please refer to Table 5 for a description of the fatty acyl molecular species associated to the m/z.

A.)

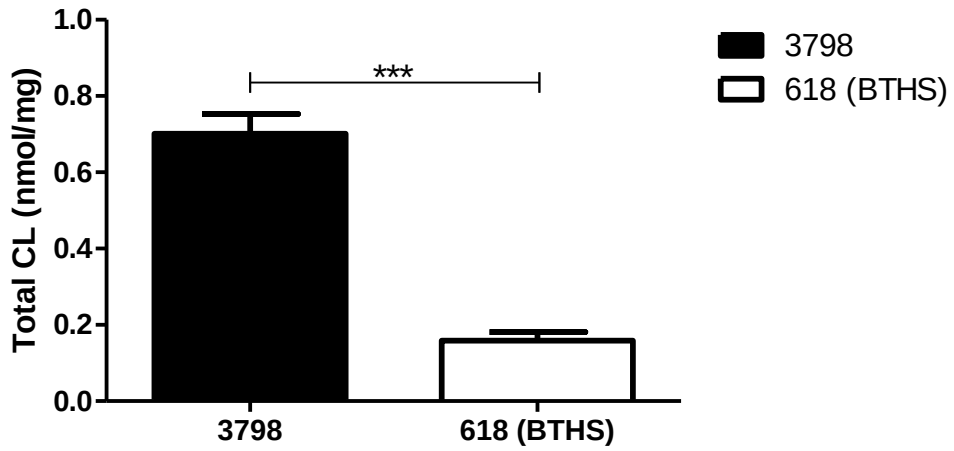

B.)

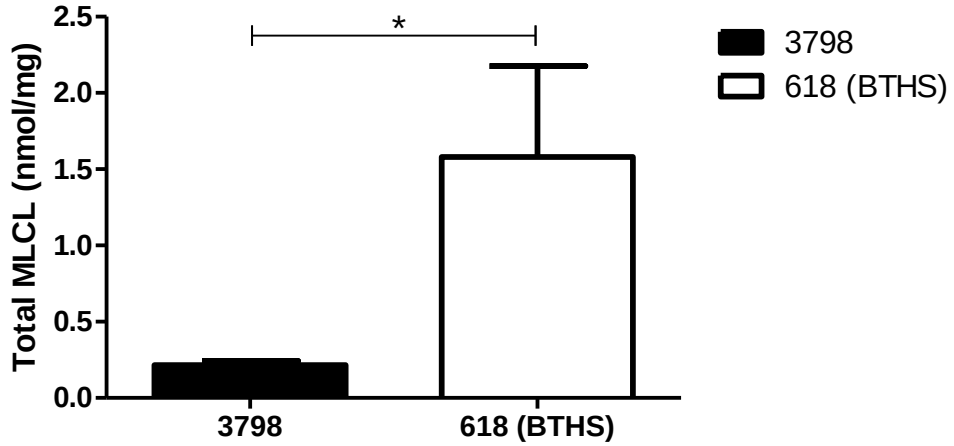

Figure 7: Measurement of the total CL and MLCL found in 3798 healthy and 618 BTHS lymphoblasts.

Quantification of the total pool of A.) CL and B.) MLCL from 3798 and 618 lymphoblasts using ESI-MS coupled with HPLC (data represent the mean ± SD, n = 3, ***p<0.001, *p<0.05)

2) *TAZ* and *MLCL AT-1* Gene Expression in Healthy and BTHS Lymphoblasts

To examine the relationship between TAZ and MLCL AT-1, the relative gene expression of both these genes was measured in healthy (3798) and BTHS (618) lymphoblasts using RT-PCR. KD of *TAZ* was performed in 3798 cells to determine if the various phenotypes exhibited by 618 cells were a direct result of *TAZ* reductions. *TAZ* KD in 3798 cells resulted in a 45% decrease in *TAZ* gene expression ($p<0.001$, Fig.8A), and conversely, an approximate 2-fold increase in *MLCL AT-1* gene expression ($p<0.05$, Fig.8B). A comparison of the *TAZ* gene expression between healthy and BTHS cells revealed a 50% reduction ($p<0.01$, Fig.8C). Surprisingly however, a comparison of the *MLCL AT-1* gene expression between healthy and BTHS cells revealed a 45% reduction in BTHS cells ($p<0.001$, Fig.8D). To determine if the BTHS phenotypes could be improved, *MLCL AT-1* was expressed in 618 cells. Expression of *MLCL AT-1* in BTHS cells resulted in a 2.5 fold increase in *MLCL AT-1* gene expression compared to mock transfected BTHS cells ($p<0.01$, Fig.8E).

A.)

B.)

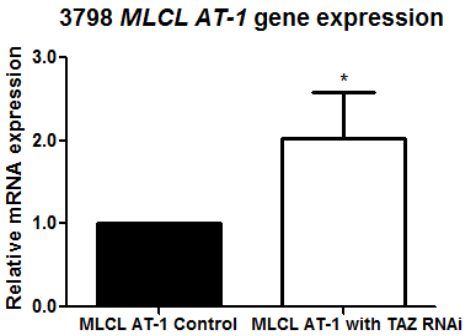

C.)

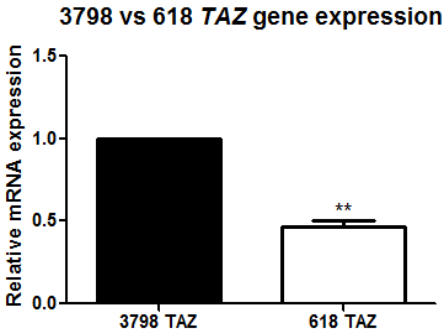

D.)

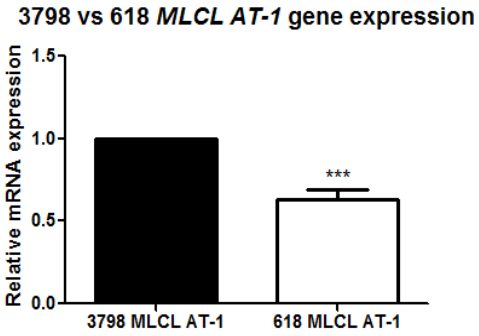

E.)

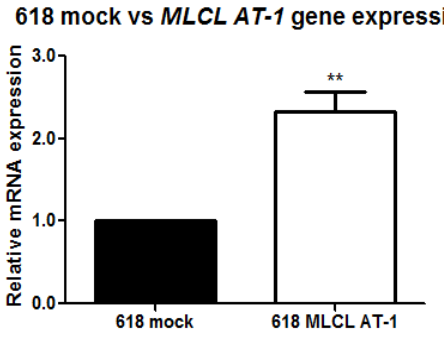

Figure 8: TAZ and MLCL AT-1 relative gene expression.

Relative gene expression measured via RT PCR. Data represent the specified mean ± SD. A) *TAZ* expression in 3798 cells with KD of *TAZ*, n = 4, ***p<0.001. B.) *MLCL AT-1* gene expression in 3798 cells with KD of *TAZ*, n = 4, *p<0.05. C.) 3798 vs 618 *TAZ* expression, n = 3, **p<0.01. D.) 3798 vs 618 *MLCL AT-1* expression, n = 4, ***p<0.001. E.) MLCL AT-1 expression in 618 cells expressing *MLCL AT-1*, n = 4, **p<0.01.

3) TAZ and MLCL AT-1 Protein Expression in Healthy and BTHS Cells

KD of *TAZ* in 3798 cells resulted in a corresponding 40% decrease in TAZ protein expression compared to controls observed via Western Blot analysis ($p<0.001$, Fig.9). As expected, BTHS cells expressed significantly lower levels of TAZ protein as demonstrated by our results showing a 90% decrease ($p<0.001$, Fig.9). *TAZ* KD in 3798 cells resulted in a significant 1.5 fold increase in MLCL AT-1 protein expression ($p<0.001$, Fig.10). In contrast, BTHS cells displayed an MLCL AT-1 protein expression that was significantly reduced (75% decrease, $p<0.001$, Fig.10). Expression of *MLCL AT-1* in BTHS cells resulted in a significant 3-fold increase in MLCL AT-1 protein expression (when using 20 µg of *MLCL AT-1* plasmid) compared to mock transfected (when using 20 µg of empty vector) cells (Fig.11A and B). Expression of various amounts of *MLCL AT-1* plasmid did not result in significant changes in αTFP expression compared to controls (Fig.11A and C).

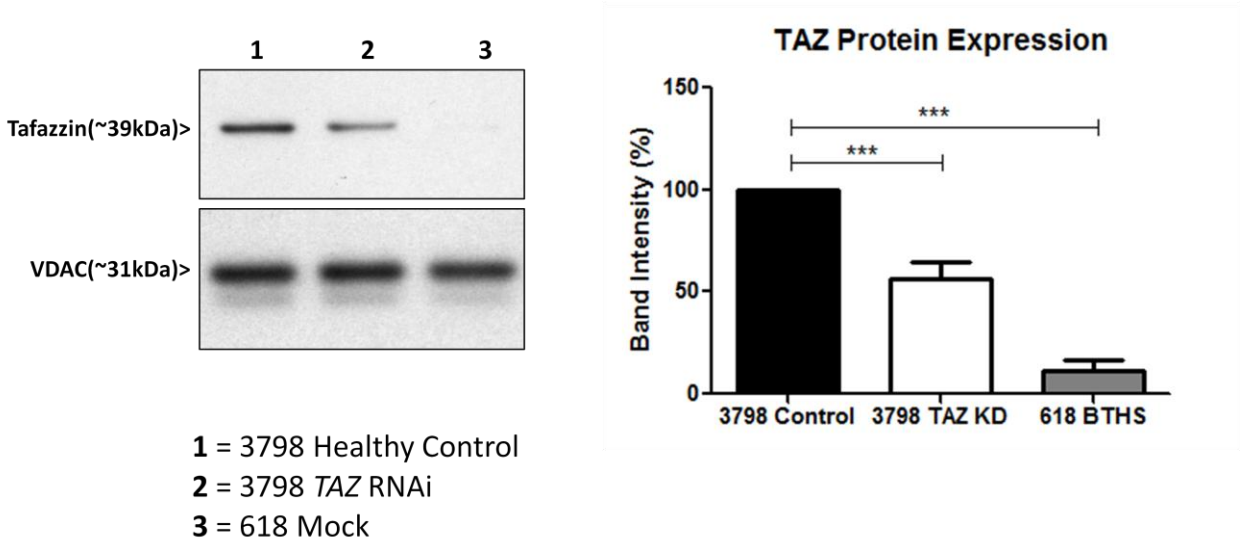

Figure 9: Detection of TAZ protein in isolated mitochondria from 3798 healthy and 618 BTHS lymphoblasts.

Mitochondria were isolated from our healthy and BTHS cell lines and TAZ protein was examined using western blot analysis. In addition, *TAZ* RNAi was used to knock down TAZ in healthy cells and TAZ protein expression was also examined (data represent means ± SD of n = 3, ***p<0.001, VDAC = voltage-dependent anion channel, used as loading control).

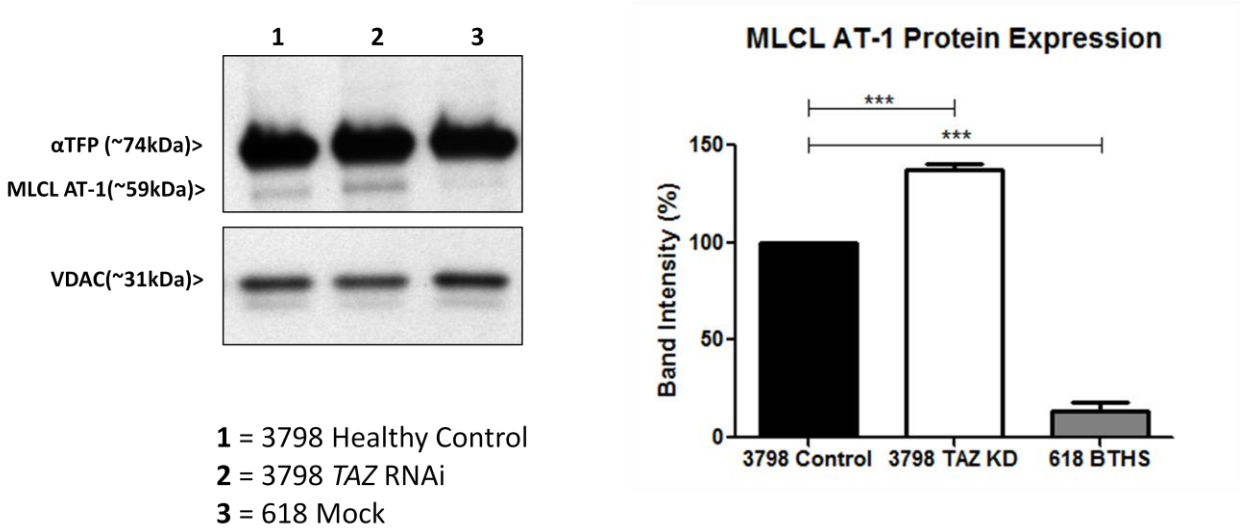

Figure 10: αTFP and MLCL AT-1 protein expression in isolated mitochondria from 3798 healthy and 618 BTHS lymphoblasts.

Using mitochondrial protein from 3798, 3798 with knock down of *TAZ* and 618 BTHS cells, αTFP and MLCL AT-1 protein expression was examined using western blot analysis (data represent mean ± SD of n = 3, ***p<0.001). VDAC = voltage-dependent anion channel, used as loading control.

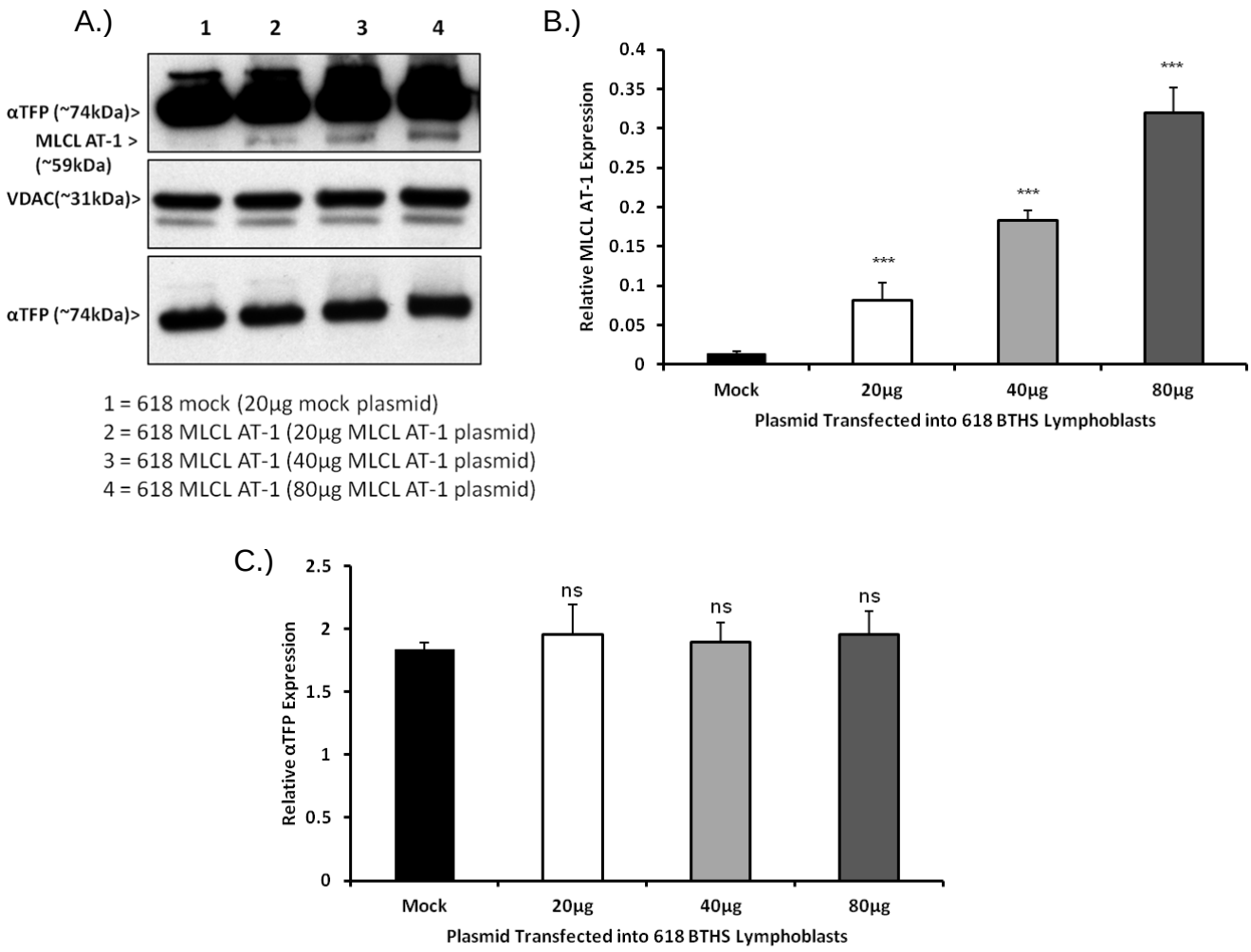

Figure 11: Increasing MLCL AT-1 protein expression in BTHS lymphoblasts.

The transfection of 618 BTHS cells with an MLCL AT-1-carrying plasmid results in the elevated expression of MLCL AT-1 protein (A and B), but not αTFP (A and C). The expression of MLCL AT-1 is directly proportional to the amount of plasmid transfected into cells. VDAC was used as a loading control. The blot showing MLCL AT-1 protein expression was subjected to longer exposure times compared to the αTFP blot in order to better visualize the MLCL AT-1 band (data represent mean ± SD of n = 3, ***$p<0.001$ compared to Mock, ns = not significant compared to Mock).

4) MLCL AT-1 Enzyme Activity is Elevated by Expression of *MLCL AT-1*

The enzymatic activity of MLCL AT-1 was measured in mitochondrial fractions of both 3798 (healthy) and 618 BTHS lymphoblasts under different experimental conditions. This experiment was conducted to test the correlation between MLCL AT-1 protein expression and enzyme activity. Figure 12 shows that *TAZ* KD in healthy (3798) lymphoblasts led to a significant 1.5-fold increase in MLCL AT-1 enzyme activity ($p<0.01$) compared to control. Co-transfection of 3798 lymphoblasts with *TAZ* RNAi and *MLCL AT-1* resulted in a significant 2.5-fold increase in MLCL AT-1 enzyme activity compared to control ($p<0.01$). MLCL AT-1 enzyme activity was significantly lower in BTHS cells compared to 3798 healthy cells ($p<0.05$, Fig.12). Expression of *MLCL AT-1* in BTHS lymphoblasts resulted in an approximate 2-fold increase in MLCL AT-1 enzyme activity compared to control ($p<0.001$, Fig.12). These results demonstrate that MLCL AT-1 enzyme activity can be increased via the expression of *MLCL AT-1* in control and BTHS lymphoblasts.

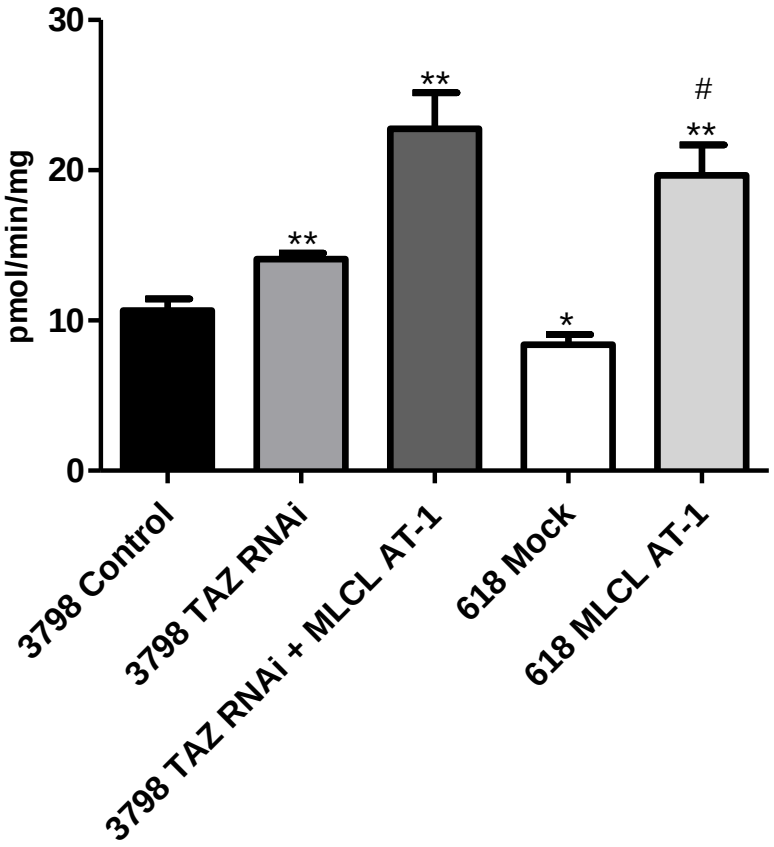

Figure 12: MLCL AT-1 enzyme activity detected in 3798 healthy and 618 BTHS lymphoblasts

Isolated mitochondria from 3798 control, 3798 *TAZ* RNAi, 3798 *TAZ* RNAi + MLCL AT-1, 618 mock and 618 expressing MLCL AT-1 cells were used to determine MLCL AT-1 enzyme activity using ^{14}C linoleoyl CoA as a substrate (data represent mean ± SD of n = 3, **p<0.01 compared to 3798 control, *p<0.05 compared to 3798 control, #p<0.001 compared to 618 mock).

5) Incorporation of ^{14}C Linoleic Acid Into CL is not Elevated by Expression of MLCL AT-1

Reports indicate that MLCL AT-1 preferentially incorporates linoleic acid into CL [18]. Therefore, healthy and BTHS cells were cultured for 24 h in the presence of ^{14}C linoleic acid and the incorporation of radiolabel into CL was determined. *TAZ* KD in healthy cells did not result in a significant change in ^{14}C linoleic acid incorporation into CL (Fig.13). In addition, no significant change was observed in healthy cells with a *TAZ* KD and expression of *MLCL AT-1* (Fig.13). The percent incorporation of ^{14}C linoleic acid into BTHS cells was significantly lower compared to control healthy cells (Fig.13). BTHS cells expressing *MLCL AT-1* did not exhibit a significant change in percent ^{14}C linoleic acid incorporation into CL compared to mock-transfected BTHS cells. Thus, BTHS cells expressing MLCL AT-1 still exhibited significantly lower levels of ^{14}C linoleic acid incorporation into CL compared to 3798 healthy controls (Fig.13).

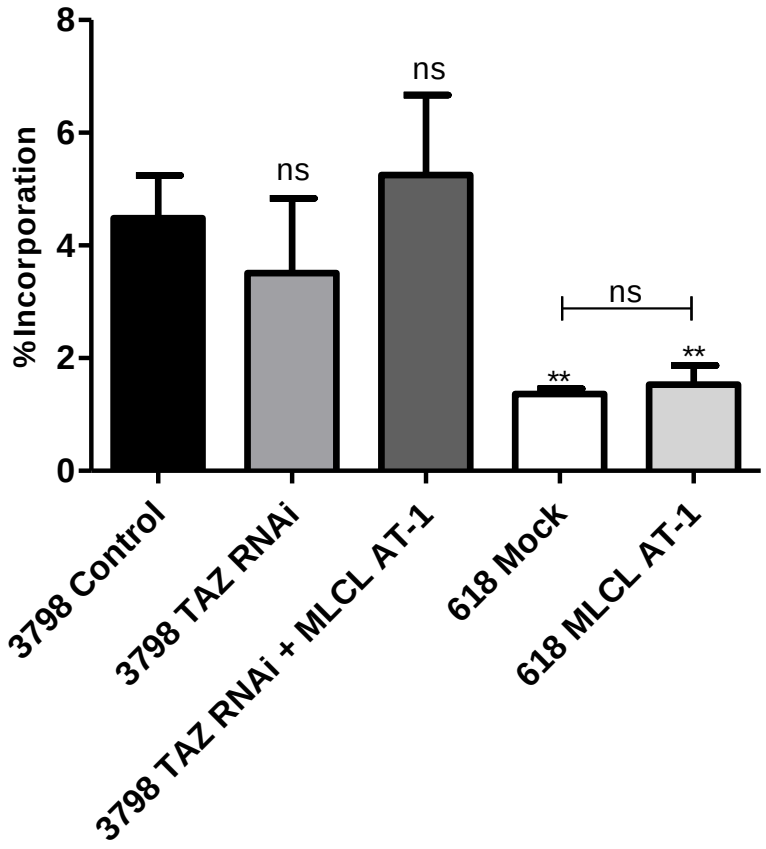

Figure 13: **Incorporation of ^{14}C linoleic acid into CL from 3798 healthy and 618 BTHS lymphoblasts.**

Percent incorporation of ^{14}C linoleic acid into CL in 3798 control, 3798 *TAZ* RNAi, 3798 *TAZ* RNAi + *MLCL AT-1*, 618 mock and 618 expressing *MLCL AT-1* cells (data represent mean ± SD of n = 3. Unless specified, ns = not significant compared to 3798 control. **p<0.01 compared to 3798 control).

6) Expression of MLCL AT-1 Increases CL Mass in Healthy and BTHS Lymphoblasts

To determine if *MLCL AT-1* expression in both cell lines affected CL mass, a sensitive lipid phosphorous assay was performed on the isolated lipid fraction from 3798 and 618 lymphoblasts from whole cell lysates. Total CL mass in 3798 cells was two-fold higher compared to 618 cells ($p<0.001$, Fig.14). This confirms that BTHS cells have significantly lower levels of CL compared with healthy cells. *TAZ* KD in 3798 cells did not significantly decrease overall CL mass (Fig.14). However, *TAZ* KD in conjunction with the expression of *MLCL AT-1* resulted in a significant 2-fold increase in CL mass in 3798 cells ($p<0.05$, Fig.14). Expression of *MLCL AT-1* significantly elevated CL mass in BTHS cells ($p<0.001$, Fig.14).

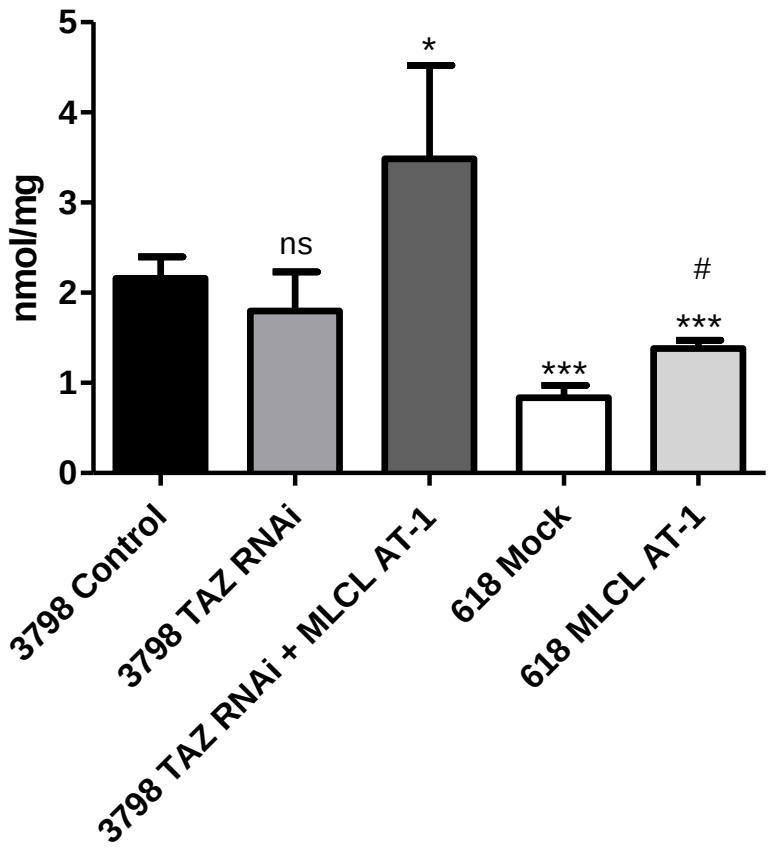

Figure 14: CL mass measured via sensitive lipid phosphorous assay in 3798 healthy and 618 BTHS lymphoblasts.

CL mass measured from whole-cell lysates of 3798 control, 3798 *TAZ* RNAi , 3798 *TAZ* RNAi + MLCL AT-1, 618 BTHS mock and 618 BTHS cells expressing MLCL AT-1 (data represent mean ± SD of n = 4, *p<0.05 compared to 3798 control, ns = not significant, ***p<0.001 compared to 3798 healthy controls, #p<0.001 compared to 618 mock-transfected BTHS cells).

7) BN PAGE & Complex I In-Gel Activity Assay in Healthy and BTHS Lymphoblasts

Mitochondria were isolated from healthy and BTHS lymphoblasts, treated with a mild detergent (0.2% DDM) and centrifuged at 20,000X g for 30 min. at 4ºC to isolate the mitochondrial membrane protein fraction. This fraction was then separated on a 3-12% Bis-Tris gradient gel to isolate the ETC complexes and supercomplexes. BN-PAGE analysis indicated that higher order SCs were absent in 618 cells (Fig.15, lanes 3 and 4) compared to 3798 cells (Fig.15, lanes 1 and 2).

IGAAs were performed to detect complex I (CI) activity in these cells. Figure 16 shows the presence of CI as well as CI-containing SCs at higher molecular weights. Knock down of *TAZ* in 3798 cells resulted in a significant decrease in the formation of these SCs compared to control (Fig.16, lane 2 compared to lane 1 respectively). In BTHS lymphoblasts, there was a reduction in CI expression as well as CI-containing supercomplex formation (Fig.16, lane 3). Expression of *MLCL AT-1* expression in BTHS cells did not affect CI or SC formation (Fig.16, lane 4).

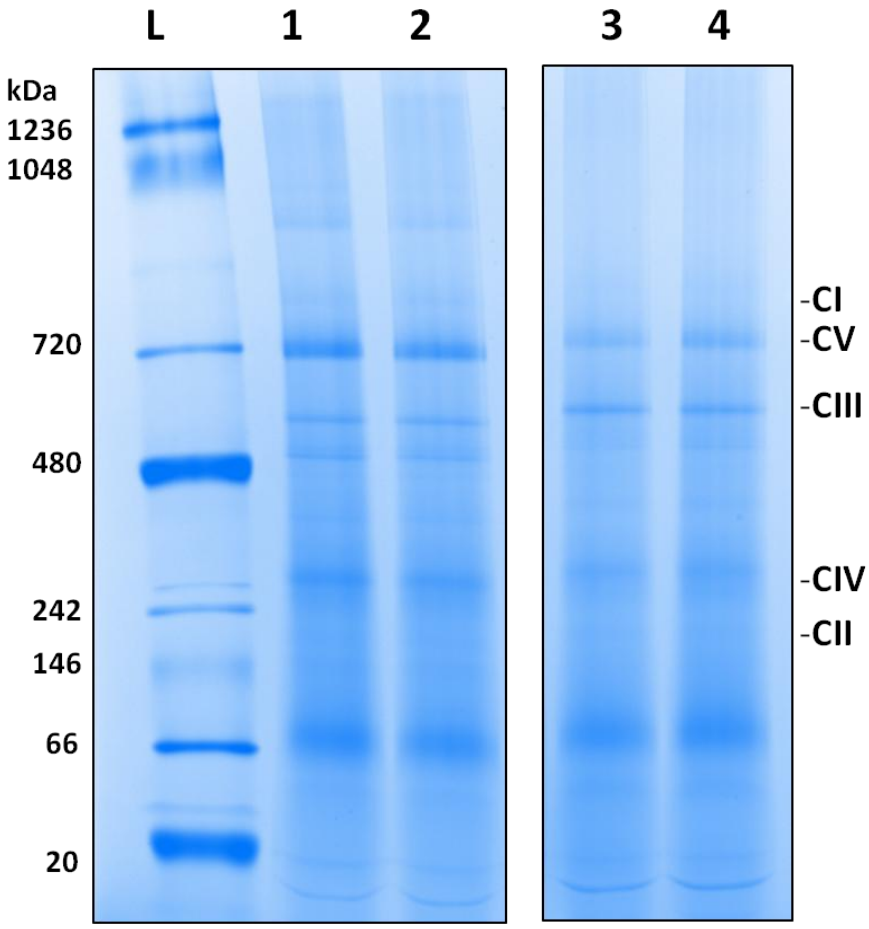

Figure 15: BN-PAGE used for the separation of ETC complexes and SCs from 3798 healthy and 618 BTHS lymphoblasts.

Representative image of a coomassie-stained gel (BN-PAGE). Isolated mitochondria from healthy and BTHS lymphoblasts were used to separate ETC complexes and SCs (n = 3. CI = complex I, CII = complex II, CIII = complex III, CIV = complex IV and CV = complex V. L = protein standard ladder, 1 = 3798 healthy control, 2 = 3798 *TAZ* RNAi, 3 = 618 mock-transfected BTHS, 4 = 618 MLCL AT-1).

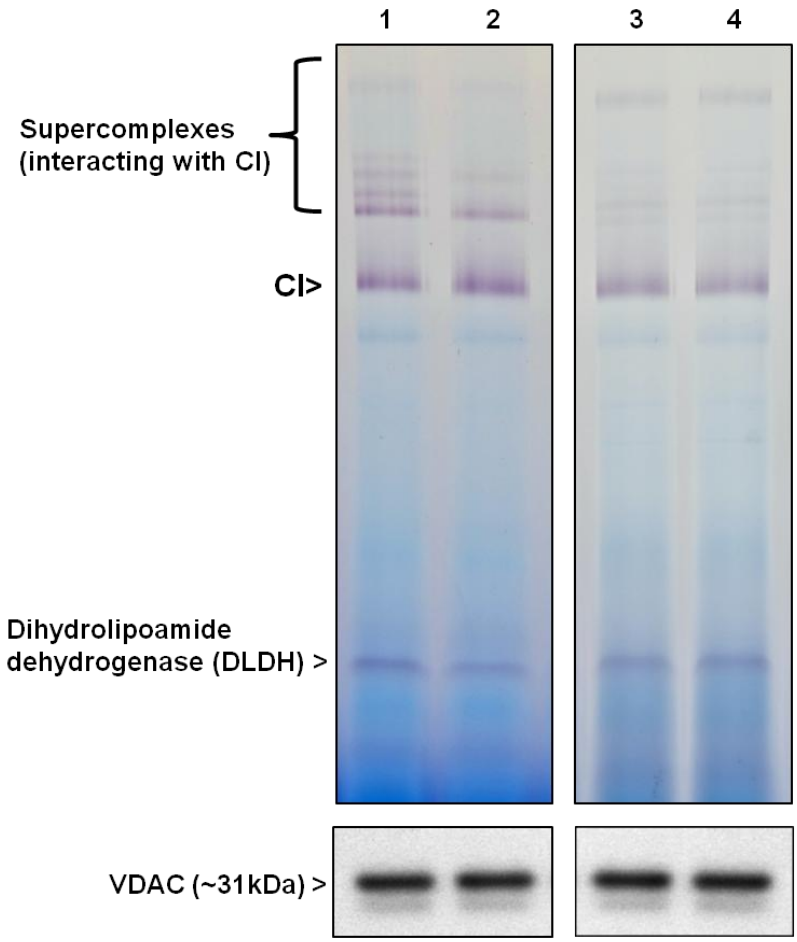

Figure 16: Complex I in-gel activity assay in 3798 healthy and 618 BTHS lymphoblasts.

Representative image of an in-gel activity assay for CI. Mitochondrial protein from healthy and BTHS lymphoblasts was used and BN-PAGE was performed as described in Experimental Methods section (n = 3). Subsequent western blot (SDS denaturing) was performed using VDAC as a loading control. 1 = 3798 healthy control, 2 = 3798 *TAZ* RNAi, 3 = 618 mock-transfected BTHS, 4 = 618 *MLCL AT-1*.

8) Mitochondrial Function in Healthy and BTHS Lymphoblasts

Mitochondrial oxygen consumption rate (OCR) analysis in healthy and BTHS lymphoblasts using a Seahorse XF24 Analyzer, revealed a number of differences between these two cell lines (Fig.17A). Basal respiration (measured as OCR [pmol/min/100k cells] before the addition of oligomycin) was approximately four-fold higher in 618 lymphoblasts compared to 3798 cells ($p<0.001$, Fig.17B). Knock down of *TAZ* in 3798 cells resulted in approximately a three-fold increase in basal respiration compared to control ($p<0.001$, Fig.17B). Expression of *MLCL AT-1* in BTHS cells resulted in a significant decrease in basal respiration ($p<0.001$ compared to mock-transfected BTHS cells, Fig.17B) that more closely mimicked the basal respiration observed in healthy cells. However, despite the improved basal respiration in BTHS cells that expressed *MLCL AT-1*, basal respiration was still significantly higher compared to healthy cells ($p<0.001$, Fig.17B). Proton leak was significantly higher in BTHS lymphoblasts compared to healthy controls ($p<0.001$, Fig.17C). The *TAZ* KD in 3798 cells resulted in a significant increase in proton leak compared to control ($p<0.001$, Fig.17C). However, expression of *MLCL AT-1* in BTHS cells resulted in a significant decrease in proton leak compared to mock-transfected BTHS cells ($p<0.001$, Fig.17C). Proton leak in BTHS cells that expressed *MLCL AT-1* was still significantly higher compared to healthy cells ($p<0.001$, Fig.17C). Spare respiratory capacity was significantly decreased in 618 lymphoblasts compared to healthy 3798 cells ($p<0.001$, Fig.17D). Healthy 3798 lymphoblasts had a spare respiratory capacity of nearly 50% while 618 lymphoblasts had a 30% capacity (Fig.17D). Surprisingly, *TAZ* KD in 3798 cells led to a significant increase in spare respiratory capacity compared to control

($p<0.01$, Fig.17D). The expression of *MLCL AT-1* in BTHS cells did not result in a significant change in spare respiratory capacity compared to mock-transfected BTHS cells. Our tests also revealed that approximately 70% of mitochondrial respiration is coupled to ATP production in 3798 cells (Fig.17E). This coupling efficiency was significantly decreased over time in 618 lymphoblasts from 62.5% to 37.5% (Fig.17E). *TAZ* KD in 3798 cells led to a significant decrease in ATP coupling compared to healthy cells ($p<0.001$, Fig.17E). The expression of *MLCL AT-1* in BTHS cells did not lead to a significant change in ATP coupling efficiency compared to mock-transfected BTHS cells. Non-mitochondrial respiration, which was measured after subjecting the cells in each well to a 1 µM concentration of Rotenone and 1 µM of Antimycin A, was not significantly different between healthy and BTHS lymphoblasts.

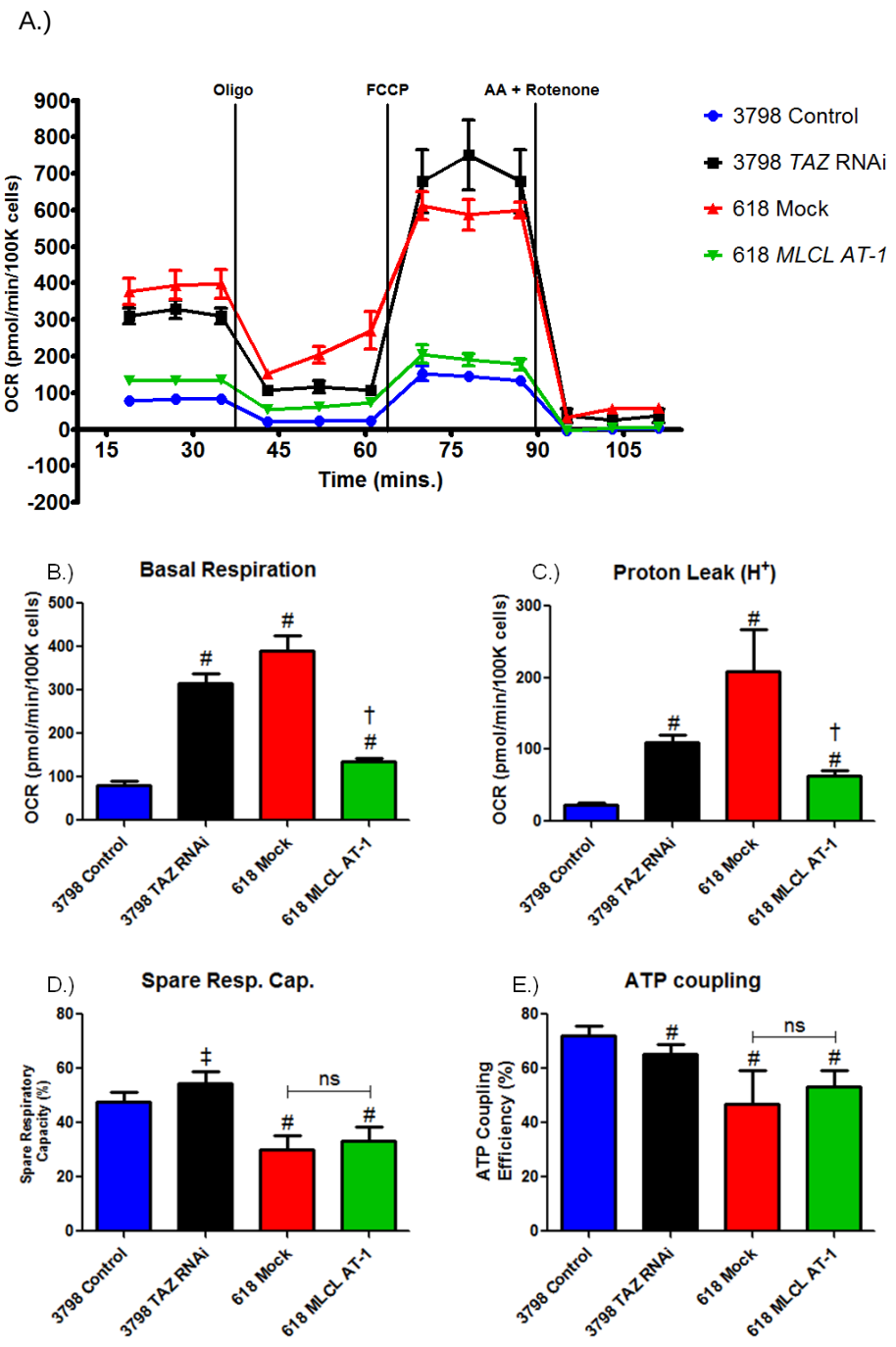

Figure 17: Mitochondrial function measured via oxygen consumption rates in 3798 healthy and 618 BTHS lymphoblasts.

A.) Cell respiratory control assessments in 3798 healthy and 618 BTHS lymphoblasts via measurements of B.) basal respiration, C.) proton leak, D.) spare respiratory capacity and E.) ATP coupling (data represent mean ± SD of n = 3, # = p< 0.001 compared to 3798 control, ‡ = p< 0.01 compared to 3798 control, † = p< 0.001 compared to 618 mock, ns = not significant compared to 618 mock).

9) Glycolytic Activity in 3798 and 618 Lymphoblasts

Using the Seahorse XF24 Analyzer, we demonstrated that 618 BTHS cells exhibit mitochondrial dysfunction compared to healthy controls. Next, we compared glycolytic activity in both cell lines to better assess how energy production may be affected in BTHS cells. To compare the rates of glycolysis between healthy and BTHS cells, ECAR was measured before and after the addition of glucose using a Seahorse XF24 Analyzer. Compared to healthy cells, BTHS cells demonstrated a rate of glycolysis that was approximately 1.5 fold higher compared to healthy controls (Fig.18A &B, $n = 3$, $p<0.001$).

A.)

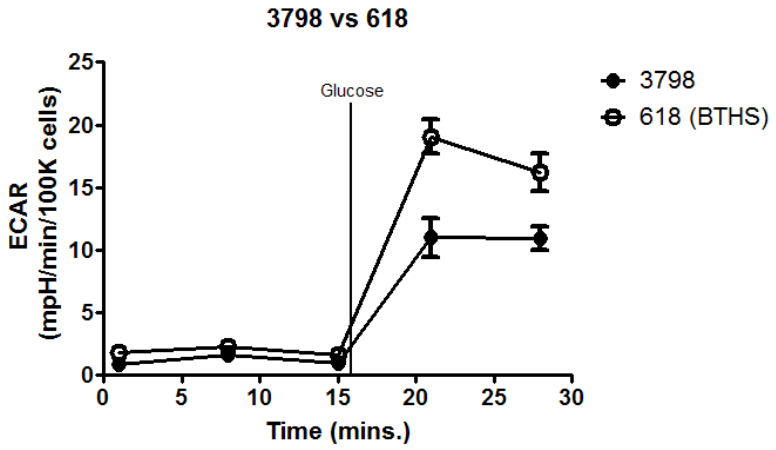

B.)

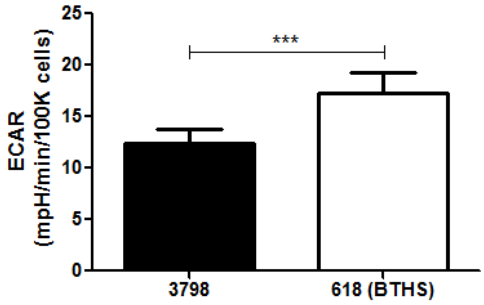

Figure 18: **Rates of glycolysis measured via ECAR in 3798 healthy and 618 BTHS lymphoblasts.**

A.) Comparison of extracellular acidification rates (ECAR) between healthy (3798) and BTHS (618) lymphoblasts (n = 3). B.) Comparison of ECAR between 3798 healthy and 618 BTHS lymphoblasts after addition of glucose (data represent mean ± SD of n = 3, ***p<0.001 compared to 3798 cells).

10) Citrate Synthase Activity in Mitochondria from Healthy and BTHS Lymphoblasts

Mitochondria from 3798 healthy and 618 BTHS lymphoblasts were isolated as described above and citrate synthase activity measured to detect changes in mitochondrial content. Any changes detected may help explain the differences in mitochondrial function between the two cell lines. BTHS mitochondria exhibited citrate synthase activity that was approximately 20% higher compared to healthy controls (Fig.19, n =1 for 3798 cells, n = 3 for BTHS cells). Expression of MLCL AT-1 in 618 BTHS cells resulted in a significant reduction in citrate synthase activity (n = 3, $p<0.05$ compared to 618 BTHS cells) that was comparable to the levels observed in 3798 cells.

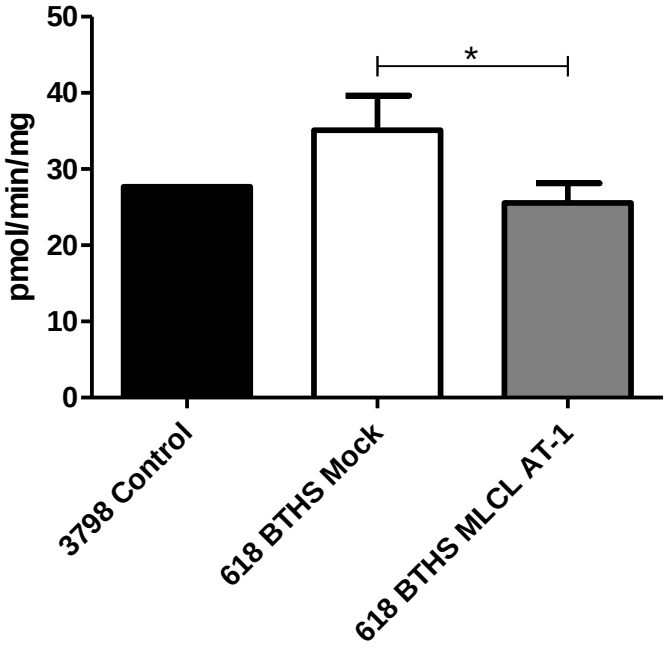

Figure 19: Citrate synthase activity comparison between 3798 healthy and 618 BTHS lymphoblasts.

Citrate synthase activity was measured in isolated mitochondria from healthy and BTHS lymphoblasts. Data represent the mean ± SD (n = 1 for 3798 cells, n = 3 for 618 BTHS mock and 618 BTHS MLCL AT-1, *$p<0.05$ compared to 618 BTHS mock).

11) ROS Production in Healthy and BTHS Lymphoblasts

Lymphoblast cell lines (3798 and 618) were stained with MitoSOX (an indicator of superoxide production) and flow cytometry analysis was performed (Fig.20). Two separate and distinct fluorescence intensity peaks were observed (Fig.20C). The right peak indicated the proportion of cells positive for MitoSOX staining while the left peak indicated the proportion of cells that were not positive for MitoSOX staining. The proportion of cells positive for superoxide production was higher in BTHS cells compared to healthy cells (approximately 75% versus 50%, respectively, Fig.20C & E). Expression of *MLCL AT-1* in BTHS cells lead to a reduction in the proportion of cells positive for superoxide production (approximately 75%→60%, Fig.20D) . As a positive control, addition of antimycin A (an inducer of superoxide production) resulted in 100% of cells analyzed to be positive for superoxide production, with no significant differences between healthy and BTHS cells (Fig.21A & B).

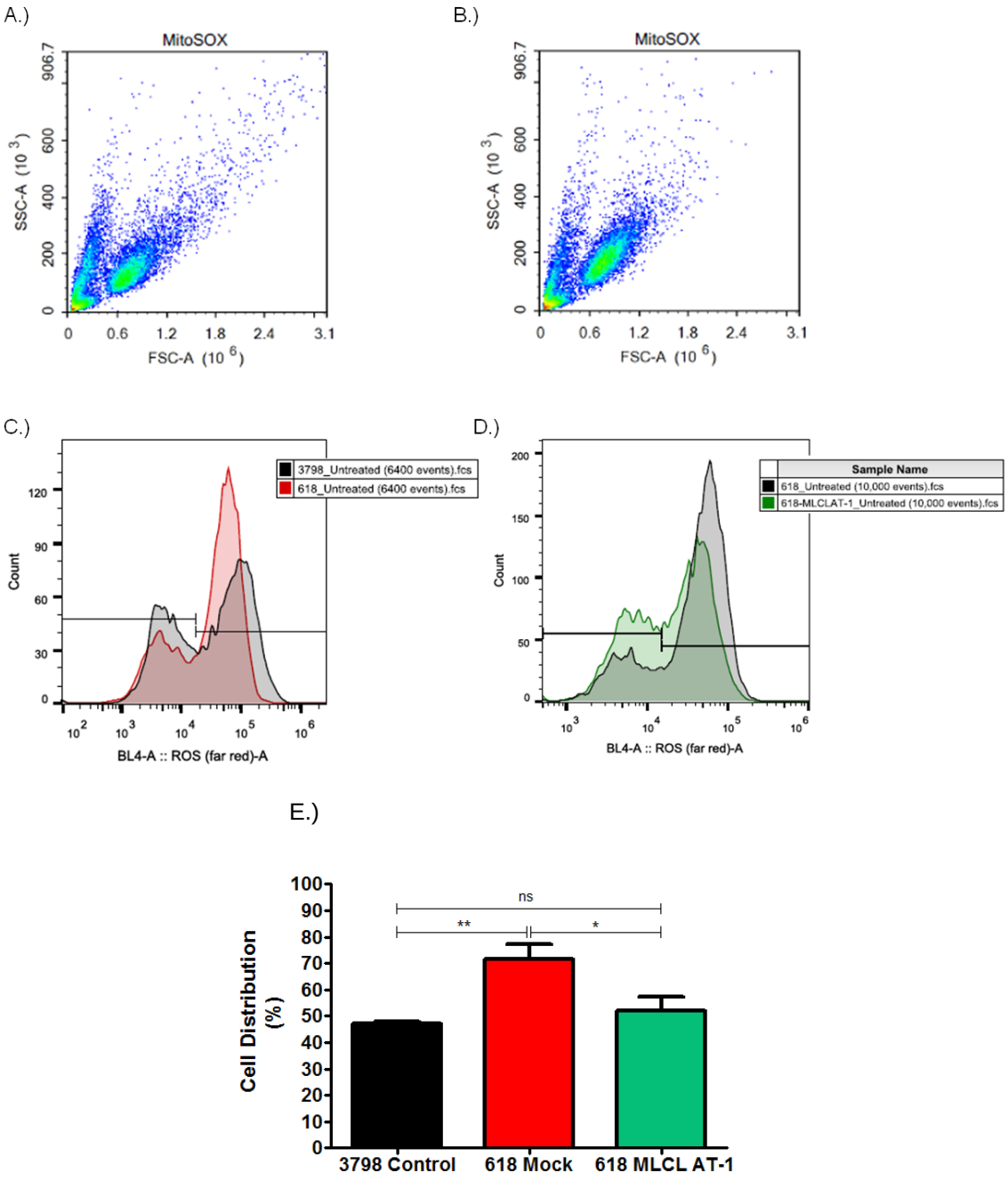

Figure 20: Measurement of ROS in 3798 healthy and 618 BTHS lymphoblasts via flow cytometry.

A.), B.) Representative scatter plots for 3798 & 618 cells (respectively). C.) ROS production comparison between 3798 & 618 cells and D.) 618 Mock & 618 cells expressing MLCL AT-1. E.) Distribution of cells positive for superoxide production (data represent mean ± SD of n = 3, **p<0.01compared to 3798 control, *p<0.05 compared to 618 mock, ns = not significant compared to 3798 control).

A.)

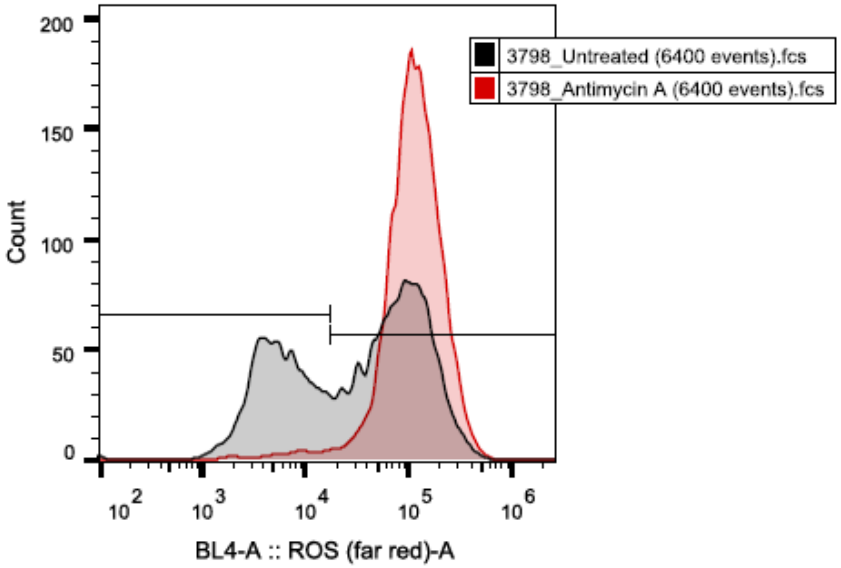

B.)

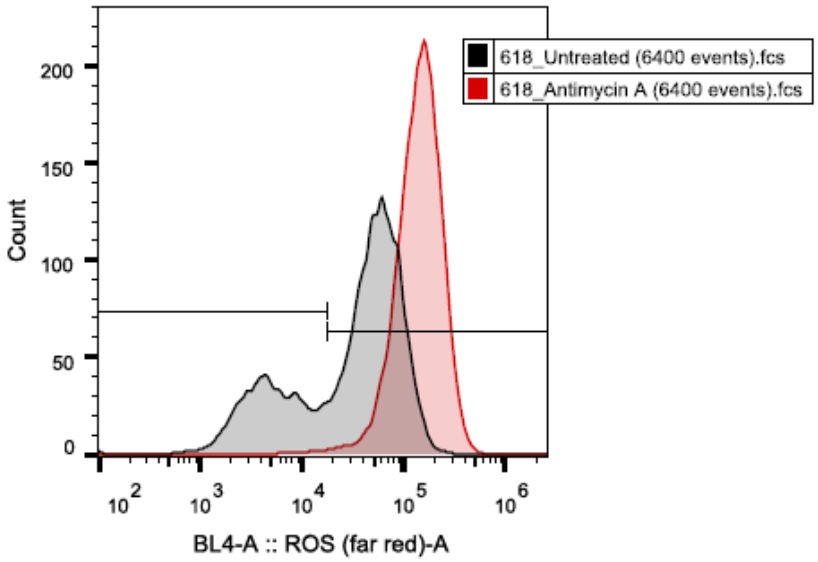

Figure 21: **Detection of ROS in 3798 healthy and 618 BTHS lymphoblasts after exposure to antimycin A.**

Addition of antimycin A to cells induces their production of superoxide, resulting in nearly 100% of A.) 3798 or B.) 618 lymphoblasts being positive for superoxide production.

12) BN-PAGE and IGAAs in WT and *Taz* KD Mice

BN-PAGE and IGAAs were performed to examine SC assembly and CI, CII and CIV activity in heart, skeletal muscle and liver of mitochondria prepared from WT and *Taz* KD mice. BN-PAGE analysis indicated that mitochondrial SC assembly was disrupted in heart and skeletal muscle of *Taz* KD mice compared to WT (Fig. 22A, 23A). CI-containing SC formation was disrupted resulting in decreased SC formation in hearts of *Taz* KD mice compared to WT (Fig.22B). The band intensity of CI and lower molecular weight CI-containing SCs was higher in heart mitochondria of *Taz* KD mice compared to WT (Fig.22B). A similar observation was apparent in skeletal muscle tissue of *Taz* KD mice compared to WT (Fig.23B). A lower CIV SC formation and increased CIV band intensity was observed in the hearts of *Taz* KD mice compared to WT (Fig.22D). Similar results for CI were observed in skeletal muscle (Fig.23D). In contrast to heart and skeletal muscle mitochondria, SC assembly was unaltered in the livers of *Taz* KD mice compared to WT (Fig.24A). In addition, CI and CIV activities were unaffected in liver of *Taz* KD mice compared to WT, as well as their corresponding CI and CIV SCs (Fig.24B & D). The number of CI and CIV SC formations in the liver of both WT and *Taz* KD mice was much lower than that of heart and skeletal muscle (Fig.22B & D, Fig.23B & D, Fig.24B & D). There were no differences in CII activity between WT and *Taz* KD mice in all three tissue samples (Fig.22C, Fig.23C and Fig.24C).

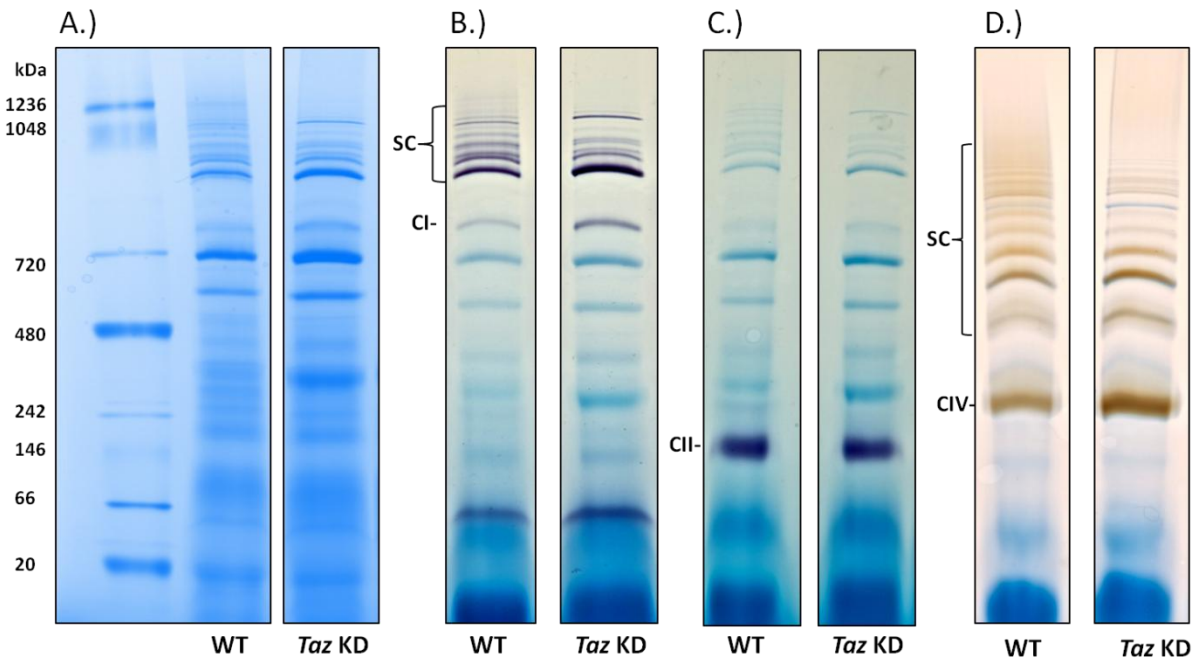

Figure 22: BN-PAGE and IGAAs using heart mitochondria from WT and *Taz* KD mice.

Mitochondria from WT (n = 6) & *Taz* KD (n = 6) mouse heart were used. A.) BN-PAGE performed to separate complexes (coomassie-stained). B.) IGAA performed to detect Complex I activity. C.) IGAA used to detect Complex II activity. D.) IGAA used to detect Complex IV activity. IGAA = in-gel activity assay, SC = supercomplexes.

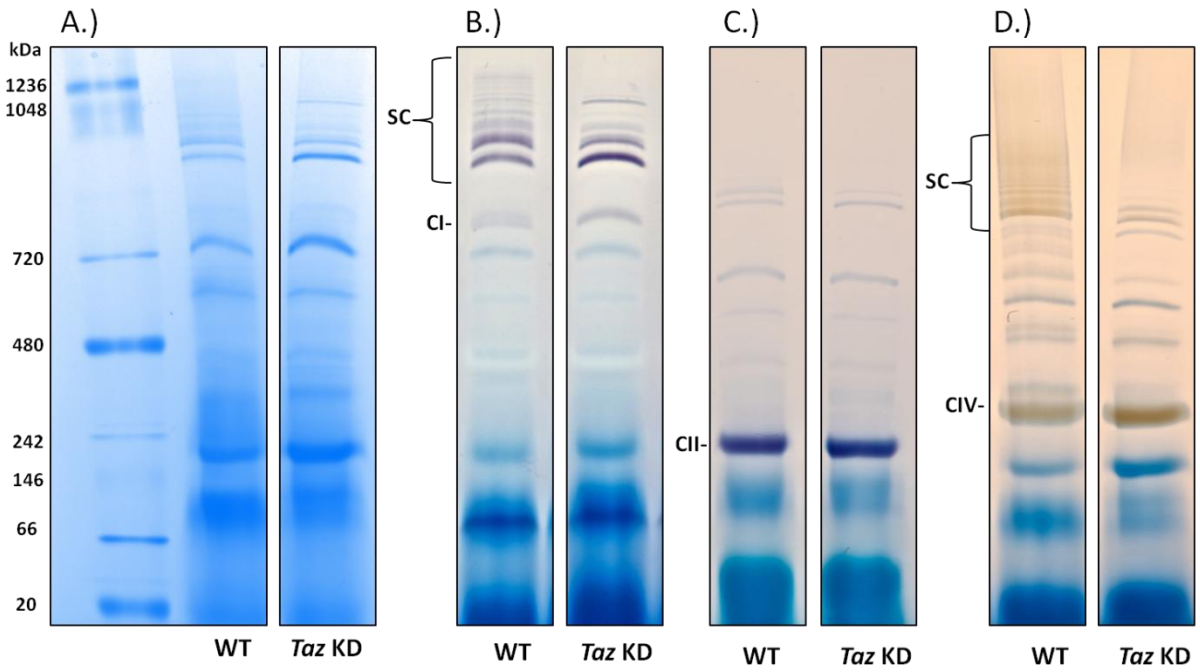

Figure 23: BN-PAGE and IGAAs using skeletal muscle mitochondria from WT and *Taz* KD mice.

A.) Mitochondria from WT (n = 5) & *Taz* KD (n = 3) mouse skeletal muscle use to perform BN-PAGE to separate complex proteins. B.) IGAA performed to detect Complex 1 activity. C.) IGAA used to detect Complex II activity. D.) IGAA performed to detect Complex IV activity.

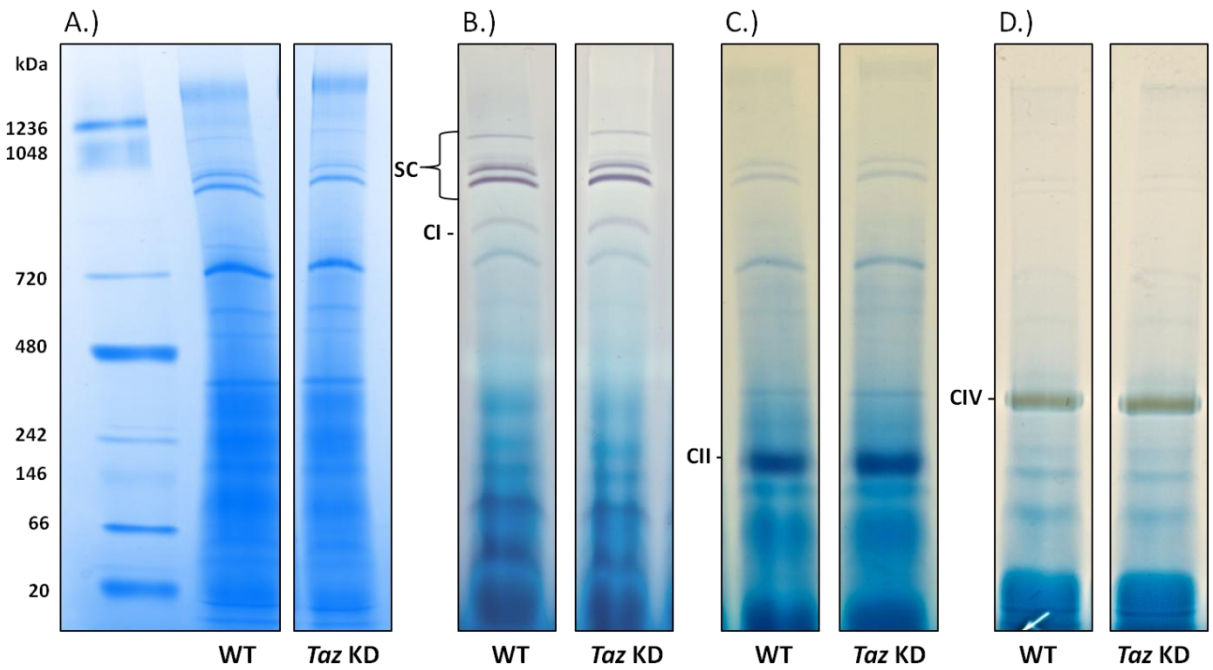

Figure 24: BN-PAGE and IGAAs using liver mitochondria from WT and *Taz* KD mice.

A.) Mitochondria from WT (n = 6) & *Taz* KD (n = 6) mouse liver used to perform BN-PAGE to separate complex proteins. B.) IGAA performed to detect Complex I activity. C.) IGAA used to detect Complex II activity. D.) IGAA for Complex IV.

13) ROS Production in WT and *Taz* KD Mice

To examine the potential correlation between SC disturbance and ROS production, hydrogen peroxide (H_2O_2) production was measured. Mitochondria were isolated from the heart, skeletal muscle and liver of WT and *Taz* KD mice and H_2O_2 was detected in these mitochondria using Amplex ® UltraRed Reagent. The heart and skeletal muscle mitochondria of *Taz* KD mice produced significantly elevated concentrations of H_2O_2 compared to mitochondria form WT animals (Fig.25A & B). In contrast, liver mitochondria of *Taz* KD mice produced a significantly lower concentration of H_2O_2 compared to the live mitochondria of WT mice (Fig.25C).

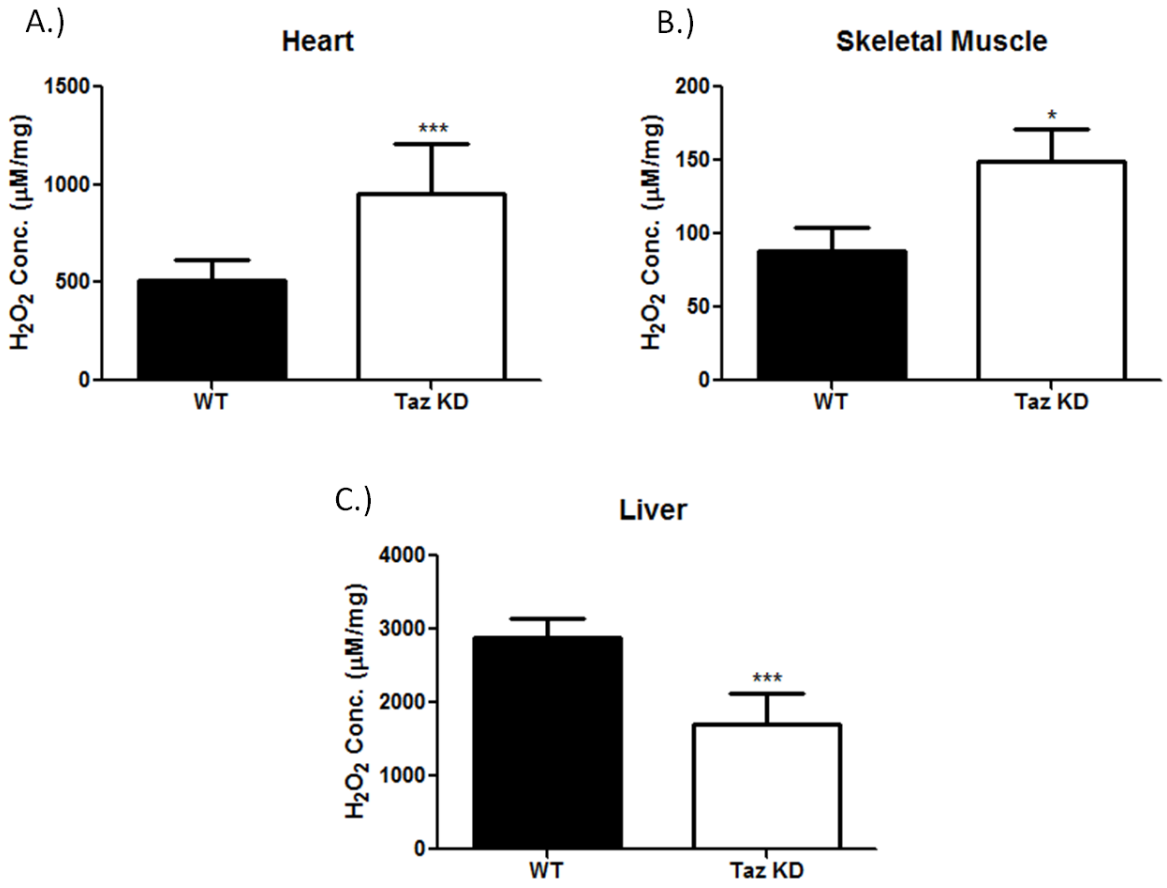

Figure 25: Measurement of H_2O_2 generation by mitochondria from tissues of WT and *Taz* KD mice.

Detection of H_2O_2 in A.) heart (n = 5, ***p < 0.001 compared to WT), B.) skeletal muscle (n = 4, *p < 0.05 compared to WT) and in C.) liver mitochondria (n = 3, ***p < 0.001 compared to WT).

Discussion

BTHS patients suffer from various symptoms that can include cardiomyopathies, neutropenia and skeletal myopathy [1, 2]. These symptoms occur as a result of *TAZ* gene mutations on the X-chromosome that lead to a decrease in functional TAZ and ultimately, a decrease in CL. Our *in vitro* work demonstrated that our BTHS cell line exhibited the common BTHS phenotypes including: low CL levels, increased MLCL and decreased expression of TAZ (compared to the healthy lymphoblast cell line). An interesting observation was made when comparing *TAZ* gene expression between BTHS and healthy cells. Given the type of mutation found on the *TAZ* gene of 618 cells (deletion of adenine nucleotide on exon 2 causing a frameshift mutation), and the fact that the primers used to detect *TAZ* gene expression were down stream of this mutation, we expected to find almost no production of mRNA. As our results show, we did find a significant decrease in *TAZ* mRNA production, but it was only a 50% reduction. Our Western blot analysis of TAZ protein found in the 618 BTHS cells shows almost no production of TAZ, which was not surprising given the nature of the mutation. However, why do we still detect *TAZ* mRNA production in the 618 BTHS lymphoblasts? This is an observation that requires further investigation. Interestingly, a 2013 study conducted by Kirwin *et al* that examined the different *TAZ* splice variants found in blood samples from BTHS patients, reported findings similar to ours [140]. In their study, Kirwin *et al* show that different BTHS individuals and healthy controls produce a greater variety of splice variants than previously described [140]. Not only do BTHS individuals produce detectable *TAZ* mRNA, but they also produce a number of TAZ isoforms [140]. Interestingly, a BTHS patient from their study has the same mutation that our 618 BTHS

lymphoblasts contain. Kirwin *et al* show that this BTHS patient exhibited five different *TAZ* transcripts with the isoform missing exon 5 comprising 57% of all the variants [140]. Therefore, it appears that BTHS patients have the ability to produce a number of detectable *TAZ* transcripts that may not lead to protein production.

In our study, we demonstrated that the expression of the remodelling enzyme, MLCL AT-1, is dependent on TAZ expression in healthy cells. *TAZ* KD in 3798 healthy lymphoblasts resulted in an approximate two-fold increase in *MLCL AT-1* gene expression. This correlated with our protein expression studies in which we observed a similar increase in MLCL AT-1 when *TAZ* was knocked down in 3798 lymphoblasts. In BTHS lymphoblasts, however, we did not observe an increase in MLCL AT-1 gene or protein expression compared to healthy cells. In fact, compared to 3798 healthy cells, there was a significant decrease in the expression of MLCL AT-1 in 618 BTHS lymphoblasts. Why did we not observe the increase in MLCL AT-1 expression in 618 BTHS cells that we observed in healthy 3798 cells in which *TAZ* was knocked down? The main difference between the 3798 and 618 lymphoblasts used in our experiments is that 618 cells contain a *TAZ* gene mutation. The original study conducted by Dr. Peter Barth in 1983 reported that BTHS patients exhibited mitochondria with significant ultrastructural damage [1]. Our BN-PAGE results indicated that mitochondria from 618 BTHS cells have significant ultrastructural damage due to their reduced SC formation. Thus, it is possible that these cells were simply too 'unhealthy' for MLCL AT-1 to employ any form of endogenous compensatory mechanism of CL remodelling. In healthy 3798 lymphoblasts, we achieved only a 40-50% reduction in TAZ gene and protein expression. This level of TAZ protein is still significantly higher than the levels of TAZ

found in BTHS cells. Thus, given a comparatively moderate reduction in TAZ enzyme expression, healthy cells may still be able to produce endogenous MLCL AT-1 allowing CL remodelling to continue. Another interesting observation from our western blot analysis experiments was that αTFP expression was unaffected in BTHS cells. This indicates that perhaps αTFP expression does not depend on TAZ or CL content. The relationship between αTFP and MLCL AT-1 will be discussed in a later section.

We used a *TAZ* RNAi sequence to KD *TAZ* in healthy lymphoblasts. After optimization, a 40-50% maximum KD was achieved in 3798 cells. In addition, TAZ protein expression levels were not reduced to the levels observed in BTHS lymphoblasts. This could be due, in part, to the type of cells used in our study. However, another study using neonatal ventricular fibroblasts to KD *TAZ* using a *TAZ* shRNA adenovirus reported only a moderate decrease (approximately 50% compared to control) in *TAZ* mRNA levels [141]. Another possible explanation for the relatively low level of *TAZ* KD could be the incubation period after cell transfection. This proved to not be the case as optimization experiments showed that this transient KD had a maximal effect on *TAZ* mRNA reduction after 48 h of incubation. The KD was transient as *TAZ* mRNA levels began to rise after this time (data not shown). This 40-50% reduction in TAZ gene and protein expression resulted in only a very moderate (but not significant) decrease in CL mass in healthy cells. Similar results were observed by He *et al* who reported only a 20% reduction in CL content after *TAZ* KD in neonatal ventricular fibroblasts [141]. These results indicate that perhaps cell type may have little to do with the efficiency to KD *TAZ in vitro*. The *TAZ* gene produces a number of isoforms that are expressed ubiquitously in mammals, with the potential for some of

these isoforms to be present only in certain tissues [6, 103]. Current studies do not agree on whether only one or several isoforms are functional or whether different isoforms are present in different tissues. As mentioned previously, it was widely believed that only one *TAZ* gene splice variant was the functional TAZ isoform [102]. A more recent study suggested that in humans, at least two TAZ isoforms express similar transacylase activity [142]. In that study, the full-length TAZ and the TAZ lacking exon 5 displayed transacylase activity and had the capability to restore normal CL patterns [142]. Thus, it is possible that current experiments that attempt to KD *TAZ* have to compete with different isoforms that may still be functional. It is also possible that knocking down one isoform results in a compensatory increase in another isoform, thus preventing significant decreases in the CL pool. The TAZ enzyme is an essential part of CL biosynthesis and any disturbances in its production may lead to devastating symptoms and even result in death. Thus, it is not surprising that an organism would employ various mechanisms to ensure the prevention of any disturbances to the functions of CL remodelling.

Despite the moderate *TAZ* KD achieved in our experiments, one might expect to see a measureable decrease in the CL pool in the healthy lymphoblasts. A decrease in TAZ in BTHS cells resulted in significantly lower levels of CL compared to controls. However, a KD of *TAZ* did not lead to a significant decrease in CL mass in healthy cells. One possible explanation for this outcome is the slow turnover rate of CL. Compared to other phospholipids, CL has among the slowest turnover rates [143, 144]. Landriscina *et al* reported that in rat liver mitochondria, ^{32}P phosphate incorporated into CL had a half-life of 10.4 days compared to other phospholipids which exhibited an average half-

life of 5.4 days [143]. A more recent study aimed at understanding the dynamics of CL found evidence that supported that finding. Using mammalian cell cultures, Yang *et al* compared the turnover rates of CL to other phospholipids, including PC and PE [144]. The authors concluded that once CL is incorporated into mitochondrial membranes, it is degraded very slowly and does not undergo acyl remodelling [144]. Taking these studies into consideration, it was not surprising that our *in vitro* results demonstrated only a moderate decrease in CL mass. The 3798 healthy lymphoblasts were incubated for 48 h post transfection with *TAZ* RNAi. Even though significant reduction in *TAZ* was achieved, this may have not been enough time to deplete or even diminish CL pools. It is findings such as these that illustrate the importance of advancing from transient KD models to an animal model that would better mimic the phenotypes observed in BTHS patients.

The development of an animal model of BTHS was and will continue to be an invaluable tool to help us better understand the mechanisms of BTHS. Acehan *et al* used a dox-inducible *Taz* KD mouse model and compared *Taz* gene expression between dox-fed mice and transgenic mice withdrawn from the dox-containing diet for one month [133]. The dox-fed mice displayed significant decreases in Taz gene and protein expression in various tissues. After a one month withdrawal period from the dox diet, *Taz* mRNA levels measured in these mice were significantly elevated compared to the dox-fed mice[133]. This finding illustrated that consistent dox feeding was required to maintain low levels of *Taz*. Other studies that have used the *Taz* KD mouse model reported major reductions in Taz gene and protein expression as well as the CL pool [145, 146]. A study from our laboratory using the dox-inducible *Taz* KD mouse model

revealed similar decreases in Taz and CL that more closely mimic the phenotypes expressed in BTHS patients [28]. Despite the limitations of our cellular *in vitro* work in BTHS lymphoblasts, it afforded us the opportunity to study the possibility of elevating MLCL AT-1 enzyme activities and observe the effect this had on CL pools in both healthy and BTHS cells.

Before the identification of the human MLCL AT-1 enzyme by Taylor *et al* in 2009 [18], there were already reports indicating that a MLCL AT enzyme may play a compensatory role in cells by preventing CL pools from diminishing under conditions of cellular duress [132]. Danos *et al* observed an increase in MLCL AT enzyme activity in H9c2 cells incubated with 2-deoxyglucose (2-DG) [132]. These cells had higher levels of cleaved caspase-3 and poly(ADP-ribose) polymerase compared to untreated controls, an indication of apoptosis induction [132]. However, the CL pool size and fatty acyl molecular composition of CL were unaltered. As Danos *et al* suggested [132], the observed increase in MLCL AT activity could be a cellular mechanism implemented to ensure CL pools do not diminish under conditions of stress. As seen in BTHS patients, a prolonged decrease in TAZ has detrimental consequences. Thus, an increase in MLCL AT-1 activity may be one of the compensatory mechanisms employed by cells to combat loss of TAZ. Another possible explanation for the observed increase in MLCL AT-1 activity in 3798 healthy cells after *TAZ* KD could be due to a change in substrate availability. Taylor *et al* suggested that a larger pool of endogenous MLCL in BTHS lymphoblasts could have been the reason why CL mass was increased in MLCL AT-1-tranfected BTHS lymphoblasts [126]. A similar phenomena could take place in healthy cells that have undergone *TAZ* KD. Several studies have shown that in BTHS patients

there is a significant decrease in CL which is linked to an increase in MLCL (reviewed in [147]). In fact, this increase in MLCL is the basis behind the bloodspot assay which is used to diagnose BTHS patients [114]. When *TAZ* is knocked down in healthy cells, the transacylase activity of TAZ is inhibited which prevents the acylation of MLCL to produce CL. Due to the slow turnover rate of CL, only moderate drops in the total CL pool may be observed. In contrast, there may be a large increase in the smaller cellular MLCL pool, similar to results observed in BTHS cells. This might provide an increase in MLCL, a substrate for MLCL AT-1 to utilize which could result in higher *in vitro* MLCL AT-1 activity in healthy cells with a KD of *TAZ*. However, due to the grossly impaired mitochondrial function in BTHS lymphoblasts, this compensatory mechanism may be absent in these cells.

The incorporation of ^{14}C linoleic acid into CL was significantly decreased in BTHS cells compared to healthy controls. RT PCR and Western blot analysis revealed that TAZ expression was significantly lower in BTHS cells compared to healthy controls. This was not surprising considering that BTHS occurs as a result of *TAZ* gene mutations [6]. Therefore, the ability of the TAZ enzyme to transfer linoleic acid from PC or PE to MLCL to create CL would be reduced. *TAZ* KD in healthy lymphoblasts did not result in a significant change in ^{14}C linoleic acid incorporation into CL. If a decrease in TAZ, like that observed in 618 BTHS cells, was responsible for a decrease in ^{14}C linoleic acid incorporation into CL, then why did we not observe a similar decrease in ^{14}C linoleic incorporation into CL in *TAZ* KD 3798 healthy cells? As previously discussed, *TAZ* KD in healthy cells resulted in a compensatory increase in MLCL AT-1 activity. This increase in MLCL AT-1 activity was likely responsible for preventing a

reduced incorporation of linoleic acid into CL in 3798 cells with KD of *TAZ*. The most surprising finding from this experiment was the fact that expression of *MLCL AT-1* both in healthy cells (also transfected with a *TAZ* RNAi) or in BTHS cells did not result in significant increases in ^{14}C linoleic acid incorporation into CL. If MLCL AT-1 indeed plays a compensatory role in healthy cells with decreased TAZ expression, then why did we not see an increase in ^{14}C linoleic acid incorporated into CL? Similarly, why was ^{14}C linoleic acid incorporation into CL in BTHS cells not significantly elevated by expression of *MLCL AT-1*? It was previously reported that in rat liver mitochondria, MLCL AT-1uses (in order of preference) linoleoyl coenzyme A > oleoyl coenzyme A > and palmitoyl coenzyme A to transfer acyl groups to MLCL to produce CL [18]. Therefore, in the presence of exogenous ^{14}C linoleic acid, newly formed ^{14}C linoleoyl CoA should be able to transfer linoleic acid to MLCL to produce ^{14}C CL. It is important to remember, however, that the study conducted by Taylor *et al* used rat liver mitochondria to arrive at this conclusion [18]. Tissues such as heart and liver are rich in L_4-CL [17]. Thus, the incorporation of ^{14}C linoleic acid into CL would not be surprising. Lymphoblasts, on the other hand, contain CL species primarily composed of oleic acid chains [17], an indication that remodelling enzymes such as TAZ and MLCL AT-1 may use oleic acid as one of their primary substrates. Our lipid mass spectrometry results, used to analyze the CL acyl species of the lymphoblast cell lines used in this study, were in agreement with a previous report which demonstrated that oleoyl-containing CL species are the dominant species in lymphoblasts [17]. In addition, the oleic acid-containing CL species were the CL species that exhibited the greatest decrease in 618 BTHS lymphoblasts. Thus, our results demonstrated only a trend towards an increase, but not a significant

rise in ^{14}C linoleoyl-CL formation when MLCL AT-1 was expressed in healthy and BTHS lymphoblasts. Perhaps the use of ^{14}C oleic acid to study fatty acid incorporation into CL may prove to be more effective in demonstrating the ability of MLCL AT-1 to increase acyl chain incorporation into CL. Why oleic and not linoleic acid is the predominant acyl species found in lymphoblasts is yet to be determined.

The results obtained from our RT PCR, western blot and MLCL AT-1 enzyme activity assay experiments were consistent in demonstrating that MLCL AT-1 expression can be elevated in both healthy and BTHS lymphoblasts. The ability to increase MLCL AT-1 expression in BTHS cells was not just limited to the 618 BTHS lymphoblasts used in these experiments. Taylor *et al* used Epstein-Barr virus transformed lymphoblasts from a different BTHS patient (patient ID: 596) with a different *TAZ* gene mutation and transfected them with a *MLCL AT-1*-carrying plasmid [18]. They observed a significant increase in MLCL AT-1 enzyme activity in the 596 BTHS lymphoblasts expressing MLCL AT-1. Other results from that study included a lower basal MLCL AT-1 enzyme activity in 596 BTHS cells compared to healthy controls that mirrored the results obtained in our study in 618 BTHS cells. Taken together, these findings suggest that MLCL AT-1 expression may be dependent on TAZ expression. However, in our BTHS lymphoblasts, the amount of MLCL AT-1 enzyme present was significantly lower compared to healthy control cells. In addition, the results from the previous study [18] also show that it is possible to elevate MLCL AT-1 expression in healthy cells, but more importantly, in BTHS lymphoblasts. Increased MLCL AT-1 expression correlated with elevated CL mass in BTHS cells in both studies. Following these observations, the next step was to conduct additional experiments to determine if

this increase in CL mass mediated by expression of MLCL AT-1 in 618 BTHS cells had a beneficial effect on mitochondrial structure and function.

Transfection of BTHS lymphoblasts with a MLCL AT-1-carrying plasmid led to significant increases in MLCL AT-1 gene and protein expression which was mirrored by an increase in enzyme activity. This, in turn, resulted in a significant increase in CL mass. CL is essential for mitochondrial SC assembly [25-28]. We examined if the elevated CL achieved in BTHS cells as a result of MLCL AT-1 expression led to changes in SC formation. Previous studies have demonstrated that in lymphoblasts from BTHS patients, SC formation is disrupted [22, 83]. Our results showed that *TAZ* KD in healthy cells led to a disruption of SC formation. Therefore, decreasing TAZ expression leads to decreased CL and ultimately, may lead to a decreased ability for complexes to assemble into SCs. In BTHS cells, where TAZ expression and CL levels are low, we observed a reduction in SC formation, which correlates with results obtained by other laboratories [22, 83]. Taken together, these results raise an interesting question. Does TAZ regulate SC formation independent of CL? From our CL mass experiments we observed that despite a 40-50% reduction in TAZ protein in healthy lymphoblasts, CL mass did not significantly decrease. However, *TAZ* KD in healthy cells did result in the disruption of CI-containing SCs. BTHS cells, which have TAZ protein expression levels that are drastically lower than *TAZ* KD cells, had little SC formation. Based on these results, it would appear that SC formation may be directly related to TAZ expression but not to CL. In support of this hypothesis was our observation that SC formation remained unaltered in BTHS cells expressing *MLCL AT-1* which exhibit elevated CL levels. The hypothesis that TAZ is the primary determinant of

SC formation (and CL a secondary component) is not a new concept. Claypool *et al* studied the association of Taz with mitochondrial membrane proteins in yeast mitochondria [148]. Using 2D BN-PAGE, the ATP-synthase and the ADP/ATP2 carrier (AAC2) in yeast were identified in separate stable interactions with Taz. In addition, CL synthase (CLS, required for *de novo* biosynthesis of CL) KD resulted in a significant decrease in CL, but this did not result in the elimination of interactions between Taz and mitochondrial complexes, but simply reduced abundance of these complex interactions [148]. In another study by Pfeiffer *et al*, it was demonstrated that CL was required for the stabilization of SCs in yeast but was not essential for their formation [25]. With the use of a CLS mutant yeast strain, CL levels were drastically reduced compared to controls, and this resulted in the decreased formation of the $CIII_2/CIV_{(2)}$ SCs detected by BN-PAGE. However, using Clear Native (CN)-PAGE, a technique that is milder than BN-PAGE [149], the authors observed that SC formation was not entirely absent in CL-deficient yeast strains [25]. The authors concluded that CL helps improve the stability of SCs, but does not direct their formation. Therefore, it is possible that TAZ may play a currently unknown role in SC formation that may not directly involve the presence of CL. This is currently a controversial hypothesis in this field as it has been widely accepted that CL is the 'glue' that holds SCs together. This is primarily based on studies that have used BTHS patient cells or BTHS yeast or animal models to study SC formation [22, 51, 83]. Since *TAZ* KD is typically accompanied by a reduction in CL levels, it is difficult to separate which of these two factors is primarily responsible for SC formation. As discussed previously, one way to get around this issue is to KD other enzymes responsible for CL formation such as CLS. A study in *Arabidopsis thaliana* showed that

CLS is not only required for proper mitochondrial function, but also mitochondrial ultrastructure [150]. Using BN-PAGE and complex I (CI) in-gel activity assays, $CI/CIII_2$ SC formation was reduced by CLS KD. The difference between this study [150] and the one conducted by Pfeiffer *et al* [25] is that the former study used BN-PAGE while the latter study used CN-PAGE. This procedural difference could be a key factor in determining whether or not SC formation is truly affected in CLS KD experiments. Diminished CLS production would interfere with the *de novo* biosynthesis of CL and result in an overall decrease in CL. This decrease would, at the very least, result in the destabilization of SCs. Still, the question remains: what is more important for SC formation, the presence of CL or TAZ? A study by Kiebish *et al* using the dox-inducible *Taz* KD mouse model attempted to reverse the phenotype caused by decreased Taz levels [146]. In their study, the signature phenotypes were observed, including: decreases in Taz, L_4-CL, CIII and CIV expression as well as increases in MLCL [146]. Using double genetic crossed mice (*Taz* KD X *CLS* transgenic), the authors over-expressed CLS in an attempt to reverse the phenotype observed in *Taz* KD mice. One of the major conclusions of this study was that the transgenic expression of CLS did not rescue the phenotype. This was an interesting observation because it indicated that increased CLS expression accompanied by increases in immature CL, were not enough to rescue ETC complex protein function. Findings such as these once again demonstrate that healthy TAZ expression is required for proper mitochondrial SC function. The findings reported by Kiebish *et al* [146] are very similar to our results which showed that expression of MLCL AT-1 in BTHS lymphoblasts lead to increases in CL mass, yet no improvement in SC formation. Observations similar to the ones

discussed have also been reported in studies outside the field of BTHS research. A study published by Mejia *et al* (2015) examined the phenotype of an αTFP heterozygous knockout mouse model (Mtpa(+/-)) and observed moderate decreases in L_4-CL in the hearts and livers of these animals [151]. The αTFP is a subunit of the mitochondrial trifunctional protein responsible for catalysing 3 out of the four reactions involved in the β-oxidation cycle [128]. In this mouse model, we observed a 55% and 50% reduction in αTFP in the heart and liver respectively compared to WT samples (Fig.26). This was accompanied by significant reductions in MLCL AT-1 protein expression and enzyme activity, but surprisingly, this was only observed in the heart and not in liver tissue [151]. In the heart, a 30% reduction in the CL pool was also observed in Mtpa(+/-) animals compared to WT. No significant changes in the CL pool were observed in the liver. Examination of CI-containing SCs using BN-PAGE and in-gel activity assays revealed no significant differences between Mtpa(+/-) and WT mice in both heart and liver (Fig.27) [151]. This, once again, illustrates that despite significant decreases in CL, SC formation was not affected. For the time being, our current results, and those of others, demonstrate that mitochondrial membrane complexes and SCs are primarily dependent on TAZ for proper function and formation. It is evident that further studies are required to better understand the biochemical roles that both TAZ and CL play in the formation of SCs. Despite the number of results (including our own) indicating that CL may not be essential for SC formation, it is important to keep in mind that every study has one or more limitations. In our own investigations using BTHS lymphoblasts, we were only able to elevate but not rescue CL mass. BTHS cells with increased CL mass still had significantly lower levels of CL compared to healthy cells.

This may be one explanation as to why SC formation was not rescued in these cells. In addition, the *MLCL AT-1* transfections carried out in our *in vitro* experiments were transient. Therefore, it would be interesting to determine the effect of a stable and prolonged *MLCL AT-1* expression in the *Taz* KD animal model. Future experiments may reveal that it is possible to rescue SC formation in BTHS cells.

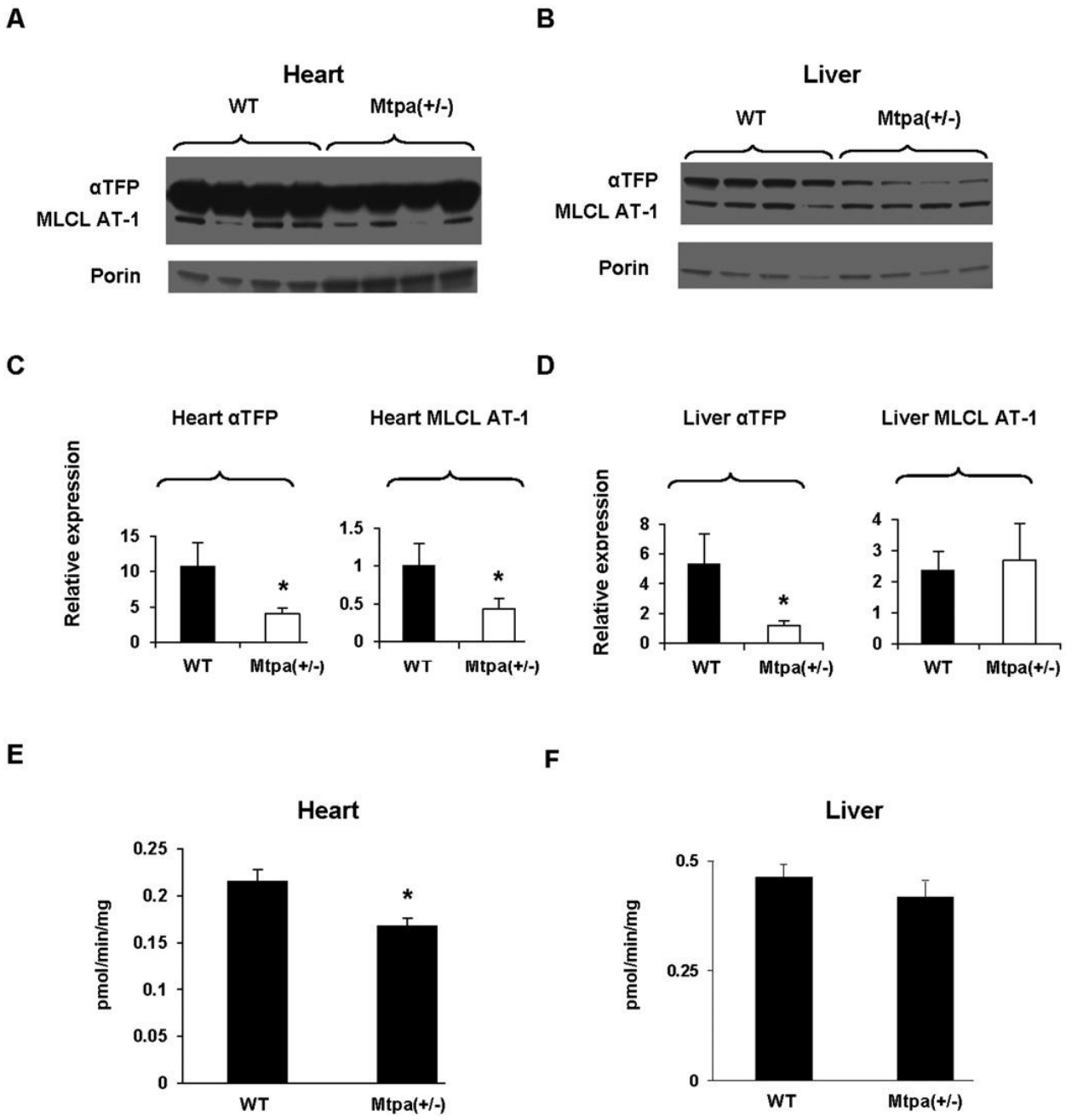

Figure 26: Expression of Mtpa/αTFP and MLCL AT-1 in the heart and liver of WT and Mtpa (+/-) mice.

(A and B) Mitochondria were isolated from WT and Mtpa (+/−) hearts (A) and livers (B), and protein levels of *α*TFP, MLCL AT-1 and porin were determined by Western blot analysis as described in the Materials and methods section. Representative blots are depicted. (C and D) The relative expression of *α*TFP or MLCL AT-1 to porin in heart (C) and liver (D). (F and G) Mitochondria were isolated from WT and Mtpa (+/−) hearts (E) and livers (F), and MLCL AT enzyme activity determined as described in the Materials and methods section. Data represent the means ± SD for four animals, *p<0.05 compared to WT. [151]

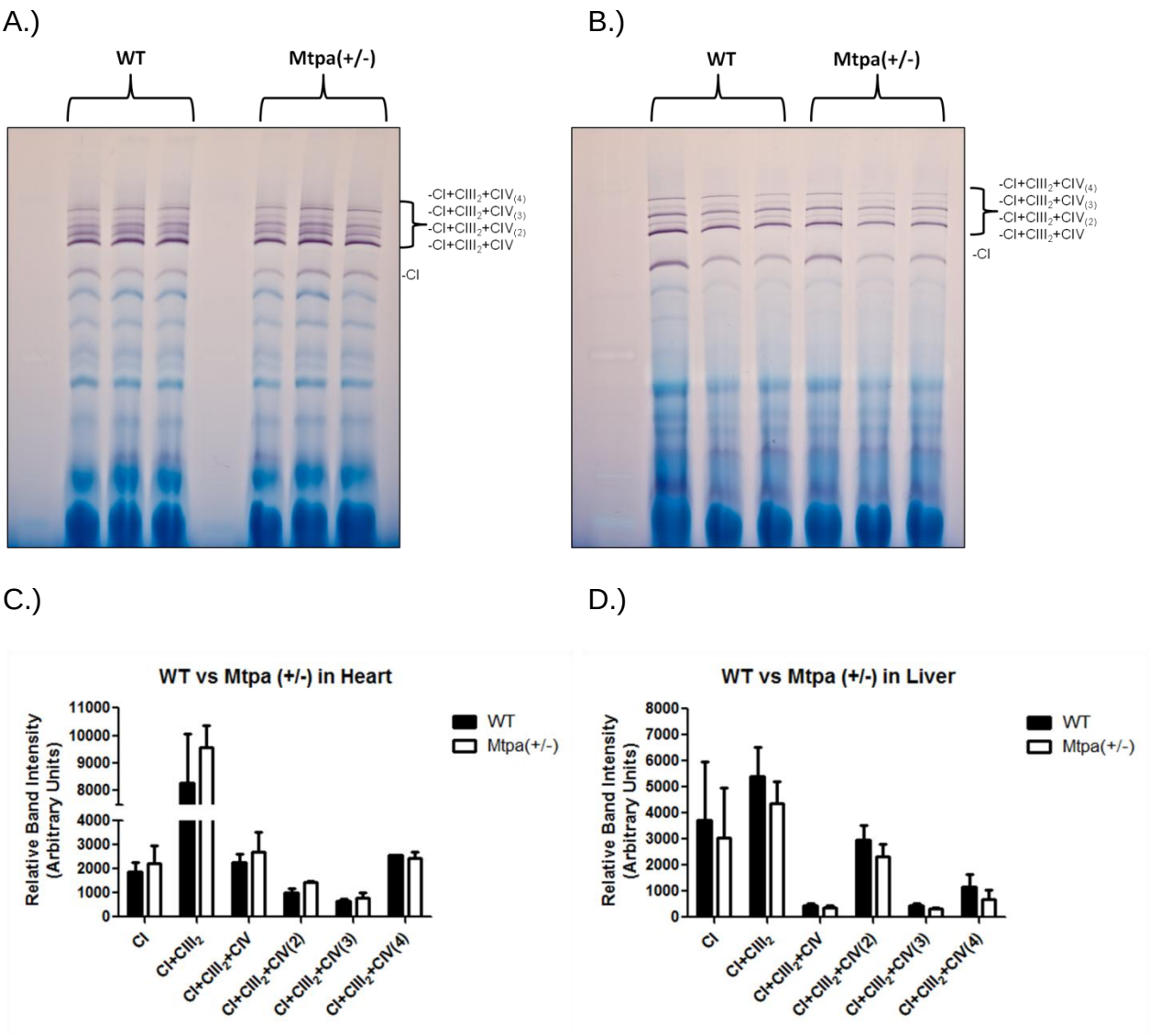

Figure 27: Cardiac and liver mitochondrial respiratory protein SC assembly and CI IGAA in WT and Mtpa(+/-) mice.

Mitochondria were isolated from WT and Mtpa(+/−) hearts (A) and livers (B), and mitochondrial protein was subjected to BN PAGE analysis as described in the Materials and methods section. A representative gel of three WT and Mtpa(+/−) hearts and livers is depicted. Complex I activity was determined in heart (A) and liver (B) using the in-gel activity assay described in the Materials and methods section. Complex I and complex I-containing supercomplexes are indicated on the right. The relative band intensities of complex I activity and complex I activity within supercomplexes is indicated for heart (C) and liver (D). [151]

Our BN-PAGE experiments revealed that expression of *MLCL AT-1* in BTHS lymphoblasts did not rescue the impaired SC formation phenotype found in these cells. We followed up these observations by analyzing mitochondrial function in healthy and BTHS lymphoblasts using a Seahorse XF24 Extracellular Flux analyzer. This instrument can be used to perform what is known as a mitochondrial stress test which can provide a wealth of information with regards to mitochondrial function in cells. Through measuring the rate of change of dissolved O_2 in media, the oxygen consumption rates (OCR) of cells can be determined. When this is combined with the introduction of various mitochondrial inhibitors at different time intervals, this allows for the determination of the bioenergetic profiles of cells. Specific parameters measured using the XF analyzer included: basal respiration, ATP coupling efficiency, spare respiratory capacity and proton leak (H^+ leak). Before our results can be discussed, it is important to understand the meaning of each these measurements. The cell's basal respiration is its OCR before the addition of drugs/inhibitors. It is controlled by the cell's ATP turnover and therefore changes in response to ATP demand [152]. ATP coupling efficiency can be measured after the introduction of oligomycin into the media of the cells. Oligomycin is an ATP synthase inhibitor. Thus, exposing cells to oligomycin results in a drop in OCR. This measurement can be used to calculate the amount of respiration that is coupled to the production of ATP. Spare respiratory capacity is measured after the addition of carbonyl cyanide 4-(trifluoromethoxy) phenylhydrazone (FCCP). This compound is described as a protonophore (H^+ ionophore) and acts as an uncoupler of oxidative phosphorylation [153]. The addition of this compound introduces instability in cellular respiration due to the fact that ATP demands are not being met. As

a result, mitochondrial respiration is stimulated as a compensatory mechanism for the decreased production of ATP. Finally, mitochondrial proton leak is measured after the addition of oligomycin. When ATP synthase is inhibited, respiration is heavily affected by proton leak kinetics, and is thus very sensitive to mitochondrial uncoupling [152]. A high proton leak measurement can be an indication of mitochondrial membrane damage. These four mitochondrial function parameters were analyzed and compared between healthy and BTHS lymphoblasts. Other compounds that comprise part of the mitochondrial stress test include the mitochondrial CI and CIII inhibitors rotenone antimycin A (respectively). These compounds are used to completely shut down mitochondrial respiration, leaving behind only non-mitochondrial OCRs which are subtracted from other rates [152].

We observed that basal respiration in 618 BTHS cells was significantly higher than that of 3798 healthy cells. The higher OCRs observed in BTHS cells were an indication that ATP demand was higher compared to healthy cells. At first, one could assume that this is a result of a higher number of mitochondria found in BTHS cells. This is something that can be addressed by future experiments such as mtDNA quantification or the use of MitoTracker to detect mitochondria through fluorescent signals. However, a likely explanation for this observed increase in basal respiration in BTHS cells could be due to an increase in their mitochondrial mass as a way to compensate for depleted ATP levels. A number of studies which are in support of this idea showed that BTHS lymphoblasts exhibited inconsistent mitochondrial size with a tendency for an increase in mitochondrial mass [123, 124]. Our BN-PAGE results are consistent with these observations as they provided an indirect view of the IMM and the

SC disturbance that occurs in BTHS cells. In addition, we also measured citrate synthase enzyme activity in both healthy and BTHS cells. Citrate synthase is a mitochondrial enzyme that is responsible for the production of citrate, a key substrate in the Krebs cycle which is used for the production of ATP and reducing equivalents for the ETC [154]. Our results show that citrate synthase activity is approximately 20% higher in BTHS lymphoblasts compared to healthy controls. Also, expressing MLCL AT-1 in 618 BTHS cells resulted in a significant reduction in citrate synthase activity compared to mock-transfected 618 BTHS cells. This is also an indication that mitochondrial mass is greater in the 618 BTHS lymphoblasts and that the use of MLCL AT-1 may ameliorate this condition. A study by Gonzalvez *et al* using immortalized lymphoblasts from BTHS patients reported findings that correlate with our results [22]. In this study, the authors also found that BTHS cells exhibited greater mitochondrial mass compared to healthy controls as shown by electron microscopy. In addition, citrate synthase enzyme activity was significantly higher in BTHS cells compared to healthy controls [22]. Therefore, it is possible that instead of more mitochondria, the 618 BTHS cells contain mitochondria with damaged mitochondrial membranes affecting cristae formation and thus result in inconsistent mitochondria of larger mass compared to healthy mitochondria.

ATP coupling efficiency was significantly decreased in 618 BTHS cells compared to healthy 3798 cells. This was not surprising considering the predicted mitochondrial membrane damage present in BTHS cells. This decreased ATP coupling efficiency indicates that despite high basal respiration, oxygen consumption in BTHS cells is not being used efficiently for the production of ATP, potentially due to mitochondrial

uncoupling. Reduced coupling efficiency may also be the result of impaired F_1F_o ATP synthase (CV) activity. Previous studies showed that in CLS mutant *Drosophila* and lymphoblasts from BTHS patients, decreased CL led to not only impaired CV function, but also impaired CV dimerization into supramolecular structures [22, 155]. A similar effect may occur in our 618 BTHS cells which have reduced CL, although we did not examine this. The proton leak in 618 BTHS cells was significantly higher compared to 3798 healthy cells. Under normal physiological conditions, the energy harvested from the electron transfer across the IMM drives complexes I, III and IV to pump protons into the intermembrane space producing the proton motive force (Δp) [156]. The controlled dissipation of the Δp is necessary to drive the phosphorylation of ADP through rotary catalysis for the production of ATP [157, 158]. Uncoupling proteins (UCPs) in the IMM allow protons to flow back into the mitochondrial matrix [156]. However, the specific role of UCPs is still not fully understood. The elevated proton leak in 618 BTHS cells was a predictable result that goes hand in hand with the increased basal respiration and decreased ATP coupling efficiency in BTHS cells. Increased respiration that is not efficiently coupled to ATP production could be caused by a leaky membrane that allows the flow of protons back into mitochondria. This would result in uncoupled respiration causing energy to be dissipated as heat instead of being stored to produce the Δp, thus leading to high basal respiration and low ATP coupling efficiency. Finally, spare respiratory capacity measured in 618 BTHS cells was significantly lower compared to 3798 healthy cells. Upon initial inspection, the OCRs after the addition of FCCP were significantly higher in BTHS cells compared to healthy cells. However, this was due to the higher basal respiration and proton leak in the BTHS cells. Calculation of the spare

respiratory capacity revealed that compared to healthy 3798 cells, 618 BTHS cells were not able to increase their respiration to compensate for the mitochondrial uncoupling caused by FCCP. Mitochondrial spare respiratory capacity is an important physiological process required by various types of cells, especially those that experience variable ATP demands (for example: neurons and skeletal muscle cells) [152]. Cells use their spare respiratory capacity in response to stress or increased workloads. The failure of cells to do this may result in a number of disorders including heart disease and cell death in smooth muscle cells [159, 160]. Considering the fact that BTHS patients experience symptoms such as skeletal myopathies and exercise intolerance [1, 2], it comes as no surprise that spare respiratory capacity was impaired in 618 BTHS cells. A clinical link between abnormal mitochondrial function in BTHS and impaired ability of skeletal muscle to utilize O_2 has been proposed. In a study by Spencer *et al*, diminished cardiac reserves as well as O_2 utilization by skeletal muscle and its link with the exercise intolerance experienced in BTHS patients was examined [161]. The authors found that skeletal muscle O_2 extraction was impaired in BTHS patients during peak exercise. In addition, ejection fractions were significantly lower in BTHS patients compared to healthy individuals. The authors concluded that their findings of both cardiac and skeletal muscle impairment were consistent with cardiac and skeletal mitochondrial myopathy previously observed in BTHS patients [161]. Therefore, taken together, it is clear that the four mitochondrial function parameters tested in our study show that BTHS cells experience mitochondrial dysfunction. Other studies utilizing the Seahorse XF analyzer to study mitochondrial function in BTHS cell models have shown similar results. Wang *et al* generated cardiomyocytes from induced pluripotent stem

cells (iPSCs) from BTHS patients and studied various structural and functional abnormalities associated with BTHS [88]. Similar to our results, Wang *et al* showed that basal respiration and proton leak were elevated while spare respiratory capacity was decreased [88]. The only difference between the mitochondrial function results from that study and our results was that they observed higher ATP coupling efficiencies in the BTHS cardiomyocytes compared to their controls, while we observed the opposite finding. This could simply be due to the different cells used in each study. Nevertheless, our studies provide insight into the bioenergetic profile of BTHS lymphoblasts. Mitochondrial stress tests were also conducted on healthy lymphoblasts transfected with a *TAZ* RNAi as well as BTHS cells transfected with MLCL AT-1. Healthy *TAZ* KD cells displayed a bioenergetic profile that was very similar to mock-transfected BTHS cells. This included elevated basal respiration and proton leak, as well as decreased ATP coupling efficiency. Surprisingly, spare respiratory capacity was not only different from BTHS cells, but it was also significantly higher than healthy cells. There are a number of explanations for this observation. As mentioned previously, *TAZ* KD in healthy 3798 cells led to increased MLCL AT-1 expression and unaltered CL mass. We also observed SC disruption, but not to the extent seen in BTHS cells. These results indicate that healthy cells express more robust rescue mechanisms compared to BTHS cells. Therefore, even though a number of mitochondrial functions were affected by the *TAZ* KD, the healthy cells appeared to be better able to cope with these cellular insults. The healthy 3798 lymphoblasts used in our study provided an excellent demonstration of the spare respiratory capacity mechanism observed in cells under normal conditions. Healthy cells should be able to respond to stress conditions

and increased workloads. These results may also be an indication that the major driving force behind the symptoms experienced by BTHS patients is their impaired mitochondrial spare respiratory capacity. Interestingly, 618 BTHS cells expressing *MLCL AT-1* showed significant improvements in certain aspects of mitochondrial function. Compared to mock transfected BTHS cells, *MLCL AT-1* expressing cells displayed significantly improved basal respiration and proton leak that more closely mimicked what was observed in healthy cells. Spare respiratory capacity and ATP coupling efficiency were not improved with the use *MLCL AT-1*. Despite the inability to show complete rescue of mitochondrial function, these results are very promising because they demonstrate that *MLCL AT-1* expression improves certain aspects of the BTHS mitochondrial phenotype. It is also important to remember that these results are reflective of a transient expression of MLCL AT-1 *in vitro*. Future experiments conducted *in vivo* may show improvement in overall mitochondrial function. Our current results provide us with a unique perspective of the potential mechanism behind the impaired mitochondrial function in BTHS cells. The improved basal respiration in MLCL AT-1 expressing BTHS cells is indicative of decreased ATP demand. This could potentially be the result of improved CV activity. As mentioned before, CL has been shown to be essential for the proper function and dimerization of CV [22, 155]. Thus, the increase in CL mass mediated by *MLCL AT-1* expression in BTHS cells may improve the function of CV. This would result in more efficient ATP production and thus, a lower basal respiration. Studies have shown that CV does not interact with other complexes of the ETC to form SCs, but instead exists in a dimeric form [51]. Thus, rescue of SC formation in BTHS cells may not be necessary for improved CV function.

As mentioned above, when ATP synthase is inhibited, respiration is heavily affected by proton leak kinetics and is thus very sensitive to mitochondrial uncoupling [152]. Our results indicated that 618 BTHS lymphoblasts may have significant mitochondrial uncoupling due to IMM damage, and thus, high proton leak. A likely reason for the reduction in proton leak observed in BTHS cells expressing *MLCL AT-1* is that the elevated CL pools may have led to diminished mitochondrial membrane damage. However, further investigation is required to determine if this has in fact occurred. Future experiments might involve examining the quality of the mitochondrial membrane potential in BTHS cells expressing *MLCL AT-1*. This potential mitochondrial membrane repair combined with improved complex function might be the reason for the improved mitochondrial function in BTHS cells expressing *MLCL AT-1*.

The Seahorse XF24 analyzer also serves to examine the extracellular acidification rates (ECARs) of cells. This feature helped us to compare the differences in glycolysis that exist between healthy and BTHS cells, and ultimately, aid in the understanding of the observed phenotypes in BTHS patients. We observed that 618 BTHS lymphoblasts exhibited higher rates of glycolysis compared to 3798 healthy cells. Currently, there are few studies that have examined glycolytic activity in BTHS cells. This is an important area of research that may help further explain the pathology of BTHS and also aid in the development of treatments. Under aerobic conditions, cells primarily utilize oxidative phosphorylation (Oxphos) as a fast and efficient way to generate ATP (reviewed in [162]). Glycolysis on the other hand, is utilized under anaerobic conditions. Oxphos is the preferred biochemical process for ATP production due to the fact that 36 ATP molecules can be made per metabolite, compared to

glycolysis which only produces two ATPs per metabolite [162]. A shift from oxphos to glycolysis is not ideal, but it may be necessary in BTHS cells to compensate for the lack of ATP produced as a result of impaired mitochondrial function. This dynamic shift from oxphos to glycolysis is potentially one of the main reasons why some BTHS patients are able to survive. Unfortunately, this shift may be the main reason why BTHS patients exhibit exercise intolerance. In the cytoplasm, glucose is converted to pyruvate which is then converted to lactate, which is ultimately excreted into the extracellular space. If the body produces lactate faster than it can process it then this results in fatigue and hence, exercise intolerance. The high glycolytic rates would explain why BTHS patients express this particular phenotype. Future studies will reveal if the use of MLCL AT-1 can alleviate this symptom by switching energy production from glycolysis to oxphos.

A number of diseases are associated with elevated ROS production including cardiovascular diseases [70], diabetes [71] and neurodegenerative disorders [72]. This has led to the hypothesis that excessive ROS generation may be playing a major role in the disease progression of BTHS. Despite this fact, there are only a few studies that have provided results comparing ROS production in BTHS cells and healthy controls. Using mitochondria from induced pluripotent stem cells (iPSC) derived from BTHS patients, Dudek *et al* measured ROS production using H_2DFFDA and compared it to controls [27]. They observed that iPSCs derived from BTHS patients displayed significantly higher levels of ROS compared to controls. Another study by Wang *et al*, generated cardiomyocytes derived from iPSCs and reported similar findings [88]. The only difference between the two studies was that Wang *et al* used the superoxide indicator MitoSOX to detect ROS production in their experiments [88] instead of

H_2DFFDA. Thus, these studies are in agreement that ROS production is elevated in BTHS cells. However, our study is among the first to demonstrate that this phenotype is in fact present in BTHS lymphoblasts obtained from a donor patient. Using flow cytometry to detect MitoSOX staining in our lymphoblast cell lines, our results showed that a significantly greater proportion of BTHS cells were positive for superoxide production compared to healthy controls. Interestingly, expression of *MLCL AT-1* in BTHS cells resulted in a reduced number of cells positive for superoxide production similar to that observed in healthy 3798 cells implying a reduction in ROS production in BTHS cells expressing MLCL AT-1. A limitation of this technique to study ROS production is that we cannot measure how much superoxide BTHS cells are producing compared to healthy controls. Instead, the technique allows for the detection of how many cells are positive for superoxide production at a specific fluorescence intensity. As shown in our results, the flow cytometry histograms generated displayed two distinct fluorescence peaks. To determine which peaks represent cells positive for superoxide production, a positive control was used in which cells were incubated with MitoSOX along with Antimycin A (AA). AA is a known inducer of superoxide production [163]. Thus, its addition should result in a larger proportion of cells producing superoxide. Indeed, the addition of AA resulted in nearly 100% of cells being positive for superoxide production. In addition, there was no difference in fluorescence intensity in all samples tested. This indicates that under our experimental conditions, AA does not induce cells to produce more superoxide, but increases the number of cells producing superoxide. Nevertheless, these experiments revealed that a significant difference in ROS production exists between 618 BTHS and 3798 healthy cells. Our current results agree

with previous reports [27, 88] and indicate the high likelihood that BTHS patients produce higher levels of ROS compared to healthy individuals. These results also correlated with our BN-PAGE results which demonstrated SC disruption in BTHS cells. Previous studies have shown that a decrease in SC formation leads to an increase in ROS production [79, 80]. Thus, the conclusion could be made that elevated ROS in BTHS cells is caused by SC disruption. However, *MLCL AT-1* expression in BTHS cells did not affect SC formation. Then, why did the proportion of cells positive for superoxide production decrease in these cells? There is currently no data to definitively answer this question. However, our mitochondrial function results may shed some light on this issue. As described previously, 618 BTHS lymphoblasts exhibited a significantly higher proton leak compared to 3798 healthy controls. Considering that a number of studies have shown that elevated ROS levels may cause significant increases in proton leak (reviewed by [164]), it is possible that the same phenomenon occurred in our BTHS cells. Studies conducted by Echtay *et al* showed that superoxide directly activated the proton leak pathway mediated by mitochondrial uncoupling proteins (UCPs) [165, 166]. Another important observation made by a number of studies is that CL plays a major role in the stabilization of UCPs [167, 168]. Taking this into consideration, it is possible that in BTHS cells, decreases in CL cause the destabilization of SCs leading to increased ROS production. Elevated ROS in the form of superoxide may up-regulate the activities of UCPs which in turn, induce proton leak. This, however, still does not explain the lack of SC formation in BTHS cells expressing *MLCL AT-1*. It is possible that the elevated CL levels observed in BTHS cells expressing *MLCL AT-1* are in fact improving SC production. As reported by Wittig *et al*, CL may be important for SC

stabilization, not formation [149]. Thus, perhaps the BN-PAGE technique used to isolate SCs in our lymphoblast experiments was too harsh to detect any improvements made possible by *MLCL AT-1* expression. The use of CN-PAGE, as described by Wittig *et al* [149], could reveal that *MLCL AT-1* expression in BTHS cells may stabilize SCs.

We used an inducible *Taz* KD mouse model to further investigate the role of *MLCL AT-1* in CL remodelling. Mejia *et al* previously showed that SC formation was decreased in the hearts of *Taz* KD mice, and this was correlated with decreased CI-containing SC activity in 10 month-old animals [28]. In addition, these mice exhibited significantly lower Taz protein expression in the heart (~50% KD), skeletal muscle (~85% KD) and liver (~80% KD), which was accompanied by significant reductions in overall CL mass compared to WT animals (~50%, ~70% and ~25% reductions in respective tissues, Cole L.K., unpublished data). One of the phenotypes we were interested in studying in this animal model was the SC formation in different tissues. Previous studies have observed that this *Taz* KD mouse model exhibits individual ETC complex dysfunction [146] as well as SC formation disturbances in heart tissue [28, 82]. However, the function of ETC complexes and their SC formations had not been examined in other tissues.

In our study, we examined CI, CII and CIV SC formation in heart, skeletal muscle and liver tissues of WT and *Taz* KD mice. Our results, similar to reports from other laboratories [28, 82], demonstrated that SC formation was disturbed in the heart mitochondria of *Taz* KD mice compared to control (Fig.21A, B and D). In addition, we observed SC dysfunction in skeletal muscle mitochondria of *Taz* KD mice compared to

control (Fig.22A, B and D). Surprisingly, no SC disturbance was observed in the liver mitochondria of *Taz* KD mice compared to control (Fig.23). Interestingly, SC formation in heart and skeletal muscle tissue of *Taz* KD mice was not entirely absent as observed in BTHS lymphoblasts. In fact, a few of the SC bands in *Taz* KD heart and skeletal muscle mitochondria displayed higher band intensity compared to WT. We hypothesize that this is not due to higher protein expression of respective complexes. Instead, this observation could be reflective of de-stabilization of higher order SCs as a result of decreased CL levels. As predicted by Pfeiffer *et al*, CL may only be responsible for SC stabilization, not formation [25]. Therefore, when performing BN-PAGE experiments to isolate SCs, the higher molecular weight SCs will be found at the top of the gel. If destabilized (via CL reduction), these SCs will break apart resulting in lower molecular weight complexes settling at lower parts of the gel. This may explain why, when looking at our CI and CIV in-gel activity assays, we see the un-complexed CI and CIV bands display significantly higher band intensities in *Taz* KD mice compared to WT. It appeared that CI and CIV were breaking apart from each other, thus, giving the impression that the activities of these complexes are elevated in *Taz* KD mice. Since BTHS lymphoblasts demonstrated little to no SC formation, it was surprising to see SCs were still present in the hearts and skeletal muscle mitochondria of *Taz* KD mice. As mentioned before, this could be due to differences in experimental conditions. Perhaps the use of the milder CN-PAGE to isolate SCs in BTHS lymphoblasts, as suggested by Pfeiffer *et al* [25], will allow observation of SCs in these cells. During our BN-PAGE optimization experiments using *T*az KD mice, we also observed that the isolation of SCs was dependent on the type of detergent used as well as its concentration. Isolated

mitochondria from WT and *Taz* KD mice were treated with 0.5% DDM before the separation of proteins via BN-PAGE. This resulted in the isolation of only a few SC bands in WT samples while no SCs were visualized in *Taz* KD samples (Fig.28). In our current study, we used 1% digitonin to isolate complexes from tissue mitochondria and observed that SCs were indeed present albeit at lower levels in heart and skeletal muscle mitochondria of *Taz* KD mice. Therefore, it is possible that BTHS patients may exhibit SC formation similar to healthy individuals, but they may be more unstable and easily disturbed.

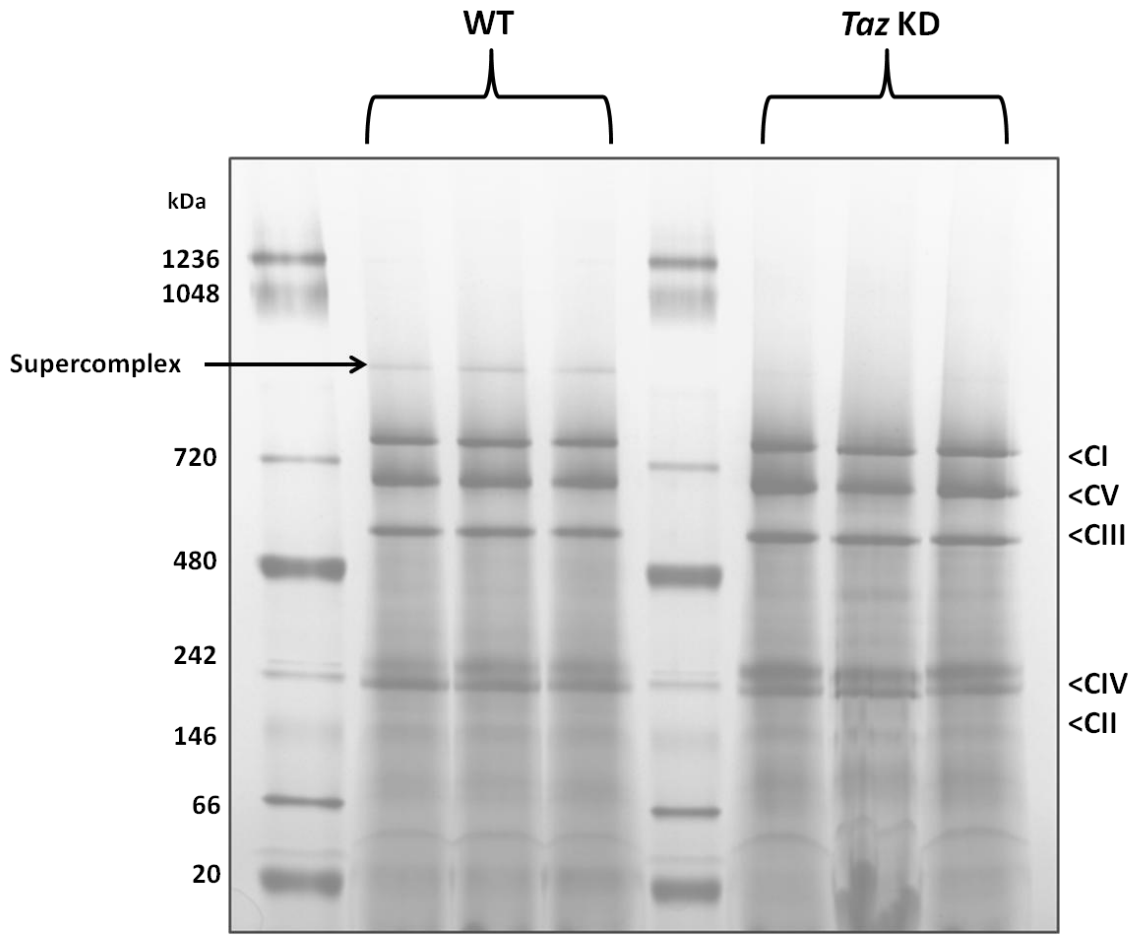

Figure 28: Cardiac mitochondria from WT and *Taz* KD mice subjected to BN-PAGE for the detection of ETC complexes.

Mitochondrial protein was isolated from WT and *Taz* KD heart and treated with 0.5% DDM followed by BN-PAGE. This image depicts a coomassie stained gel showing the separation of complexes I-V and the presence of SCs in the WT samples (n = 3 for both WT and *Taz* KD samples).

In addition to analyzing CI and CIV SCs and their activities, CII was studied in tissues of WT and *Taz* KD mice. Consistent with previous studies showing that CII does not assemble into SCs [51, 60, 61], our results showed that CII did not form SCs in any of the tissues examined. Also, there was no significant difference in CII expression or activity in all tissues examined between WT and *Taz* KD samples. This may be an indication that CII does not rely heavily on CL or TAZ for proper function. Other studies, however, have shown that CII associates with CL and its function is dependent on the presence of CL [169, 170]. Therefore, it is possible that CL is necessary for CII to perform various other biochemical functions, however, its enzymatic activity does not appear to be impaired when CL and TAZ are significantly reduced. Out of the three complexes analyzed in this study, CII was the only complex to maintain constant and unchanging expression in the heart, skeletal muscle and liver of both WT and *Taz* KD mice. Interestingly, CI and CIV SC expression varied between all three tissues tested. Currently, there are no studies that describe the different SC variations that may exist between different tissues. However, studies conducted on a wide variety of different cells from different organisms show that variations in SC formation exist. In our own results, we can see that SC formation differs between human lymphoblasts and mouse tissue. These observed differences between different cells and tissues are predicted by the 'plasticity' model of SC organization. As mentioned previously, this model hypothesizes that the organization of SCs can be adjusted depending on the cell type and also on the different metabolic demands of different tissues [58] . Essentially, SCs do not exist in a fixed state, but rather are dynamic and flexible components of the ETC that can rearrange their interactions with other complexes to meet certain metabolic

demands. For example, a study conducted by Ramirez-Aguilar *et al* showed that under hypoxic conditions, individual CI and CIV activities increased while SC formation decreased in potato tubers [59]. SC formation could be recovered once the plants were placed in normoxic conditions. Our results demonstrate that lymphoblasts, heart and skeletal muscle, display a greater number of SCs compared to liver. In fact, our BN-PAGE experiments revealed that liver tissue expressed little to no CIV SC formation. The differences we observed between heart, skeletal muscle and liver could explain why BTHS patients experience certain symptoms. BTHS patients primarily suffer from cardiomyopathies, skeletal myopathies, neutropenia and exercise intolerance [1, 2]. Symptoms involving liver dysfunctions, however, are not common in BTHS patients. Some BTHS patients exhibit a mild hypocholesterolemia [171], but for the most part this is an uncommon symptom. Our data indicates that SC formation is not only essential in heart and skeletal muscle, but is also significantly affected by decreases in Taz and CL. The differences in SC formation observed between the liver and the heart and skeletal muscle may be explained by the fact that the heart and skeletal muscle have similar metabolic demands that vary from those of the liver. This is not surprising considering the fact that cells in heart and skeletal muscle tissue experience variable and often high ATP demand. The brain is also another organ that is known to have very high energy demands and as such, neurons also experience variable ATP requirements. A study by Buck *et al* conducted in mouse brain mitochondria to analyze SC formation correlated with our own results and shows a high degree of CI, CIII and CIV SC formation [172]. Although SC analysis is yet to be conducted on *Taz* KD mouse brain, SC disturbances in this tissue would not be surprising considering that there have been reports showing

a cognitive phenotype in BTHS patients [3]. Therefore, our BN-PAGE experiments conducted on *Taz* KD mouse tissue demonstrate that this animal model is well suited for BTHS studies.

Our BN-PAGE experiments conducted in *Taz* KD mice showed that SCs were significantly affected. However, this was only apparent in the heart and skeletal muscle of these animals. Liver tissue on the other hand, not only had significantly lower CI and CV SCs, but exhibited no detectable differences between WT and *Taz* KD animals. Although it is possible that the difference in SC formation between liver and other tissues could be due to different metabolic demands, this does not explain the unaltered SC formation in *Taz* KD mice. Mejia *et al* used an αTFP heterozygous knockout mouse model (Mtpa(+/-)) to investigate differences in CL and MLCL AT-1 expression in heart and liver tissue [151]. In that study, Mtpa(+/-) mice had significant decreases in CL in both heart and liver tissue (~30% and ~20% reductions compared to WT, respectively) (Fig.25). Interestingly, MLCL AT-1 protein expression and enzyme activity was significantly reduced in the hearts of Mtpa(+/-) mice compared to controls. Even more surprising was that in liver, MLCL AT-1 protein and enzyme activity were not significantly different in Mtpa(+/-) mice compared to WT animals. In addition, MLCL AT-1 protein expression is greater in liver compared to heart mitochondria. BN-PAGE experiments revealed no significant differences in CI-containing SCs between WT and Mtpa(+/-) mice in both heart and liver tissue (Fig.26). It was concluded that the lack of SC disturbance in Mtpa(+/-) mice may be due to an insufficient decrease in CL. These results demonstrated that MLCL AT-1 exhibits differential expression in heart and liver, a topic that will require further investigation. However, these results may explain why

SCs from *Taz* KD liver mitochondria did not differ from WT samples. Higher MLCL AT-1 expression in the livers of *Taz* KD mice may compensate for a decrease in Taz. MLCL AT-1 expression in heart (and possibly skeletal muscle) may not be sufficient to counteract the effects of lower *Taz* and CL in Taz KD mice. Our recent study using the Mtpa(+/-) mouse model, also revealed that the heart experienced greater decreases in CL compared to the liver (Fig.25) [151], an indication that perhaps other mechanisms in the liver are present that can compensate for any potential mitochondrial disturbances. The differences we observed in αTFP and MLCL AT-1 protein levels between the heart and liver could be a result of differences in energy metabolism in these tissues. The heart predominantly uses fatty acids (catabolized by β-oxidation) as its main energy source, accounting for 60-90% of the total energy production [173]. The liver on the other hand, utilizes glucose as its main energy source when carbohydrates are abundant [174]. The αTFP is a subunit of the MTP, an enzyme complex responsible for performing 3 out of the 4 reactions involved in fatty acid β-oxidation [128]. Therefore, it was not surprising that the αTFP subunit was significantly more abundant in heart tissue compared to the liver (Fig.25A & B) [151]. The heart's heavy reliance on fatty acid oxidation for energy may be the reason why the production of MLCL AT-1 is significantly lower compared to the liver. It is possible that translation of the full-length αTFP mRNA takes priority over the production of the MLCL AT-1 splice variant in heart tissue, whereas in the liver, the production of both αTFP and MLCL AT-1 may be less regulated. Thus, alterations in αTFP may have little to no effect on MLCL AT-1 expression in the liver. In the event of a loss of Taz, MLCL AT-1 would be more readily available to compensate for its decrease in the liver.

Previous studies have shown that SC formation helps to minimize ROS production by mitochondria [79, 80]. Elevated ROS levels can cause mtDNA mutations [73], oxidize the complexes of the ETC themselves [74] and cause phospholipid peroxidation [75]. Our own results have shown that a greater proportion of BTHS lymphoblasts produced superoxide compared to healthy controls. Thus, we set out to measure ROS production in the hearts, skeletal muscle and livers of both WT and *Taz* KD mice. Our results show that both heart and skeletal muscle mitochondria from *Taz* KD mice produce significantly greater amounts of hydrogen peroxide (H_2O_2) compared to WT samples. The livers of *Taz* KD mice on the other hand, produce significantly less H_2O_2 compared to WT mice. The primary ROS product from mitochondria is superoxide [175, 176]. However, due to its low biochemical reactivity and its negative charge, which prevents its entry into mitochondrial membranes [175], it is not believed to be the main culprit in ROS-induced cellular damage. Upon its initial production, superoxide is quickly converted to H_2O_2 by superoxide dismutase (SOD). It is H_2O_2 that is electrically neutral allowing it to cross membranes and react with cellular targets such as protein SH groups [177]. This can also lead to the production of electrically neutral yet highly reactive hydroxyl radicals. Therefore, excessive H_2O_2 production can lead to many cellular defects and could be a driving force in the symptoms experienced by BTHS patients. The significantly higher ROS levels observed in heart and skeletal muscle mitochondria of *Taz* KD mice compared to WT correlated with the SC disturbances observed in these tissues. This is an indication that destabilizing SCs can lead to higher ROS levels which are potentially contributing to or are responsible for the cardiomyopathies and skeletal myopathies observed in BTHS patients. Links between

cardiomyopathies and oxidative stress have already been established by many studies (reviewed in [178, 179]). Thus, if excessive ROS production is a key factor in the development of BTHS, a potential therapeutic approach would be the administration of antioxidants. This approach has already been explored via numerous clinical trials that have examined the potential for antioxidants to prevent or even treat cardiovascular diseases (reviewed in [70]). Unfortunately, results from these clinical trials have yielded conflicting and often deleterious effects caused by the use of antioxidants to treat cardiovascular diseases (reviewed in [70]). This is most likely due to the fact that ROS are more than just by-products of mitochondrial respiration, but are also molecules that play key roles in various signalling pathways [68, 69]. Thus, direct interference with their production can have negative consequences. A more effective therapeutic approach might be targeting the causes that lead to elevated ROS production instead of targeting ROS itself.

Interestingly, liver mitochondria were shown to produce significantly lower concentrations of H_2O_2 in *Taz* KD mice compared to WT. Whether or not this is a beneficial or detrimental phenotype caused by Taz reductions requires further investigation. Much like elevated ROS produced by the hearts and skeletal muscle in this BTHS animal model, this phenotype could be the cause or the result of cellular dysfunctions. As mentioned previously, ROS species have been shown to play important signalling roles in cellular pathways [68, 69], and any interference may have adverse effects. Based on our observations in the livers of *Taz* KD mouse mice, the phenotypes displayed do not indicate that decreased ROS production results in cellular disruptions. *Taz* KD mice have lean bodies, elevated fatty acid oxidation (FAO) and are

not prone to insulin resistance under a high fat diet (Cole L.K., unpublished data). How a decreased production of ROS in these mice fits with the rest of the phenotypes is something that is still under investigation. One thing we know for sure is that compared to the heart and skeletal muscle, the liver is unique. Unlike the heart and skeletal muscle, the liver does not experience SC disruption. In addition, the liver experienced the least amount of total CL decrease compared to the other tissues (Cole L.K., unpublished data). We also know from our studies in the Mtpa(+/-) mice that MLCL AT-1 expression is greater in the liver compared to the heart and is independent of αTFP function [151]. Taking all of these observations into consideration, it is evident that the liver is equipped with compensatory mechanisms to minimize the effects of Taz loss. Similar to results obtained from healthy lymphoblasts in which *TAZ* was knocked down, it is possible that MLCL AT-1 expression is elevated in *Taz* KD mice preventing large decreases in CL mass. This hypothesis may also be a gateway to understanding how MLCL AT-1 works in relation to ROS production in the liver. Since H_2O_2 concentrations were decreased in the livers of *Taz* KD mice, it is worth considering the possibility that catalase may play a role in this animal model. Catalases are a group of enzymes found in nearly all living organisms exposed to oxygen, that catalyze the breakdown of H_2O_2 into water and oxygen [180]. As previously mentioned, excessive H_2O_2 may be harmful to cells, and so catalases must break it down to water and oxygen which are compounds that are less reactive in cells [180, 181]. Therefore, an elevated expression of catalase would result in a reduction in H_2O_2 concentrations. A number of studies have shown that catalase expression is increased in certain pathological conditions. A study conducted by Sundaram *et al* using spontaneously hypertensive rats (SHR)

showed that H_2O_2 levels in the kidneys of these rats were significantly lower compared to WT [182]. The authors also reported that pre-hypertensive SHRs produced significantly higher catalase activity compared to WT rats. The authors hypothesized that an increase in catalase activity precedes the development of hypertension [182]. Other studies have investigated the role of catalase in metabolic syndrome and have reported increases in catalase activity [183, 184]. However, there are inconsistencies in this claim do to the fact that other studies have shown the opposite effect of catalase in metabolic syndrome [185]. Nevertheless, it can be seen that catalase may be playing an essential role in a number of diseases. The same may be true in BTHS patients. A significant decrease in CL has been shown to produce a number of cellular insults. In the liver, however, the effects are diminished by rescue mechanisms that prevent large decreases in CL. These same mechanisms may be allowing catalase to breakdown the elevated H_2O_2 levels produced as a result of decreased mitochondrial function. This is a topic that warrants further investigation in future studies.

To date over one-hundred different TAZ mutations have been recorded in BTHS patients [109]. However, no link between genotype and phenotype has been described. When *TAZ* was knocked down in 3798 healthy cells, CL mass did not decrease significantly. The increase in *MLCL AT-1* expression observed in 3798 *TAZ* KD cells may be a compensatory mechanism that helps prevent a decrease in CL similar to that observed in BTHS cells. It is possible that MLCL AT-1 may play a role of varying significance in different BTHS patients. This might explain why some patients experience severe and wide-spread symptoms while others are asymptomatic. Thus, the increase in *MLCL AT-1* expression following a decrease in *TAZ* gene expression

may explain how some BTHS patients are able to survive despite the loss of tafazzin, an enzyme which is crucial for proper cardiac development.

Conclusion

For this thesis, my objectives were: 1) to gain a better understanding of the inter-relationship that may or may not exist between TAZ and MLCL AT-1, 2) to determine if MLCL AT-1 expression in BTHS lymphoblasts lead to improvements in mitochondrial function, and 3) to use the *Taz* KD mouse model to get a better understanding of the phenotypes displayed by BTHS patients. Our *in vitro* work using Epstein-Barr virus transformed lymphoblasts from a BTHS patient and an age-matched healthy control helped us achieve our first two objectives. Our results demonstrated that healthy lymphoblasts transfected with a *TAZ* RNAi had significantly lower TAZ mRNA and protein expression. These cells responded to TAZ reductions by significantly elevating their expression of MLCL AT-1. In healthy lymphoblasts with *TAZ* KD, CL mass was not reduced, potentially due to compensatory mechanisms employed by these cells via elevated MLCL AT-1 expression. In BTHS lymphoblasts, TAZ and MLCL AT-1 expression was significantly reduced. These results correlated with a significantly lower CL mass in BTHS cells compared to healthy controls. Transfection of healthy and BTHS lymphoblasts with a MLCL AT-1-carrying plasmid, elevated MLCL AT-1 gene, protein and enzyme activity in both cell lines. This resulted in a significantly higher CL mass in both of these cell lines. Knock down of *TAZ* in healthy lymphoblasts resulted in CI-containing SC disturbance compared to healthy controls. BTHS cells also displayed

CI-containing SC disturbance that was more severe than that observed in healthy cells with *TAZ* KD. In addition, mitochondrial function tests (using a Seahorse XF analyzer) revealed that BTHS cells experience significant mitochondrial dysfunction compared to healthy controls. Knock down of *TAZ* in healthy cells resulted in a mitochondrial function profile that mimics that of BTHS cells. However, unlike BTHS cells, healthy cells were better able to cope with the *TAZ* KD by increasing their spare respiratory capacity. We were also able to analyze rates of glycolysis in healthy and BTHS lymphoblasts using the XF analyzer. Our results showed that BTHS cells have significantly higher rates of glycolysis compared to healthy controls, which indicates that BTHS cells require alternative means to meet their ATP demands. Mitochondrial ROS production was also measured in these cell lines and our data showed that a greater proportion of BTHS cells produced superoxide compared to healthy controls. Since MLCL AT-1 expression could be elevated in BTHS cells, and its expression lead to significant increases in CL mass, we wanted to determine if MLCL AT-1 could reverse any of the observed phenotypes. Our results showed that SC formation could not be improved in BTHS cells expressing *MLCL AT-1*, however, certain aspects of mitochondrial function were significantly improved. The proportion of BTHS cells positive for superoxide production was significantly lower in BTHS cells expressing MLCL AT-1.

Using a dox-inducible *Taz* KD mouse model, we studied SC formation in heart, skeletal muscle and liver mitochondria. Our *ex vivo* results showed that mitochondrial SC formation was disturbed in the hearts and skeletal muscle of the *Taz* KD mice compared to WT samples. No differences in SC formation were observed in liver

mitochondria between WT and *Taz* KD mice. These results correlated with results obtained from our ROS experiments using mitochondria isolated from these tissues. Heart and skeletal muscle mitochondria from *Taz* KD mice produced significantly higher concentrations of H_2O_2 compared to WT samples. On the other hand, liver mitochondria from *Taz* KD mice produced significantly less H_2O_2 compared to WT liver.

In conclusion, our results have demonstrated that MLCL AT-1 expression is dependent on the presence of functional TAZ. Our results also indicate that MLCL AT-1 has a compensatory role in cells to ensure that CL levels remain unaffected despite cellular insult. In addition, expression of MLCL AT-1 in BTHS cells improves some aspects of mitochondrial function, however, this compensatory mechanism may only be possible provided that mitochondrial function is not grossly impaired. In addition, the use of the *Taz* KD mouse model has proven to be highly effective in helping us gain a better understanding of the phenotypes associated with BTHS. Its use in future research to determine the effects of MLCL AT-1 expression is highly warranted. Thus, MLCL AT-1 may potentially be a new therapeutic approach for the treatment of BTHS.

Future Directions

The work conducted in this study has helped improve our understanding of the role MLCL AT-1 plays in CL remodelling. Research conducted on MLCL AT-1 has come a long way, from the initial acyl CoA-dependent acyltransferase activity detected by Ma *et al* [131], to the identification of the human MLCL AT-1 enzyme by Taylor *et al*

[18]. However, additional work is still required to address some of the questions that remain unanswered.

From our current study and the work conducted by Taylor *et al* [18], we know that MLCL AT-1 elevates CL mass in BTHS cells. However, the use of additional BTHS cell lines is still required to test various findings from this study. For example, the use of 618 BTHS lymphoblasts revealed that MLCL AT-1 expression was significantly lower than in healthy 3798 cells. It would be interesting to see if this is true for all BTHS patients, or if there exist differences in MLCL AT-1 expression between patients. This type of information would shed light on the current observation that the genotype of BTHS patients does not match their phenotype [110]. Perhaps MLCL AT-1 compensatory mechanisms play a role in determining which patients suffer from severe symptoms and which ones are asymptomatic.

Compensatory mechanisms are predicted to play important roles in BTHS patients. As mentioned previously, a common characteristic in BTHS lymphoblasts is an increased mitochondrial mass [123]. This correlates with results from our own study showing increased mitochondrial basal respiration, which we hypothesize to be due to increased ATP demand by BTHS cells. In addition, significantly elevated rates of glycolysis and citrate synthase activity have been found in these cells, which also indicate an attempt to compensate for their inefficient ATP production. Expression of *MLCL AT-1* in BTHS cells has been shown to improve mitochondrial function by decreasing the basal respiration as well as the proton leak to levels that more closely resemble those of healthy cells. Future experiments need to be conducted to better understand the specific effect that MLCL AT-1 is having on BTHS cells. One possibility

is that perhaps MLCL AT-1 is affecting mitochondrial membrane potentials. Tetramethylrhodamin-methylester (TMRM), is a cationic fluorescent dye that is readily taken up by mitochondria due to its negatively charged interior. TMRM may be used to measure mitochondrial membrane potential in a variety of cells. The use of TMRM in future experiments may help elucidate how MLCL AT-1 is helping improve mitochondrial function in BTHS cells. Since MLCL AT-1 is predicted to improve mitochondrial function in BTHS cells, it would be interesting to see the effects that MLCL AT-1 has on glycolysis. We hypothesize that the rate of glycolysis would decrease after the expression of MLCL AT-1 in BTHS cells due to improved mitochondrial function resulting in more efficient oxidative phosphorylation.

The future work conducted on this project will primarily involve the use of the *Taz* KD mouse model. Currently, this animal model has provided us with a wealth of information about the characteristic phenotypes found in BTHS patients. Analysis of the mitochondrial SCs has shown us that specific tissues (e.g. heart and skeletal muscle) are more susceptible to decreases in *Taz*. The next step in our research will be to study the effects of MLCL AT-1 expression in the *Taz* KD mouse model. Our laboratory has already established a lentiviral-mediated gene delivery system which we plan to use to transfect *MLCL AT-1* into the *Taz* KD mouse. We will then examine if SC disturbance can be reversed if not improved, and we will test to see if mitochondrial function can also be improved in this animal model. Preliminary mitochondrial function experiments have already revealed mitochondrial dysfunction in heart, skeletal muscle and liver cells in the *Taz* KD mouse (Cole L.K., unpublished data). Since our experiments have revealed that certain tissues are more susceptible to *Taz* disturbances, it may be

necessary to also work on a tissue-specific expression of *MLCL AT-1* to minimize any potential side-effects.

The results obtained from the analysis of SCs in the *Taz* KD mouse revealed that the liver does not behave like the heart or skeletal muscle. In the liver of *Taz* KD mice, SC formation is not affected and there is a decrease in ROS compared to WT controls. These observations will require further research in order to understand the unique nature of the liver. As mentioned previously, we hypothesize that MLCL AT-1 expression is higher in the liver, which could be compensating for a decrease in Taz. It would be interesting to selectively KD both *Taz* and *MLCL AT-1* in the liver to determine if this would have an effect on SC formation and ROS production. The BN-PAGE work conducted in the *Taz* KD mouse has helped us gain a better understanding of the symptoms experienced by BTHS patients. We now know that the heart and skeletal muscle are particularly susceptible to changes in *Taz* levels. This is why a better understanding of MLCL AT-1 in these (and other tissues) is necessary. If in fact this is due to the differences in MLCL AT-1 expression in these tissues, it would indicate that the BTHS phenotype can be treated with the use of MLCL AT-1.

Ultimately, our goal is to one day administer MLCL AT-1 to BTHS patients. This novel therapeutic approach addresses some of the issues affecting the current treatments available, including: invasive surgeries and pharmacotherapeutic approaches that target only one symptom.

References

1. Barth, P.G., et al., *An X-linked mitochondrial disease affecting cardiac muscle, skeletal muscle and neutrophil leucocytes.* Journal of the neurological sciences, 1983. **62**(1-3): p. 327-355.
2. Kelley, R.I., et al., *X-linked dilated cardiomyopathy with neutropenia, growth retardation, and 3-methylglutaconic aciduria.* The Journal of pediatrics, 1991. **119**(5): p. 738-747.
3. Mazzocco, M.M., A.E. Henry, and R.I. Kelly, *Barth syndrome is associated with a cognitive phenotype.* Journal of developmental and behavioral pediatrics : JDBP, 2007. **28**(1): p. 22-30.
4. Bolhuis, P.A., et al., *Mapping of the locus for X-linked cardioskeletal myopathy with neutropenia and abnormal mitochondria (Barth syndrome) to Xq28.* American Journal of Human Genetics, 1991. **48**(3): p. 481-485.
5. Ades, L.C., et al., *Barth syndrome: clinical features and confirmation of gene localisation to distal Xq28.* American Journal of Medical Genetics, 1993. **45**(3): p. 327-334.
6. Bione, S., et al., *A novel X-linked gene, G4.5. is responsible for Barth syndrome.* Nature genetics, 1996. **12**(4): p. 385-389.
7. Xu, Y., et al., *The enzymatic function of tafazzin.* The Journal of biological chemistry, 2006. **281**(51): p. 39217-39224.
8. Daum, G., *Lipids of mitochondria.* Biochim Biophys Acta, 1985. **822**(1): p. 1-42.

9. Hostetler, K.Y., *Polyglycerophospholipids: phosphatidylglycerol, diphosphatidylglycerol and bis (monoacylglycero) phosphate*, in *Phospholipids*, J.N. Hawthorne and G.B. Ansell, Editors. 1982. p. 215.
10. Hatch, G.M., *Cell biology of cardiac mitochondrial phospholipids.* Biochemistry and cell biology = Biochimie et biologie cellulaire, 2004. **82**(1): p. 99-112.
11. Pangborn, M., *Isolation and purfication of a serologically active phospholipid from beef heart.* J.Biol.Chem., 1942. **143**: p. 247.
12. Schlame, M. and D. Haldar, *Cardiolipin is synthesized on the matrix side of the inner membrane in rat liver mitochondria.* The Journal of biological chemistry, 1993. **268**(1): p. 74-79.
13. de Kroon, A.I., et al., *Phospholipid composition of highly purified mitochondrial outer membranes of rat liver and Neurospora crassa. Is cardiolipin present in the mitochondrial outer membrane?* Biochimica et biophysica acta, 1997. **1325**(1): p. 108-116.
14. Daum, G. and J.E. Vance, *Import of lipids into mitochondria.* Progress in lipid research, 1997. **36**(2-3): p. 103-130.
15. Mejia, E.M. and G.M. Hatch, *Mitochondrial phospholipids: role in mitochondrial function.* J Bioenerg Biomembr, 2015.
16. Renner, L.D. and D.B. Weibel, *Cardiolipin microdomains localize to negatively curved regions of Escherichia coli membranes.* Proc Natl Acad Sci U S A, 2011. **108**(15): p. 6264-9.

17. Schlame, M., et al., *Molecular symmetry in mitochondrial cardiolipins.* Chemistry and physics of lipids, 2005. **138**(1-2): p. 38-49.

18. Taylor, W.A. and G.M. Hatch, *Identification of the human mitochondrial linoleoyl-coenzyme A monolysocardiolipin acyltransferase (MLCL AT-1).* The Journal of biological chemistry, 2009. **284**(44): p. 30360-30371.

19. Gebert, N., et al., *Mitochondrial cardiolipin involved in outer-membrane protein biogenesis: implications for Barth syndrome.* Current biology : CB, 2009. **19**(24): p. 2133-2139.

20. Chen, S., et al., *Cardiolipin mediates cross-talk between mitochondria and the vacuole.* Molecular biology of the cell, 2008. **19**(12): p. 5047-5058.

21. Gonzalvez, F., et al., *Cardiolipin provides an essential activating platform for caspase-8 on mitochondria.* The Journal of cell biology, 2008. **183**(4): p. 681-696.

22. Gonzalvez, F., et al., *Barth syndrome: cellular compensation of mitochondrial dysfunction and apoptosis inhibition due to changes in cardiolipin remodeling linked to tafazzin (TAZ) gene mutation.* Biochimica et biophysica acta, 2013. **1832**(8): p. 1194-1206.

23. Lutter, M., et al., *Cardiolipin provides specificity for targeting of tBid to mitochondria.* Nature cell biology, 2000. **2**(10): p. 754-761.

24. Kuwana, T., et al., *Bid, Bax, and lipids cooperate to form supramolecular openings in the outer mitochondrial membrane.* Cell, 2002. **111**(3): p. 331-342.

25. Pfeiffer, K., et al., *Cardiolipin stabilizes respiratory chain supercomplexes.* The Journal of biological chemistry, 2003. **278**(52): p. 52873-52880.

26. Zhang, M., E. Mileykovskaya, and W. Dowhan, *Gluing the respiratory chain together. Cardiolipin is required for supercomplex formation in the inner mitochondrial membrane.* The Journal of biological chemistry, 2002. **277**(46): p. 43553-43556.

27. Dudek, J., et al., *Cardiolipin deficiency affects respiratory chain function and organization in an induced pluripotent stem cell model of Barth syndrome.* Stem cell research, 2013. **11**(2): p. 806-819.

28. Mejia, E.M., L. Cole, and G.M. Hatch, *Cardiolipin metabolism and the role it plays in heart failure and mitochondrial supercomplex formation.* Cardiovasc. Haematol. Disord. Drug Targets, 2014.

29. Elmore, S., *Apoptosis: a review of programmed cell death.* Toxicol Pathol, 2007. **35**(4): p. 495-516.

30. Youle, R.J. and D.P. Narendra, *Mechanisms of mitophagy.* Nat Rev Mol Cell Biol, 2011. **12**(1): p. 9-14.

31. Chu, C.T., H. Bayir, and V.E. Kagan, *LC3 binds externalized cardiolipin on injured mitochondria to signal mitophagy in neurons: implications for Parkinson disease.* Autophagy, 2014. **10**(2): p. 376-8.

32. Wang, Y. and J.S. Morrow, *Identification and characterization of human SLP-2, a novel homologue of stomatin (band 7.2b) present in erythrocytes and other tissues.* J Biol Chem, 2000. **275**(11): p. 8062-71.

33. Owczarek, C.M., et al., *A novel member of the STOMATIN/EPB72/mec-2 family, stomatin-like 2 (STOML2), is ubiquitously expressed and localizes to HSA chromosome 9p13.1.* Cytogenet Cell Genet, 2001. **92**(3-4): p. 196-203.

34. Kirchhof, M.G., et al., *Modulation of T cell activation by stomatin-like protein 2.* J Immunol, 2008. **181**(3): p. 1927-36.

35. Christie, D.A., et al., *Stomatin-like protein 2 binds cardiolipin and regulates mitochondrial biogenesis and function.* Molecular and cellular biology, 2011. **31**(18): p. 3845-3856.

36. Da Cruz, S., et al., *SLP-2 interacts with prohibitins in the mitochondrial inner membrane and contributes to their stability.* Biochim Biophys Acta, 2008. **1783**(5): p. 904-11.

37. Tatsuta, T., K. Model, and T. Langer, *Formation of membrane-bound ring complexes by prohibitins in mitochondria.* Mol Biol Cell, 2005. **16**(1): p. 248-59.

38. Steglich, G., W. Neupert, and T. Langer, *Prohibitins regulate membrane protein degradation by the m-AAA protease in mitochondria.* Mol Cell Biol, 1999. **19**(5): p. 3435-42.

39. Nijtmans, L.G., et al., *Prohibitins act as a membrane-bound chaperone for the stabilization of mitochondrial proteins.* EMBO J, 2000. **19**(11): p. 2444-51.

40. Artal-Sanz, M., et al., *The mitochondrial prohibitin complex is essential for embryonic viability and germline function in Caenorhabditis elegans.* J Biol Chem, 2003. **278**(34): p. 32091-9.

41. Beyer, K. and M. Klingenberg, *ADP/ATP carrier protein from beef heart mitochondria has high amounts of tightly bound cardiolipin, as revealed by 31P nuclear magnetic resonance.* Biochemistry, 1985. **24**(15): p. 3821-6.

42. Schlame, M., et al., *Molecular species of cardiolipin in relation to other mitochondrial phospholipids. Is there an acyl specificity of the interaction between cardiolipin and the ADP/ATP carrier?* Eur J Biochem, 1991. **199**(2): p. 459-66.

43. Hoffmann, B., et al., *The reconstituted ADP/ATP carrier activity has an absolute requirement for cardiolipin as shown in cysteine mutants.* J Biol Chem, 1994. **269**(3): p. 1940-4.

44. Jiang, F., et al., *Absence of cardiolipin in the crd1 null mutant results in decreased mitochondrial membrane potential and reduced mitochondrial function.* J Biol Chem, 2000. **275**(29): p. 22387-94.

45. Hostetler, K.Y., H. Van den Bosch, and L.L. Van Deenen, *Biosynthesis of cardiolipin in liver mitochondria.* Biochimica et biophysica acta, 1971. **239**(1): p. 113-119.

46. McAuley, K.E., et al., *Structural details of an interaction between cardiolipin and an integral membrane protein.* Proc Natl Acad Sci U S A, 1999. **96**(26): p. 14706-11.

47. Wakeham, M.C., et al., *Is there a conserved interaction between cardiolipin and the type II bacterial reaction center?* Biophys J, 2001. **80**(3): p. 1395-405.

48. Chance, B. and G.R. Williams, *A method for the localization of sites for oxidative phosphorylation.* Nature, 1955. **176**(4475): p. 250-254.

49. Vartak, R., C.A. Porras, and Y. Bai, *Respiratory supercomplexes: structure, function and assembly.* Protein & cell, 2013. **4**(8): p. 582-590.

50. Hatefi, Y., A.G. Haavik, and D.E. Griffiths, *Studies on the electron transfer system. XL. Preparation and properties of mitochondrial DPNH-coenzyme Q reductase.* J Biol Chem, 1962. **237**: p. 1676-80.

51. Schagger, H. and K. Pfeiffer, *Supercomplexes in the respiratory chains of yeast and mammalian mitochondria.* The EMBO journal, 2000. **19**(8): p. 1777-1783.

52. Dudkina, N.V., et al., *Structure and function of mitochondrial supercomplexes.* Biochim Biophys Acta, 2010. **1797**(6-7): p. 664-70.

53. Eubel, H., et al., *Respiratory chain supercomplexes in plant mitochondria.* Plant Physiol Biochem, 2004. **42**(12): p. 937-42.

54. Hackenbrock, C.R., B. Chazotte, and S.S. Gupte, *The random collision model and a critical assessment of diffusion and collision in mitochondrial electron transport.* J Bioenerg Biomembr, 1986. **18**(5): p. 331-68.

55. Chazotte, B. and C.R. Hackenbrock, *The multicollisional, obstructed, long-range diffusional nature of mitochondrial electron transport.* J Biol Chem, 1988. **263**(28): p. 14359-67.

56. Gupte, S.S. and C.R. Hackenbrock, *The role of cytochrome c diffusion in mitochondrial electron transport.* J Biol Chem, 1988. **263**(11): p. 5248-53.

57. Trouillard, M., B. Meunier, and F. Rappaport, *Questioning the functional relevance of mitochondrial supercomplexes by time-resolved analysis of the respiratory chain.* Proc Natl Acad Sci U S A, 2011. **108**(45): p. E1027-34.

58. Acin-Perez, R. and J.A. Enriquez, *The function of the respiratory supercomplexes: the plasticity model.* Biochim Biophys Acta, 2014. **1837**(4): p. 444-50.

59. Ramirez-Aguilar, S.J., et al., *The composition of plant mitochondrial supercomplexes changes with oxygen availability.* J Biol Chem, 2011. **286**(50): p. 43045-53.

60. Eubel, H., L. Jansch, and H.P. Braun, *New insights into the respiratory chain of plant mitochondria. Supercomplexes and a unique composition of complex II.* Plant Physiol, 2003. **133**(1): p. 274-86.

61. Acin-Perez, R., et al., *Respiratory active mitochondrial supercomplexes.* Molecular cell, 2008. **32**(4): p. 529-539.

62. Arnold, I., et al., *Yeast mitochondrial F1F0-ATP synthase exists as a dimer: identification of three dimer-specific subunits.* EMBO J, 1998. **17**(24): p. 7170-8.

63. Li, Y., et al., *An assembled complex IV maintains the stability and activity of complex I in mammalian mitochondria.* J Biol Chem, 2007. **282**(24): p. 17557-62.

64. Acin-Perez, R., et al., *Respiratory complex III is required to maintain complex I in mammalian mitochondria.* Mol Cell, 2004. **13**(6): p. 805-15.

65. Marques, I., et al., *Supramolecular organization of the respiratory chain in Neurospora crassa mitochondria.* Eukaryot Cell, 2007. **6**(12): p. 2391-405.

66. Moreno-Lastres, D., et al., *Mitochondrial complex I plays an essential role in human respirasome assembly.* Cell Metab, 2012. **15**(3): p. 324-35.

67. Murphy, M.P., *How mitochondria produce reactive oxygen species.* Biochem J, 2009. **417**(1): p. 1-13.

68. Ray, P.D., B.W. Huang, and Y. Tsuji, *Reactive oxygen species (ROS) homeostasis and redox regulation in cellular signaling.* Cell Signal, 2012. **24**(5): p. 981-90.

69. Yang, Y., et al., *Reactive oxygen species in the immune system.* Int Rev Immunol, 2013. **32**(3): p. 249-70.

70. Sugamura, K. and J.F. Keaney, Jr., *Reactive oxygen species in cardiovascular disease.* Free Radic Biol Med, 2011. **51**(5): p. 978-92.

71. Ha, H., et al., *Role of reactive oxygen species in the pathogenesis of diabetic nephropathy.* Diabetes Res Clin Pract, 2008. **82 Suppl 1**: p. S42-5.

72. Uttara, B., et al., *Oxidative stress and neurodegenerative diseases: a review of upstream and downstream antioxidant therapeutic options.* Curr Neuropharmacol, 2009. **7**(1): p. 65-74.

73. Yakes, F.M. and B. Van Houten, *Mitochondrial DNA damage is more extensive and persists longer than nuclear DNA damage in human cells following oxidative stress.* Proc Natl Acad Sci U S A, 1997. **94**(2): p. 514-9.

74. Musatov, A. and N.C. Robinson, *Susceptibility of mitochondrial electron-transport complexes to oxidative damage. Focus on cytochrome c oxidase.* Free Radic Res, 2012. **46**(11): p. 1313-26.

75. Reis, A. and C.M. Spickett, *Chemistry of phospholipid oxidation.* Biochim Biophys Acta, 2012. **1818**(10): p. 2374-87.

76. Lenaz, G., et al., *New insights into structure and function of mitochondria and their role in aging and disease.* Antioxid Redox Signal, 2006. **8**(3-4): p. 417-37.

77. Hirst, J., M.S. King, and K.R. Pryde, *The production of reactive oxygen species by complex I.* Biochem Soc Trans, 2008. **36**(Pt 5): p. 976-80.

78. Bleier, L. and S. Drose, *Superoxide generation by complex III: from mechanistic rationales to functional consequences.* Biochim Biophys Acta, 2013. **1827**(11-12): p. 1320-31.

79. Maranzana, E., et al., *Mitochondrial respiratory supercomplex association limits production of reactive oxygen species from complex I.* Antioxidants & redox signaling, 2013. **19**(13): p. 1469-1480.

80. Diaz, F., J.A. Enriquez, and C.T. Moraes, *Cells lacking Rieske iron-sulfur protein have a reactive oxygen species-associated decrease in respiratory complexes I and IV.* Mol Cell Biol, 2012. **32**(2): p. 415-29.

81. Brandner, K., et al., *Taz1, an outer mitochondrial membrane protein, affects stability and assembly of inner membrane protein complexes: implications for Barth Syndrome.* Molecular biology of the cell, 2005. **16**(11): p. 5202-5214.

82. Huang, Y., et al., *Cardiac metabolic pathways affected in the mouse model of barth syndrome.* PLoS One, 2015. **10**(6): p. e0128561.

83. McKenzie, M., et al., *Mitochondrial respiratory chain supercomplexes are destabilized in Barth Syndrome patients.* Journal of Molecular Biology, 2006. **361**(3): p. 462-469.

84. Shidoji, Y., et al., *Loss of molecular interaction between cytochrome c and cardiolipin due to lipid peroxidation.* Biochem Biophys Res Commun, 1999. **264**(2): p. 343-7.

85. Liu, X., et al., *Induction of apoptotic program in cell-free extracts: requirement for dATP and cytochrome c.* Cell, 1996. **86**(1): p. 147-57.

86. Li, P., et al., *Cytochrome c and dATP-dependent formation of Apaf-1/caspase-9 complex initiates an apoptotic protease cascade.* Cell, 1997. **91**(4): p. 479-89.

87. Kroemer, G. and J.C. Reed, *Mitochondrial control of cell death.* Nat Med, 2000. **6**(5): p. 513-9.

88. Wang, G., et al., *Modeling the mitochondrial cardiomyopathy of Barth syndrome with induced pluripotent stem cell and heart-on-chip technologies.* Nat Med, 2014. **20**(6): p. 616-23.

89. Hatch, G.M., *Regulation of cardiolipin biosynthesis in the heart.* Mol Cell Biochem, 1996. **159**(2): p. 139-48.

90. Schlame, M., *Cardiolipin synthesis for the assembly of bacterial and mitochondrial membranes.* Journal of lipid research, 2008. **49**(8): p. 1607-1620.

91. Bratschi, M.W., et al., *Glycerol-3-phosphate acyltransferases gat1p and gat2p are microsomal phosphoproteins with differential contributions to polarized cell growth.* Eukaryot Cell, 2009. **8**(8): p. 1184-96.

92. Tamura, Y., et al., *Tam41 Is a CDP-Diacylglycerol Synthase Required for Cardiolipin Biosynthesis in Mitochondria.* Cell metabolism, 2013. **17**(5): p. 709-718.

93. Chakraborty, T.R., et al., *Phosphatidic acid synthesis in mitochondria. Topography of formation and transmembrane migration.* The Journal of biological chemistry, 1999. **274**(42): p. 29786-29790.

94. Zhang, J., et al., *Mitochondrial phosphatase PTPMT1 is essential for cardiolipin biosynthesis.* Cell metabolism, 2011. **13**(6): p. 690-700.

95. Mejia, E.M., H. Nguyen, and G.M. Hatch, *Mammalian cardiolipin biosynthesis.* Chemistry and physics of lipids, 2013.

96. Hostetler, K.Y., et al., *Further studies on the formation of cardiolipin and phosphatidylglycerol in rat liver mitochondria. Effect of divalent cations and the fatty acid composition of CDP-diglyceride.* Biochimica et biophysica acta, 1975. **380**(3): p. 382-389.

97. Nowicki, M., F. Muller, and M. Frentzen, *Cardiolipin synthase of Arabidopsis thaliana.* FEBS letters, 2005. **579**(10): p. 2161-2165.

98. Houtkooper, R.H., et al., *Identification and characterization of human cardiolipin synthase.* FEBS letters, 2006. **580**(13): p. 3059-3064.

99. Claypool, S.M., J.M. McCaffery, and C.M. Koehler, *Mitochondrial mislocalization and altered assembly of a cluster of Barth syndrome mutant tafazzins.* J Cell Biol, 2006. **174**(3): p. 379-90.

100. Schlame, M., *Cardiolipin remodeling and the function of tafazzin.* Biochim Biophys Acta, 2013. **1831**(3): p. 582-8.

101. Schlame, M., et al., *Deficiency of tetralinoleoyl-cardiolipin in Barth syndrome.* Annals of Neurology, 2002. **51**(5): p. 634-637.

102. Vaz, F.M., et al., *Only one splice variant of the human TAZ gene encodes a functional protein with a role in cardiolipin metabolism.* J Biol Chem, 2003. **278**(44): p. 43089-94.

103. Houtkooper, R.H., et al., *The enigmatic role of tafazzin in cardiolipin metabolism.* Biochim Biophys Acta, 2009. **1788**(10): p. 2003-14.

104. Malhotra, A., et al., *Formation of molecular species of mitochondrial cardiolipin. 1. A novel transacylation mechanism to shuttle fatty acids between sn-1 and sn-2 positions of multiple phospholipid species.* Biochim Biophys Acta, 2009. **1791**(4): p. 314-20.

105. Schlame, M., et al., *The physical state of lipid substrates provides transacylation specificity for tafazzin.* Nat Chem Biol, 2012. **8**(10): p. 862-9.

106. Schlame, M., *Cardiolipin remodeling and the function of tafazzin.* Biochimica et biophysica acta, 2012.

107. Neuwald, A.F., *Barth syndrome may be due to an acyltransferase deficiency.* Curr Biol, 1997. **7**(8): p. R465-6.

108. Vreken, P., et al., *Defective remodeling of cardiolipin and phosphatidylglycerol in Barth syndrome.* Biochemical and biophysical research communications, 2000. **279**(2): p. 378-382.

109. IL, G. *Human tafazzin (TAZ) gene variation database.* Science and Medicine section of http://www.barthsyndrome.org 2015 March 2015.

110. Johnston, J., et al., *Mutation characterization and genotype-phenotype correlation in Barth syndrome.* Am J Hum Genet, 1997. **61**(5): p. 1053-8.

111. Clarke, S.L., et al., *Barth syndrome.* Orphanet journal of rare diseases, 2013. **8**: p. 23-1172-8-23.

112. Schlame, M. and M. Ren, *Barth syndrome, a human disorder of cardiolipin metabolism.* FEBS letters, 2006. **580**(23): p. 5450-5455.

113. *Barth Syndrome Foundation website: frequently asked question*

114. Kulik, W., et al., *Bloodspot assay using HPLC-tandem mass spectrometry for detection of Barth syndrome.* Clinical chemistry, 2008. **54**(2): p. 371-378.

115. Steward, C.G., et al., *Barth syndrome: an X-linked cause of fetal cardiomyopathy and stillbirth.* Prenatal diagnosis, 2010. **30**(10): p. 970-976.

116. Aprikyan, A.A. and Z. Khuchua, *Advances in the understanding of Barth syndrome.* British journal of haematology, 2013. **161**(3): p. 330-338.

117. Aprikyan, A.A., et al., *Impaired survival of bone marrow hematopoietic progenitor cells in cyclic neutropenia.* Blood, 2001. **97**(1): p. 147-53.

118. Devriendt, K., et al., *Constitutively activating mutation in WASP causes X-linked severe congenital neutropenia.* Nat Genet, 2001. **27**(3): p. 313-7.

119. Welte, K., C. Zeidler, and D.C. Dale, *Severe congenital neutropenia.* Semin Hematol, 2006. **43**(3): p. 189-95.

120. Klein, C. and K. Welte, *Genetic insights into congenital neutropenia.* Clin Rev Allergy Immunol, 2010. **38**(1): p. 68-74.

121. Kuijpers, T.W., et al., *Neutrophils in Barth syndrome (BTHS) avidly bind annexin-V in the absence of apoptosis.* Blood, 2004. **103**(10): p. 3915-23.

122. Massullo, P., et al., *Aberrant subcellular targeting of the G185R neutrophil elastase mutant associated with severe congenital neutropenia induces*

premature apoptosis of differentiating promyelocytes. Blood, 2005. **105**(9): p. 3397-404.

123. Xu, Y., et al., *Characterization of lymphoblast mitochondria from patients with Barth syndrome.* Lab Invest, 2005. **85**(6): p. 823-30.

124. Acehan, D., et al., *Comparison of lymphoblast mitochondria from normal subjects and patients with Barth syndrome using electron microscopic tomography.* Laboratory investigation; a journal of technical methods and pathology, 2007. **87**(1): p. 40-48.

125. Taylor, W.A. and G.M. Hatch, *Purification and characterization of monolysocardiolipin acyltransferase from pig liver mitochondria.* The Journal of biological chemistry, 2003. **278**(15): p. 12716-12721.

126. Taylor, W.A., et al., *Human trifunctional protein alpha links cardiolipin remodeling to Beta-oxidation.* PloS one, 2012. **7**(11): p. e48628.

127. Yang, B.Z., et al., *The genes for the alpha and beta subunits of the mitochondrial trifunctional protein are both located in the same region of human chromosome 2p23.* Genomics, 1996. **37**(1): p. 141-3.

128. Uchida, Y., et al., *Novel fatty acid beta-oxidation enzymes in rat liver mitochondria. II. Purification and properties of enoyl-coenzyme A (CoA) hydratase/3-hydroxyacyl-CoA dehydrogenase/3-ketoacyl-CoA thiolase trifunctional protein.* J Biol Chem, 1992. **267**(2): p. 1034-41.

129. Ushikubo, S., et al., *Molecular characterization of mitochondrial trifunctional protein deficiency: formation of the enzyme complex is important for stabilization of both alpha- and beta-subunits.* Am J Hum Genet, 1996. **58**(5): p. 979-88.

130. Weinberger, M.J., et al., *Intact alpha-subunit is required for membrane-binding of human mitochondrial trifunctional beta-oxidation protein, but is not necessary for conferring 3-ketoacyl-CoA thiolase activity to the beta-subunit.* Biochem Biophys Res Commun, 1995. **209**(1): p. 47-52.

131. Ma, B.J., et al., *Acylation of monolysocardiolipin in rat heart.* Journal of lipid research, 1999. **40**(10): p. 1837-1845.

132. Danos, M., W.A. Taylor, and G.M. Hatch, *Mitochondrial monolysocardiolipin acyltransferase is elevated in the surviving population of H9c2 cardiac myoblast cells exposed to 2-deoxyglucose-induced apoptosis.* Biochemistry and cell biology = Biochimie et biologie cellulaire, 2008. **86**(1): p. 11-20.

133. Acehan, D., et al., *Cardiac and skeletal muscle defects in a mouse model of human Barth syndrome.* The Journal of biological chemistry, 2011. **286**(2): p. 899-908.

134. Livak, K.J. and T.D. Schmittgen, *Analysis of relative gene expression data using real-time quantitative PCR and the 2(-Delta Delta C(T)) Method.* Methods, 2001. **25**(4): p. 402-8.

135. Sparagna, G.C., et al., *Quantitation of cardiolipin molecular species in spontaneously hypertensive heart failure rats using electrospray ionization mass spectrometry.* Journal of lipid research, 2005. **46**(6): p. 1196-1204.

136. Rouser, G., A.N. Siakotos, and S. Fleischer, *Quantitative analysis of phospholipids by thin-layer chromatography and phosphorus analysis of spots.* Lipids, 1966. **1**(1): p. 85-6.

137. Bradford, M.M., *A rapid and sensitive method for the quantitation of microgram quantities of protein utilizing the principle of protein-dye binding.* Anal Biochem, 1976. **72**: p. 248-54.

138. Biosciences, B., *BD Cell-Tak™ Cell and Tissue Adhesive Instructions for Use*. 2001.

139. Mukhopadhyay, P., et al., *Simultaneous detection of apoptosis and mitochondrial superoxide production in live cells by flow cytometry and confocal microscopy.* Nat Protoc, 2007. **2**(9): p. 2295-301.

140. Kirwin, S.M., et al., *Tafazzin splice variants and mutations in Barth syndrome.* Mol Genet Metab, 2014. **111**(1): p. 26-32.

141. He, Q., et al., *Tafazzin knockdown interrupts cell cycle progression in cultured neonatal ventricular fibroblasts.* Am J Physiol Heart Circ Physiol, 2013. **305**(9): p. H1332-43.

142. Xu, Y., et al., *Characterization of tafazzin splice variants from humans and fruit flies.* J Biol Chem, 2009. **284**(42): p. 29230-9.

143. Landriscina, C., F.M. Megli, and E. Quagliariello, *Turnover of fatty acids in rat liver cardiolipin: comparison with other mitochondrial phospholipids.* Lipids, 1976. **11**(1): p. 61-6.

144. Xu, Y. and M. Schlame, *The turnover of glycerol and acyl moieties of cardiolipin.* Chem Phys Lipids, 2014. **179**: p. 17-24.

145. Phoon, C.K., et al., *Tafazzin knockdown in mice leads to a developmental cardiomyopathy with early diastolic dysfunction preceding myocardial*

noncompaction. Journal of the American Heart Association, 2012. **1**(2): p. 10.1161/JAHA.111.000455. Epub 2012 Apr 24.

146. Kiebish, M.A., et al., *Dysfunctional cardiac mitochondrial bioenergetic, lipidomic, and signaling in a murine model of Barth syndrome.* Journal of lipid research, 2013. **54**(5): p. 1312-1325.

147. Hauff, K.D. and G.M. Hatch, *Cardiolipin metabolism and Barth Syndrome.* Progress in lipid research, 2006. **45**(2): p. 91-101.

148. Claypool, S.M., et al., *The cardiolipin transacylase, tafazzin, associates with two distinct respiratory components providing insight into Barth syndrome.* Mol Biol Cell, 2008. **19**(12): p. 5143-55.

149. Wittig, I. and H. Schagger, *Advantages and limitations of clear-native PAGE.* Proteomics, 2005. **5**(17): p. 4338-46.

150. Pineau, B., et al., *The importance of cardiolipin synthase for mitochondrial ultrastructure, respiratory function, plant development, and stress responses in Arabidopsis.* Plant Cell, 2013. **25**(10): p. 4195-208.

151. Mejia, E.M., et al., *Differential reduction in cardiac and liver monolysocardiolipin acyltransferase-1 and reduction in cardiac and liver tetralinoleoyl-cardiolipin in the alpha-subunit of trifunctional protein heterozygous knockout mice.* Biochem J, 2015. **471**(1): p. 123-9.

152. Brand, M.D. and D.G. Nicholls, *Assessing mitochondrial dysfunction in cells.* Biochem J, 2011. **435**(2): p. 297-312.

153. Heytler, P.G. and W.W. Prichard, *A new class of uncoupling agents--carbonyl cyanide phenylhydrazones.* Biochem Biophys Res Commun, 1962. **7**: p. 272-5.

154. Wiegand, G. and S.J. Remington, *Citrate synthase: structure, control, and mechanism.* Annu Rev Biophys Biophys Chem, 1986. **15**: p. 97-117.

155. Acehan, D., et al., *Cardiolipin affects the supramolecular organization of ATP synthase in mitochondria.* Biophys J, 2011. **100**(9): p. 2184-92.

156. Divakaruni, A.S. and M.D. Brand, *The regulation and physiology of mitochondrial proton leak.* Physiology (Bethesda), 2011. **26**(3): p. 192-205.

157. Noji, H., et al., *Direct observation of the rotation of F1-ATPase.* Nature, 1997. **386**(6622): p. 299-302.

158. Stock, D., A.G. Leslie, and J.E. Walker, *Molecular architecture of the rotary motor in ATP synthase.* Science, 1999. **286**(5445): p. 1700-5.

159. Sansbury, B.E., et al., *Bioenergetic function in cardiovascular cells: the importance of the reserve capacity and its biological regulation.* Chem Biol Interact, 2011. **191**(1-3): p. 288-95.

160. Hill, B.G., et al., *Regulation of vascular smooth muscle cell bioenergetic function by protein glutathiolation.* Biochim Biophys Acta, 2010. **1797**(2): p. 285-95.

161. Spencer, C.T., et al., *Impaired cardiac reserve and severely diminished skeletal muscle O(2) utilization mediate exercise intolerance in Barth syndrome.* Am J Physiol Heart Circ Physiol, 2011. **301**(5): p. H2122-9.

162. Zheng, J., *Energy metabolism of cancer: Glycolysis versus oxidative phosphorylation (Review).* Oncol Lett, 2012. **4**(6): p. 1151-1157.

163. Chen, Q., et al., *Production of reactive oxygen species by mitochondria: central role of complex III.* J Biol Chem, 2003. **278**(38): p. 36027-31.

164. Brookes, P.S., *Mitochondrial H(+) leak and ROS generation: an odd couple.* Free Radic Biol Med, 2005. **38**(1): p. 12-23.

165. Echtay, K.S., et al., *Superoxide activates mitochondrial uncoupling proteins.* Nature, 2002. **415**(6867): p. 96-9.

166. Echtay, K.S., et al., *Superoxide activates mitochondrial uncoupling protein 2 from the matrix side. Studies using targeted antioxidants.* J Biol Chem, 2002. **277**(49): p. 47129-35.

167. Lee, Y., et al., *Uncoupling protein 1 binds one nucleotide per monomer and is stabilized by tightly bound cardiolipin.* Proc Natl Acad Sci U S A, 2015. **112**(22): p. 6973-8.

168. Crichton, P.G., et al., *Trends in thermostability provide information on the nature of substrate, inhibitor, and lipid interactions with mitochondrial carriers.* J Biol Chem, 2015. **290**(13): p. 8206-17.

169. Schwall, C.T., V.L. Greenwood, and N.N. Alder, *The stability and activity of respiratory Complex II is cardiolipin-dependent.* Biochim Biophys Acta, 2012. **1817**(9): p. 1588-96.

170. Hwang, M.S., et al., *Mitochondrial Ca(2+) influx targets cardiolipin to disintegrate respiratory chain complex II for cell death induction.* Cell Death Differ, 2014. **21**(11): p. 1733-45.

171. Hauff, K.D. and G.M. Hatch, *Reduction in cholesterol synthesis in response to serum starvation in lymphoblasts of a patient with Barth syndrome.* Biochemistry and cell biology = Biochimie et biologie cellulaire, 2010. **88**(4): p. 595-602.

172. Buck, K.J., N.A. Walter, and D.L. Denmark, *Genetic variability of respiratory complex abundance, organization and activity in mouse brain.* Genes Brain Behav, 2014. **13**(2): p. 135-43.

173. van der Vusse, G.J., et al., *Fatty acid homeostasis in the normoxic and ischemic heart.* Physiol Rev, 1992. **72**(4): p. 881-940.

174. Rui, L., *Energy metabolism in the liver.* Compr Physiol, 2014. **4**(1): p. 177-97.

175. Turrens, J.F., *Superoxide production by the mitochondrial respiratory chain.* Biosci Rep, 1997. **17**(1): p. 3-8.

176. Andreyev, A.Y., Y.E. Kushnareva, and A.A. Starkov, *Mitochondrial metabolism of reactive oxygen species.* Biochemistry (Mosc), 2005. **70**(2): p. 200-14.

177. Starkov, A.A., *Measurement of mitochondrial ROS production.* Methods Mol Biol, 2010. **648**: p. 245-55.

178. Sawyer, D.B., et al., *Role of oxidative stress in myocardial hypertrophy and failure.* J Mol Cell Cardiol, 2002. **34**(4): p. 379-88.

179. Korantzopoulos, P., et al., *The possible role of oxidative stress in heart failure and the potential of antioxidant intervention.* Med Sci Monit, 2003. **9**(6): p. RA120-5.

180. Chelikani, P., I. Fita, and P.C. Loewen, *Diversity of structures and properties among catalases.* Cell Mol Life Sci, 2004. **61**(2): p. 192-208.

181. Gaetani, G.F., et al., *Predominant role of catalase in the disposal of hydrogen peroxide within human erythrocytes.* Blood, 1996. **87**(4): p. 1595-9.

182. Sundaram, A., et al., *Upregulation of catalase and downregulation of glutathione peroxidase activity in the kidney precede the development of hypertension in pre-hypertensive SHR.* Hypertens Res, 2013. **36**(3): p. 213-8.

183. Cardona, F., et al., *Similar increase in oxidative stress after fat overload in persons with baseline hypertriglyceridemia with or without the metabolic syndrome.* Clin Biochem, 2008. **41**(9): p. 701-5.

184. Cardona, F., et al., *Fat overload aggravates oxidative stress in patients with the metabolic syndrome.* Eur J Clin Invest, 2008. **38**(7): p. 510-5.

185. Vavrova, L., et al., *Altered activities of antioxidant enzymes in patients with metabolic syndrome.* Obes Facts, 2013. **6**(1): p. 39-47.